# Determining the Application of Small Extracellular Vesicles (SEVs) as Biomarkers of Arsenic Induced Urothelial Injury and Carcinogenesis

**Nicole Washuck**

Thesis submitted to the University of Ottawa
in the partial fulfillment of the requirements for the
Master of Science in Biology
Specialization in Chemical and Environmental Toxicology

Department of Biology

Faculty of Science

University of Ottawa

# Abstract

Arsenic is a toxic metalloid that continues to contaminate the water and food sources of millions of people globally. Among the numerous health effects of arsenic exposure are urothelial toxicity and cancer. In recent years, small extracellular vesicles (SEVs) have been shown to be vital in intracellular communication and have been used in clinical studies as biomarkers of disease. The overall goal of this thesis is to understand the mechanisms of cell communication during arsenic exposure and to develop minimally invasive biomarkers for the toxic responses. The specific objectives are to: a) determine if SEVs released from arsenic exposed urothelial cells are responsible for mediating urothelial toxicity; and b) assess the application of urinary SEVs as novel biomarkers of arsenic exposure in an exposed population. The hypothesis leading this research is that the biology and protein packaging profile of urothelial SEVs are altered following arsenic exposure because of the induction of cell stress signaling pathways. I also hypothesize that urinary SEV proteins can be used as biomarkers of arsenic exposure because they are positively correlated with urinary arsenic concentrations in an exposed population. SVHUC1 human urothelial cells were dosed with sodium meta arsenite (1, 2, and 5 uM) for 48 hours. T24 urothelial carcinoma cells were also grown in parallel to compare for carcinogenicity. A label-free quantitative proteomics approach was used to assess the differentially expressed proteins in the cell lysate and the SEVs extracted from the culture media to determine the mechanistic pathways involved and how well the protein profiles in SEVs correlate with those in the cell lysate. SEVs were isolated from the archived urine samples of participants (n=36) enrolled in the Yellow Knife Health Effects Monitoring Program (YKHEMP) and two potential biomarkers, transforming growth factor beta receptor 1 (TGFBR1) and ribonuclease inhibitor 1

(RNH1), were measured by an enzyme linked immunosorbent assay (ELISA). SEVs in all samples were successfully characterized based on their size (50-200 nm) and positive antibody array for eight protein markers indicating their endosomal biogenesis. The total number of SEVs was not shown to increase following arsenic exposure in the *in vitro* study. However, the cancerous T24 cells had nearly four times higher numbers of SEVS compared to the non-cancerous SVHUC1 cells. The changes in the protein profiles in SEVs released following arsenic dosage indicated activation of pathways important for cell survival, viability, and migration and inactivation of pathways related to cell death and necrosis which were also observed in the paired cell lysate samples. Comparison between paired SEV and cell lysate samples, however, indicated selective SEV packaging of proteins which may be for the purpose of intracellular communication. Comparative assessment of SEVs from T24 and arsenic exposed SVHUC1 cells showed similar activation of cancer related pathways including those responsible for malignant tumors and increased proliferation rates. From the *in vitro* study results, we identified 8 potential SEV biomarkers. Of which, TGFBR1 showed the most promising association, having been positively associated with both inorganic arsenic and cadmium concentrations in urine samples. This thesis showed that SEVs are important mediators of arsenic exposure in urothelial cells and highlighted the comparability of SEV and cell lysate analysis. Furthermore, TGFBR1 was identified as a promising biomarker of arsenic exposure for its positive association with increased arsenic both *in vitro* and in human biomonitoring analysis.

# Acknowledgments

First, I would like to thank my supervisor Dr. Laurie Chan for teaching me that research is so much more than what we do in lab, it is the impact we leave on those it affects and it is only through understanding that can we improve as scientists. The unwavering support of Laurie to try new techniques and learn from every failure has been pivotal to my growth as a researcher and as a person.

Moreover, I would like to thank my thesis advisory committee members, Dr. Bill Willmore, and Dr. Maxim Berezovski, for their valuable comments and guidance throughout my thesis that allowed me to see my own research in a new light.

I have been so lucky to work with such brilliant and supportive lab colleagues and importantly friends over the past two years at the University of Ottawa. I have appreciated the technical expertise of Emmanuel Yumvihoze whose ingenious solutions to analytical problems have helped me more than once. I have also had the pleasure of working with Xufeng Hu the systematic review king, whose support has allowed me to foster writing and review skills. A huge thank you to the labs long time life supports Kayla Grey, Renata Rosol, and Lynn Barwin, who have fearlessly held our large group of researchers and collaborators together. To my fellow masters' students and friends Rhiannon Ng, Chathumi De Silva, Tyler Eng, Elizabeth Wallace, and Hannah Klassen you made moving to a new city and starting a masters during a global pandemic feel normal and welcoming. We supported each other throughout all the trials of grad school and are coming out the other side with degrees, memories, and lifelong friendships. A special thanks to Janet Cheung who was my first friend in lab and has been there every day since to answer all my absurd questions and critically evaluate life decisions with. Thank you to Pu Xia (Sharp), Bai Li, Jake Drouillard, Allison Loan, and Joseph Wai-Hin Leung for being so welcoming when I first joined the lab and for all your support since.

Chan lab members aside, I would be remised not to take this opportunity to thank all the collaborators who made this research possible with their expertise. To members of the Berezovski lab, Yingxi Li (Cici), Nico Hüttmann, and Dr. Zoran Minic your expertise in the field of SEVs and proteomics is the only reason I was able to learn an entirely new area of study over the past two years. Thank you to the Gibbings lab and Ryan Reshke for use of your nanoparticle tracking analysis and technical expertise.

Finally, I would like to thank my parents; Denise Drysdale and Mike Washuck, they have taught me to see the beauty in the world and it is because of their unparalleled support and love that I am the person I am today. I also need to thank my giant and crazy family who have been my backbone through life. To all my friends who have always been there for me from game nights to phone calls during my long days in lab, thank you. Lastly, to my partner in life and my confidant Aleks Veselic, thank you for being there for every practice presentation, late-night thesis writing session, and every time I got knocked down to make sure I never stay there for long.

I am so fortunate for all the support I have received, and I will spend my life trying to pay it forward in the pursuit of knowledge.

# Table of Contents

# List of Abbreviations

| | |
|---|---|
| **ADAMTSL4** | ADAMTS-like protein 4 |
| **AKR1B1** | Aldose reductase |
| **ALDH1A3** | Aldehyde dehydrogenase family 1 member A3 |
| **ALIX** | ALG-2-interacting protein X |
| **AM** | Arithmetic mean |
| **ANXA2, A5, and A7** | Annexin A2, A5, and A7 |
| **AsB** | Arsenobetaine |
| **$As^{III}$** | Arsenite |
| **ASS1** | Argininosuccinate synthase |
| **$As^{V}$** | Arsenate |
| **AUC** | Area under the curve |
| **AXL** | Tyrosine-protein kinase receptor UFO |
| **BAG2** | Bcl-2-associated athanogene 2 |
| **BASP1** | Brain acid soluble protein 1 |
| **BC** | Bladder cancer |
| **BCA** | Bicinchoninic acid assay |
| **BMP1** | Bone morphogenetic protein 1 |
| **BSA** | Bovine serum albumin |
| **C4A** | Complement C4-A |
| **CAPZA2** | F-actin-capping protein subunit alpha-2 |
| **Cd** | Cadmium |
| **CD59** | CD59 glycoprotein |
| **CD70** | CD70 antigen |
| **CD9, CD63, CD73, CD81** | Cluster of differentiation 9, 63, 73, and 81 |
| **CDH1** | Cadherin-1 |
| **CDH2** | Cadherin-2 |
| **CEACAM-5** | Carcinoembryonic antigen-related cell adhesion molecule 5 |
| **CHMP2A** | Charged multivesicular body protein 2a |
| **CHMS** | Canadian Health measures Survey |
| **CK2** | Casein Kinase II |
| **CLDN11** | Claudin-11 |
| **CLDN4** | Claudin-4 |
| **CLDN7** | Claudin-7 |
| **CLTC** | Clathrin heavy chain 1 |
| **COL5A1** | Collagen alpha-1(V) chain |
| **COL6A1** | Collagen alpha-1(VI) chain |
| **CSNK1G1** | Casein kinase I isoform gamma-1 |
| **CTSC** | Dipeptidyl peptidase 1 |

| | |
|---|---|
| **DDAH1** | N(G)-dimethylarginine dimethylaminohydrolase 1 |
| **DEPs** | Differentially expressed proteins |
| **DHX9** | ATP-dependent RNA helicase A |
| **$DMA^{III}$** | Dimethylarsinous acid |
| **$DMA^{V}$** | Dimethylarsinic acid |
| **DNM2** | Dynamin-2 |
| **DTT** | Dithiothreitol |
| **dUC** | Differential ultracentrifugation |
| **ECM** | Extracellular matrix |
| **EDIL-3** | EGF Like Repeats And Discoidin Domains 3 |
| **EEF1A2** | Elongation factor 1-alpha 2 |
| **ELISA** | Enzye linked immunosorbent assay |
| **ENG** | Endoglin |
| **EPB41L2** | Band 4.1-like protein 2 |
| **EPCAM** | Epithelial cell adhesion molecule |
| **EpCAM** | Epithelial cellular adhestion molecule |
| **EPHA2** | Ephrin type-A receptor 2 |
| **EPS8L1** | Epidermal growth factor receptor kinase substrate 8-like protein 1 |
| **EPS8L2** | Epidermal growth factor receptor kinase substrate 8-like protein 2 |
| **ESCRTs** | Endosomal sorting complex proteins |
| **EVA1A** | Protein eva-1 homolog A |
| **EVs** | Extracellular Vesicles |
| **F11R** | Junctional adhesion molecule A |
| **FAM3C** | Protein FAM3C |
| **FAT10** | Human leukocyte antigen (HLA)-F adjacent transcript 10 |
| **FDR** | False discovery rate |
| **FERMT2** | Fermitin family homolog 2 |
| **FLOT1** | Flotillin 1 |
| **FN1** | Fibronectin 1 |
| **FOLR1** | Folate receptor 1 |
| **GDI1** | Rab GDP dissociation inhibitor alpha |
| **GM** | Geometric mean |
| **GM130** | Golgimatrix protein 130 |
| **GNA11** | Guanine nucleotide-binding protein subunit alpha-11 |
| **GNAI1** | Guanine nucleotide-binding protein G(i) subunit alpha-1 |
| **GSH** | Glutathione |
| **H2AFV** | Histone H2A.V |
| **H2AFX** | Histone H2AX |
| **H2AFY** | Core histone macro-H2A.1 |
| **H3F3A** | Histone H3.3 |

| | |
|---|---|
| **HDGF** | Heptoma-derived growth factor |
| **HEXB** | Beta-hexosaminidase subunit beta |
| **HGS** | Hepatocyte growth factor-regulated tyrosine kinase substrate |
| **HIST1H1B** | Histone H1.5 |
| **HIST1H4A** | Histone H4 |
| **HIST2H2AC** | Histone H2A type 2-C;Histone H2A type 2-A |
| **HNRNPC** | Heterogeneous nuclear ribonucleoproteins C1/C2 |
| **hnRNPK** | Heterogeneous nuclear ribonucleoprotein K |
| **HNRNPL** | Heterogeneous nuclear ribonucleoprotein L |
| **HNRNPU** | Heterogeneous nuclear ribonucleoprotein U |
| **HSPB1** | Heat shock protein beta-1 |
| **HTRA1** | Serine protease HTRA1 |
| **IARC** | International Agency for Research on Cancer |
| **iAs** | Inorganic arsenic |
| **ICAM1** | Intercellular adhesion molecule 1 |
| **ICP-MS** | Inductively coupled plasma mass spectrometry |
| **IL10RB** | Interleukin-10 receptor subunit beta |
| **ILV** | Intraluminal vesicle |
| **IPA** | Ingenuity pathway analysis |
| **ITGA2B** | Integrin alpha-Iib |
| **ITGA6** | Integrin alpha-6 |
| **ITGB4** | Integrin beta-4 |
| **ITGB5** | Integrin beta-5 |
| **ITGB6** | Integrin beta-6 |
| **iTRAQ** | Isobaric tags for relative and absolute quantification |
| **KRAS** | GTPase Kras |
| **LAMA3** | Laminin subunit alpha-3 |
| **LAMC2** | Laminin subunit gamma-2 |
| **LFC** | Log fold change |
| **LFQ** | Label free quantification |
| **LOD** | Limit of detection |
| **LRP1** | Prolow-density lipoprotein receptor-related protein 1 |
| **MAN2B1** | Lysosomal alpha-mannosidas |
| **MICB** | Muscle invasive bladder cancer |
| **MISEV** | Minimal information for studies of extracellular vesicles |
| **$MMA^{III}$** | Monomethylarsonous acid |
| **$MMA^{V}$** | Monomethylarsonic acid |
| **MNAR** | Missing not at random |
| **MVB** | Multivesicular body |
| **MYO1C** | Unconventional myosin-Ic |

| | |
|---|---|
| **NaAsO2** | Sodium meta arsenite |
| **nano-LC-MS** | Nano liquid chromatography mass spectrometry |
| **NAP1L1** | Nucleosome assembly protein 1-like 1 |
| **NF2** | Merlin |
| **NID2** | Nidogen-2 |
| **NONO** | Non-POU domain-containing octamer-binding protein |
| **NQO1** | NAD(P)H dehydrogenase [quinone] 1 |
| **Nras** | GTPase Nras |
| **NSMA** | North Slave Metis Alliance |
| **NTA** | Nanoparticle tracking analysis |
| **OCLN** | Occludin |
| **Pb** | Lead |
| **PBS** | Phosphate buffer saline |
| **PCA** | Principal component analysis |
| **PDLIM1** | PDZ and LIM domain protein 1 |
| **PDXN** | Peroxidasin |
| **PLAT** | Tissue-type plasminogen activator |
| **ppm** | Parts per million |
| **PROM2** | Prominin-2 |
| **PRSS23** | Serine protease 23 |
| **PSMA1** | Proteasome subunit alpha type-1 |
| **PSMA2** | Proteasome subunit alpha type-2 |
| **PSMA3** | Proteasome subunit alpha type-3 |
| **PSMA4** | Proteasome subunit alpha type-4 |
| **PSMA5** | Proteasome subunit alpha type-5 |
| **PSMA7** | Proteasome subunit alpha type-7 |
| **PSMB1** | Proteasome subunit beta type-1 |
| **PSMB2** | Proteasome subunit beta type-2 |
| **PSMB3** | Proteasome subunit beta type-3 |
| **PSMB3** | Proteasome 20S subunit beta3 |
| **PSMB5** | Proteasome subunit beta type-5 |
| **PTPRC** | Receptor-type tyrosine-protein phosphatase C |
| **PTPRJ** | Receptor-type tyrosine-protein phosphatase eta |
| **PTX3** | Pentraxin-related protein PTX3 |
| **PXDN** | Peroxidasin homolog |
| **RAB35** | Ras-related protein Rab-35 |
| **RAI3** | Retinoic acid-induced protein 3 |
| **RALB** | Ras-related protein RAL-B |
| **RIPA** | Rasioimmunoprecipitation assay |
| **RNH1** | Ribonuclease inhibitor |

| | |
|---|---|
| **ROS** | Reactive oxygen species |
| **RPM** | Revolutions per minute |
| **RRAS2** | Ras-related protein R-Ras2 |
| **S100A4** | Protein S100-A4 |
| **SAM** | S-adenosylmethionine |
| **SD** | Standard deviation |
| **SEVs** | Small Extracellular Vesicles |
| **SH3GL1** | Endophilin-A2 |
| **SLC20A1** | Sodium-dependent phosphate transporter 1 |
| **SLC26A2** | Sulfate transporter |
| **SMPDL3B** | Acid sphingomyelinase-like phosphodiesterase 3b |
| **SMPDL3B** | Spingomyelin phosphodiesterase acid-like 3b |
| **SND1** | Staphylococcal nuclease domain-containing protein 1 |
| **SSBP1** | Single-stranded DNA-binding protein |
| **ST14** | Suppressor of tumorigenicity 14 protein |
| **STEAP4** | Metalloreductase STEAP4 |
| **TACSTD2** | Tumor-associated calcium signal transducer 2 |
| **TAGLN** | Transgelin |
| **TALDO1** | Transaldolase |
| **TCC** | Transitional cell carcinoma |
| **TGFBR1** | TGF-beta receptor type-1 |
| **TGM2** | Protein-glutamine gamma-glutamyltransferase 2 |
| **THBS1** | Thrombospondin-1 |
| **THBS4** | Thrombospondin-4 |
| **TINAGL1** | Tubulointerstitial nephritis antigen-like |
| **TMPRSS2** | Transmembrane protease serine 2 |
| **TPP1** | Tripeptidyl-peptidase 1 |
| **TPP2** | Tripeptidyl-peptidase 2 |
| **TSG101** | Tumor susceptibility gene 101 |
| **TUBA4A** | Tubulin alpha-4A chain |
| **UAP1** | UDP-N-acetylhexosamine pyrophosphorylase |
| **VIM** | Vimetin |
| **WHO** | World Health Organization |
| **YKDFN** | Yellowknife Dene First Nations |
| **YKHEMP** | Yellowknife Health Effects Monitoring Program |
| **ZDHHC5** | Palmitoyltransferase ZDHHC5 |

# List of Tables

# List of Figures

# Chapter 1: Introduction

Arsenic is a pervasive metalloid in water, soil, and air that is derived from both natural and anthropogenic sources (Hughes, 2002). Arsenic is listed by the World Health Organization (WHO) as the most significant drinking water contaminant globally, affecting an estimated 140 million individuals across 50 countries (WHO, 2018). Chronic exposure to arsenic causes an array of adverse health effects that have been proven at a population level (Tchounwou, Centeno, & Patlolla, 2004). Included in these chronic effects is the increased risk of developing various cancers (Putila & Guo, 2011; Mendez et al, 2017; Tchounwou, Centeno, & Patlolla, 2004). Bladder cancer inparticular has been regarded as one of the most prevalant cancers linked to arsenic exposure (NTP, 2016). Urological tumors account for 25% of all human cancers, with 90-95% of these tumors originating from the bladder (Burger et al., 2017). As both arsenic exposure and bladder cancer are globally prevalent issues, it is important to understand their relationship to one another and develop diagnostic tools to aid in early disease identification.

In recent years, many novel approaches have emerged that have changed our understanding of carcinogenesis. Once such approach is the use of small extracellular vesicles (SEVs) as biomarkers of disease. SEVs are a type of extracellular vesicle (EV) that are critical for cell signalling and communication (Bowers, Hassanin, & Ramos, 2020). SEVs have been used to identify novel chemical induced disease mechanisms and have been proposed as an ideal vector for biomarker discovery (Harischandra et al., 2017; Bowers, Hassanin, & Ramos, 2020). The study of SEVs is still novel to the field of toxicology, and the roles SEVs play in arsenic-induced bladder toxicity have never been assessed.

## 1.1. Arsenic

### 1.1.1. Basic Chemistry

Arsenic is the 33rd element on the periodic table and is classified as a heavy metalloid. Arsenic is part of the pnictogen group composed of nitrogen, phosphorus, antimony, and bismuth in the periodic table with properties in between that of true metals and non-metals. Arsenic has a greater oxidation potential than that of nitrogen and phosphorous enabling arsenic to exhibit +3 and +5 oxidation states (Flora, 2015). With arsenic presenting similar electrochemical properties to phosphorus, it behaves similarly and is found in comparable compounds. Various physiochemical properties including oxidation and methylation rates and pH determine the overall species, mobility, and bioavailability of arsenic in a system (Jomova et al., 2011). Arsenic exists in inorganic and organic forms. Inorganic arsenicals are typically more toxic than their organic counterparts with trivalent arsenic ($As^{III}$) being more toxic and 50-60 times more mobile than pentavalent arsenic ($As^{IV}$). Under reducing conditions trivalent arsenic is the predominant form and under oxidizing conditions pentavalent arsenic dominates (Flora, 2015). Of the inorganic compounds, sodium arsenite, arsenic trioxide, and arsenic trichloride are the most common trivalent species and arsenate, arsenic acid, and arsenic pentoxide are the most common pentavalent compounds (IARC, 2012). These inorganic compounds can complex with other minerals and are typically found in rock, soil, air, and water (Jomova et al., 2011). Organic arsenic forms include arsenosugars, arsenolipids, arsenocholine, and arsenobetaine which are typically found in fish and seafood products (IARC, 2012).

### 1.1.2. Human Exposure

**Sources and Routes of Exposure**

Arsenic can be mobilized in the environment by natural processes such as hydrothermal or geothermal activities, biological activities, and the weathering of rocks as well as through anthropogenic activities. Anthropogenic activities responsible for elevated environmental arsenic levels include mining, use of arsenical pesticides, and the combustion of fossil fuels (Flora, 2015). The primary route of arsenic exposure for humans is through ingestion of contaminated food and water. Inorganic arsenic is typically highest in fruit juices and rice with organic arsenic found mainly in fish and shellfish (Health Canada, 2022). Concentrations of arsenic in surface freshwater is typically less than 10 $\mu$g/L but has been documented to be as high as 5 mg/L in regions near anthropogenic sources (IARC, 2012). Bangladesh and India are known as the most arsenic-affected countries in the world in based on population exposure in drinking water. In Bangladesh alone an estimated 50 million people are at risk of exposure (Ahmad et al., 2018; Bagchi, 2007). As part of the Canadian Water Network initiative researchers searched government databases to quantify arsenic in drinking water across Canada. The results of this study found several hotspots across Canada with arsenic concentrations documented above the 10 $\mu$g/L government threshold in drinking water. These hotspots spanned from British Columbia to Newfoundland and were determined to generally be the result of natural, non-anthropogenic sources (McGuigan et al., 2010). Cumulatively, the daily intake of ingested arsenic ranges from 20-300 $\mu$g/day for the general population. Inhalation of arsenic accounts for a minor amount of total exposure with estimated daily intakes of 20-200 ng in rural areas, 400-600 ng in cities, 1 $\mu$g for non-smokers living in polluted areas and up to 10 $\mu$g for smokers (Howe et al., 2001). Inhalation as well as dermal exposure to arsenic is of particular concern in occupational exposures. Industries facing occupational exposure include any mining requiring the smelting of

non-ferrous metal, coal-fired power plants, pressure-treated woodwork, battery assembly, glass manufacturing, and the electronics industry. Carcinogen Exposure Canada (CAREX) researchers estimated that 25000 Canadians are regularly exposed to elevated arsenic levels in the workplace (IARC, 2012).

**Adsorption, Distribution, Metabolism and Excretion**

After adsorption via the lungs or gastrointestinal tract arsenic is widely distributed throughout the body by the blood. Most tissues can rapidly clear arsenic except for keratin-rich tissues such as hair, skin, and nails. In keratin-rich tissues arsenic complexes with keratin rich sulfhydryl groups and accumulates (Chen et al., 2013). Absorbed arsenic is primarily metabolized in the liver; the process of arsenic metabolism involves alternating steps of two-electron reductions and oxidative methylation. Oxidative methylation of arsenic requires S-adenosyl methionine (SAM) as a methyl donor and glutathione (GSH) as an essential cofactor (**Figure 1.1**) (Chen et al., 2013). At this point, organic species have a low cellular permeability and are typically of low concern (Chung et al., 2014). Trivalent inorganic arsenic can cross most membranes via a simple diffusion mechanism and may also be taken up by aquaglyceroporins 7 and 9 and glucose transporter type 1 and 4 in mammals. Only a small proportion of pentavalent inorganic arsenic can cross cell membranes where it is then immediately reduced to trivalent inorganic arsenic. As pentavalent inorganic arsenic share similarities with phosphorous it can be taken up into cells via phosphate transporters (Rosen & Liu, 2009). The main route of arsenic excretion (70%) is through the kidneys into the urine with other possible excretion into the feces and sweat. Approximately 50% of urinary arsenic is dimethylated, followed by 25% monomethylated, and 25% as inorganic arsenic (Chen et al., 2013).

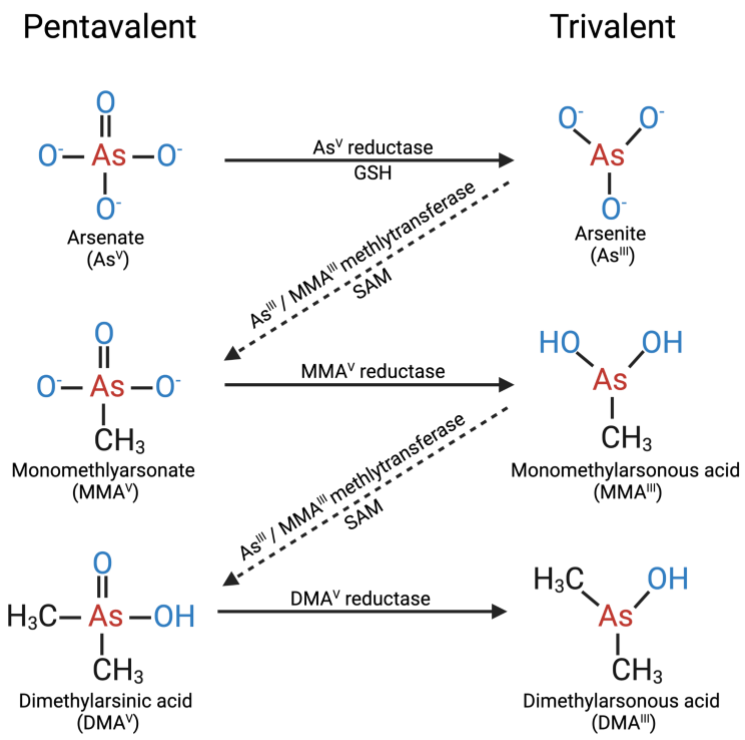


**Figure 1.1.** Molecular mechanisms of arsenic speciation. Adapted from Chen et al., 2013. Created with BioRender.com.

### 1.1.3. Associated Health Effects

The diverse toxic effects of arsenic result in several adverse health outcomes related to both acute and chronic exposure. Due to arsenics high affinity for thiol groups, keratin rich tissues such as the skin are a major target of toxicity. Dermal effects are a hallmark of arsenic poisoning and can include the development of skin lesions including hyperkeratosis and hyperpigmentation (Jomova et al., 2011). Arsenic can also affect the cardiovascular, renal, nervous, hepatic, endocrine and haematological systems resulting in a variety of disease outcomes. Some notable diseases commonly associated with arsenic exposure include blackfoot disease, diabetes mellitus,

peripheral neuropathy, kidney damage and the development of several cancers (Mohammed Abdul et al., 2015).

Inorganic arsenic has been classified by the International Agency for Research on Cancer (IARC) as a group-1 carcinogen meaning it is carcinogenic to humans. IARC based this classification on epidemiological and mechanistic data supporting arsenic induced skin, lung, urinary bladder, kidney, liver, and prostate cancer in humans (IARC, 2004). Arsenic induced carcinogenesis results from chronic exposure to moderate to high levels of arsenic, often correlated with arsenic contaminated drinking water. Arsenic-induced Bowen's disease (intraepithelial carcinoma) can appear after 10 years, whereas other skin cancers may take 20-30 years to appear (Martinez et al., 2011). In a study of 442,570 individuals living in northern China it was found that lung, bladder, and kidney cancer mortality due to arsenic had long latency times. In this study increased risk of cancer mortalities manifested 40 years after exposure reduction (Smith et al., 2018).

## 1.2. Arsenic and Bladder Cancer

### 1.2.1. Epidemiological Evidence

There is sufficient evidence across countries such as Bangladesh (Mostafa & Cherry, 2015), Taiwan (Chen et al., 2010), Chile (Steinmaus et al., 2013), Finland (Kurttio et al., 1999), Argentina (Bates et al., 2004) and the United States (Meliker et al., 2010) to support that arsenic exposure increases the risk of developing bladder cancer at chronic exposure concentrations greater than 100 $\mu$g/L in drinking water. A dose response relationship between arsenic and bladder cancer risk has previously been reported (Chiou et al., 2001; Chu & Crawford-Brown,

2007; Shao et al., 2021). In a cohort of 8,102 people, the risk for developing transitional cell carcinoma at various exposure concentrations were calculated. This study found that the relative risk for developing transitional cell carcinoma were 1.5, 2.3, and 4.9 at concentrations of arsenic in drinking water of 10.1-50, 50.1-100, and >100 $\mu$g/L, respectfully with risk being statistically significant in the 100 $\mu$g/L group (Chiou et al., 2001). A retrospective study by Chen et al. (2010) found that urinary tract tumor malignancy increased with increasing concentration of arsenic in drinking water in a population out of Taiwan.

Typically, low dose (<100-200 $\mu$g/L in drinking water) arsenic exposure has not been correlated with increased cancer risk (Lamm et al., 2021). Epidemiological studies in areas with lower levels of arsenic such as Canada have typically not reported a significantly increased risk of arsenic related cancers (Baastrup et al., 2008; Bates et al., 2004; Mink et al., 2008; C. Steinmaus et al., 2003; Tsuji et al., 2014). A recent metanalysis aiming to identify the risk low level (<150 $\mu$g/L in drinking water) arsenic exposure poses to lung and bladder cancer found insufficient evidence to support cancer risk in the 2996 bladder cancer cases studied (Boffetta & Borron, 2019). A review comparing US and Taiwan male datasets of arsenic and bladder cancer incidences showed similar regressions in the range of 3-60 $\mu$g/L arsenic in drinking water, neither of which showed increased risk in the given low dose exposure range (Lamm et al., 2021).

### 1.2.2. Effect Modifiers

There are many factors that modify the relationship between arsenic intake and bladder cancer risk; these include consumption of co-mutagenic compounds, individual methylation capabilities,

dietary nutrients, and other underlying conditions. Arsenic is not typically regarded as a mutagen on its own, but some evidence suggests that it may act as a co-mutagen when consumed by individuals who also smoke tobacco (Koutros et al., 2018). This co-mutagenesis can arise as arsenic interferes with DNA repair pathways that are crucial in repairing damage caused by tobacco carcinogens (Fischer et al., 2005; Hartwig et al., 2002; S. Shen et al., 2008). A handful of studies have not reported a significant correlation between smoking, arsenic, and bladder cancer risk, which may be due in part to the long latency period of bladder cancer (Koutros et al., 2018; Tsuji et al., 2014). Decreased arsenic methylation capacity has been correlated to elevated cancer risk and greater toxicity in vitro (Chen et al., 2003; Huang et al., 2008; Yu et al., 2000). A meta-analysis of studies examining the factors affecting interhuman methylation variation concluded that smoking, drinking, and older age are all factors in reduced methylation capabilities. Furthermore, analysis revealed that men had a 0.36-fold lower secondary methylation index than women, implying sex may play a role in arsenic methylation as well (H. Shen et al., 2016). Folate is important in the one carbon metabolism for SAM synthesis, a key step in mammalian arsenic methylation (Hall & Gamble, 2012). Increased dietary folate is correlated with increased arsenic methylation and excretion of urinary dimethylated arsenic, decreased urinary monomethylated arsenic and inorganic arsenic (iAs) (Bozack et al., 2019). Several other dietary antioxidants, including zinc, methionine, and cysteine, when used with chelating agents can increase the mobilization and excretion of arsenic while decreasing oxidative stress (Patrick, 2003).

### 1.2.3. Mechanisms of Arsenic Induced Bladder Cancer

According to the National Institute of Health, skin and bladder cancer are the most prevalent cancers associated with arsenic exposure, followed by cancer of the lungs, liver, kidney, digestive tract, lymphatic, and hematopoietic system (NTP, 2016). The inorganic trivalent form of arsenic has greater associated genotoxicity than its pentavalent counterpart, making it a more potent carcinogen (Singh et al., 2011). Unlike most carcinogens, arsenic does not conclusively cause cancer in animal models and thus *in vitro* experiments have been key to deciphering mechanisms of arsenic induced carcinogenicity (Tchounwou et al., 2004). The precise mechanism of arsenic induced bladder carcinogenesis remains unclear; however, research has shown that it likely spans genotoxic, co-mutagenic, cytotoxic pathways, and epigenetic modifications. Arsenic is well documented to induce the production of reactive oxygen species (ROS), leading to oxidative stress in mammalian cells. Besides direct production of ROS, arsenic exposure and methylation can result in the depletion of antioxidant stores, impairment of ROS-savaging enzymes, and mitochondrial dysfunction, all resulting in elevated oxidative stress (Ming Tam et al., 2020).

One proposed mechanism of arsenic induced carcinogenesis is the resulting genotoxicity of free radicals in cells and eventual DNA damage and mutations caused by these radicals. Naranmandura et al. (2011) found that acute exposure of human bladder cancer cells to inorganic and organic arsenic species induced reactive oxygen species (ROS) production and levels of glutathione were reduced by 60% following exposure to dimethylarsonous acid ($DMA^{III}$). Furthermore, the production of ROS was linked to DNA damage and impairment of tumor

protein 53 and 21 DNA repair proteins in human bladder cancer cells (Naranmandura et al., 2011). Oxidative damage from arsenic has also been linked to chromosomal aberrations in both mammalian cell and epidemiological models (L. Liu et al., 2003; Moore et al., 2002). In a case study of 123 bladder cancer patients who had been exposed to arsenic through drinking water, the total number of chromosomal alterations was higher with elevated exposure levels and were associated with the severity of tumour stage and grade (Moore et al., 2002).

Arsenic alone is a weak mutagen but may enhance the mutagenic properties of other chemicals including ultraviolet light, X-rays, diepoxybutane, and methylmethanesulfonate (Jha et al., 1992; Lee-Chen et al., 1993; Wiencke & Yager, 1992). Enhanced mutagenicity due to arsenic is related to the ability of arsenic to inhibit the repair of DNA lesions produced by other chemicals and ROS. Arsenic has been documented to affect both the expression and catalytic abilities of nucleotide excision repair and base excision repair pathways, leading to mutations and potentially cancer (Ming Tam et al., 2020).

Additionally, arsenic has been observed to interfere with cell cycle regulation, promoting cell proliferation, and decreased cell death which in turn enables the propagation of damaged DNA and mutations. Hyperproliferation of the bladder uroepithelium was demonstrated in mice exposed to 0.01% sodium meta arsenite through drinking water for 4 weeks. In the same study arsenic induced cell proliferation was reported to be correlated with the activation of the mitogen activated protein kinase pathway leading to the expression of activator protein-1-associated genes involved in cell proliferation (Luster & Simeonova, 2004).

Lastly, arsenic may promote carcinogenesis via the induction epigenetic modifications leading to the silencing of tumour suppressor genes or activation of oncogenes. Arsenic induced epigenetic modification include changes in DNA methylation, histone modification, and changes in miRNA expression (Meakin et al., 2017). In a study of 351 bladder tumours from individuals with elevated arsenic exposure, researchers determined that hypermethylation of Ras associated domain family 1 and serine protease 3 promoters was corelated with higher exposure and was related to tumour grade (Marsit et al., 2006). As stated, many mechanisms have been implicated in arsenic induced carcinogenesis. However, none of the listed mechanisms are specific to the bladder and few are fully understood, leaving gaps in our understanding of how chronic arsenic exposure can lead to the development of bladder cancer in epidemiological studies.

## 1.3. Biomarkers

Biomarkers are defined by cellular, analytical, biochemical, or molecular measurements from biological media that may be used to determine biological responses, adverse health effects or the presence of a chemical in the body (EPA, 2022). Biomarkers of exposure are used to indicate the internal dose of chemicals and their metabolites inside the body (Nordberg, 2010). Common matrices used to assess levels of arsenic exposure include measuring inorganic and methylated metabolites in urine, toenail clippings, hair, and blood. These biomarkers provide good indicators of exposure levels and can be used to predict adverse health effects based upon safety thresholds (National Research Council, 1999). Alternatively, biomarkers of effect are those indicators that are specific to adverse exposure effects including injury and disease biomarkers. Biomarkers of effect are valuable for determining the health outcomes of exposure and mitigating early signs of biological distress (Nordberg, 2010). Advancements in omics techniques are making biomarkers

of effect increasingly easier to discover using non-targeted approaches. These biomarkers are often molecules that reflect a change in chemical processes or may be key indicators of pathways of disease. An ideal biomarker is one that is (a) easily obtained in a minimally invasive manner, (b) highly indicative of pathological or physiological effects, (c) sensitive and specific, and (d) cost effective (Campion et al., 2013).

Urine provides an ideal source of biomarkers as it is readily expelled and easily obtained in high sample volumes. Furthermore, urine is rich in cells and vesicles derived from the urinary tract including the kidneys, ureter, bladder, and urethra as urine passes directly by the transitional epithelium, shedding vesicles and debris into the urine for excretion. Urinary biomarkers of chemical exposure have been widely studied and will be examined further in this thesis.

## 1.4. Small Extracellular Vesicles (SEVs)

Since their discovery in 1983 (Harding & Stahl, 1983; Pan & Johnstone, 1983), SEVs have gained the interest of many researchers due to their complex roles in physiology and disease, namely through transmission of intracellular signals. They are abundant in bodily fluids and released by potentially every cell type, making them easily accessible and ideal for candidate biomarker discovery (Bowers et al., 2020). SEVs (commonly termed “exosomes”) are a subset of extracellular vesicles (EVs) that are of endosomal origin. Alongside SEVs, other extracellular vesicles secreted by cells include plasma membrane derived “ectosomes” (microparticles/microvesicles) (30-100 nm) and apoptotic bodies (50-500 nm). The main difference between EV subtypes are their respective modes of biogenesis (X. Li et al., 2019). Since SEVs are similar in size and density to other secreted EVs, some scientists argue that EVs

should only be classified as small (< 200 nm) or large/medium (> 200 nm) rather than by modes of biogenesis (Théry et al., 2018). SEVs are commonly identified in studies by their unique protein and lipid composition, which are reminiscent of their endosomal origin. Widely accepted exosomal markers include tetraspanins (CD9, CD81, and CD63), proteins related to biogenesis (TGS 101 and Alix), heat shock proteins, membrane transport, and fusion protein such as annexins (Li et al., 2019). SEVs may carry proteins, lipids, metabolites, DNAs (single-stranded, double-stranded, and multicopy single-stranded), and RNAs (messenger, long noncoding, and micro), all of which can be taken up by recipient cells (Soung et al., 2017).

### 1.4.1. Biogenesis

SEVs are produced by the endosomal pathway. The endosomal pathway is one of the many ways in which cells communicate, regulate, and interact with their environment. Endocytosis is at the center of the endosomal pathway, and it is the process by which cells may internalize various molecules as well as surface proteins. Internalized macromolecules and proteins may be degraded by lysosomes, recycled back into the plasma membrane, or sent across polar cells in a process known as transcytosis. Endocytosis regulates key components of human health and disease and may alter glucose levels, stomach acidification, cell homeostasis, cell-cell and cell-matrix interactions and cell adhesion (Elkkin, Lakoduk, & Schmid, 2017).

SEV biogenesis is one of the many facets of the endosomal pathway and is outlined in **Figure 1.2**. Briefly, SEVs are generated from late endosomes, formed by the inward budding of the multivesicular body (MVB) membrane. Intraluminal vesicles (ILVs) are formed following invagination of the late endosomal membrane within the larger MVBs. During invagination,

cytosolic components may be engulfed in the ILVs and various surface proteins will get incorporated into the invaginating membranes. SEVs constitute those ILVs released into the extracellular space by exocytosis upon fusion with the plasma membrane (Y. Zhang et al., 2019). Various endogenous molecules as well as extrinsic factors, including microbial, viral, and non-viral infections (Crenshaw et al., 2018; Jones et al., 2018) can modulate the biogenesis pathway. The endosomal sorting complex proteins (ESCRTs) are those most widely attributed to SEV biogenesis. ESCRT-0 facilitates cargo aggregation, subsequent transfer and recruitment of ESCRT-I, ESCRT-II, and ESCRT-III to the endosomal membrane. ESCRT-I and II facilitate the budding of the endosomal membrane, and ESCRT-III facilitates membrane invagination and formation of ILVs. ESCRT components TSG101 and ALIX are examples of commonly employed SEV biomarkers. ILVs may also be formed through ESCRT-independent mechanisms involving key tetraspanins (CD9, CD63, CD81), small integral membrane proteins and lipids (Jadli et al., 2020).

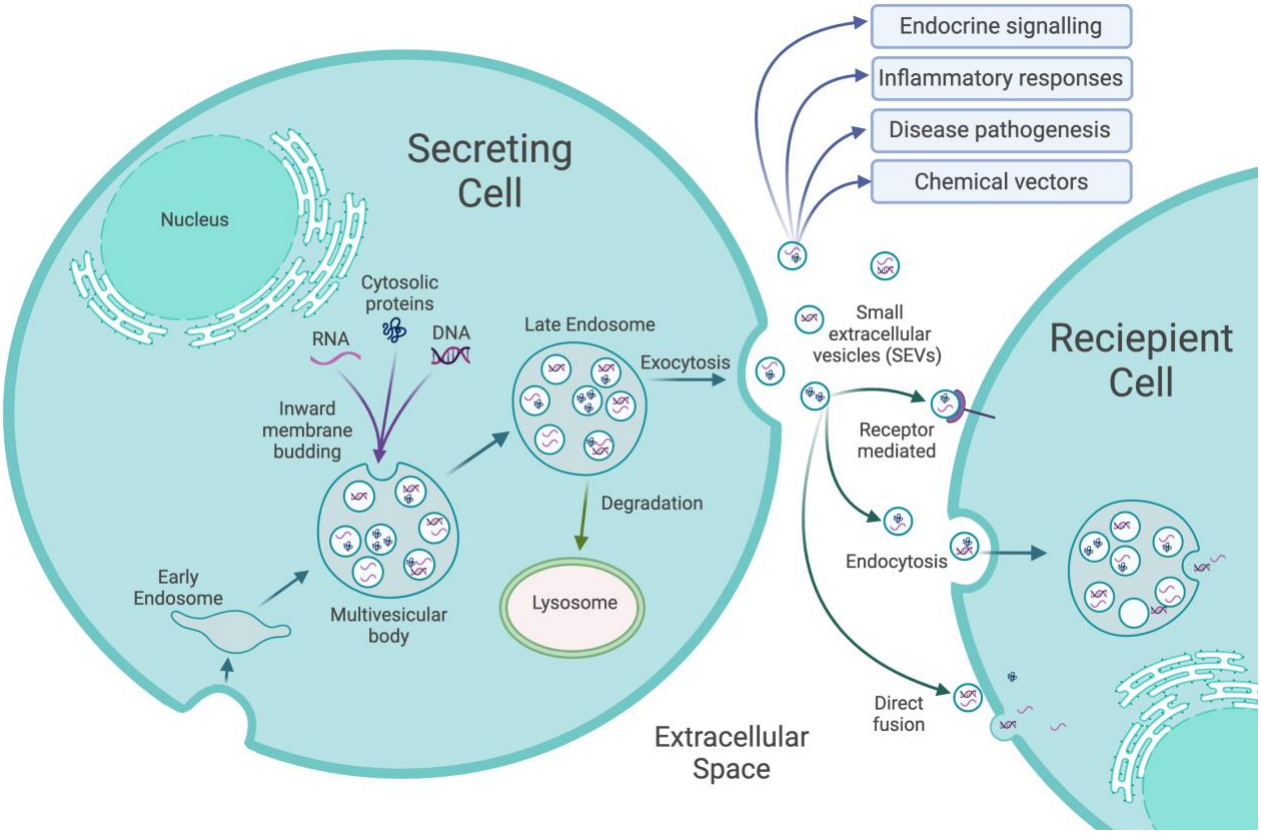


**Figure 1.2.** Biogenesis, secretion, and uptake of small extracellular vesicles (SEVs) by cells. Created with BioRender.com.

## 1.4.2. SEV Cargo Packaging

Many different mechanisms have been implicated in SEV packaging. Preferential packaging of certain RNA into SEVs suggests that packaging is not random, but rather specific mechanisms exist to shuttle select RNA into SEVs. RNA Y-box protein 1 has been implicated in the packaging of select non-coding RNA (Shurtleff et al., 2017) and miRNA (Shurtleff et al., 2016) into SEVs. Heterogenous nuclear ribonucleoprotein A2B1 can recognize specific miRNA sequence motifs and has also been associated with SEV packaging (Villarroya-Beltri et al., 2013). Precise mechanisms associated with exosomal DNA packaging are not yet known, but treatment with topoisomerase-I inhibitors (Kitai et al., 2017) and epidermal growth factor

receptor (Montermini et al., 2015) have been shown to increase DNA packaging. Various ESCRT proteins including TSG101 and EAP45 are important in packaging ubiquitinated proteins and lipids into ILVs (Piper & Katzmann, 2007). Altered protein packaging was observed in mammalian cells depleted of four key ESCRT proteins, suggesting that ESCRT-dependent mechanisms fill a specific niche of protein cargo packaging into ILVs (Stuffers et al., 2009). The tetraspanin CD63 is also important in ESCRT-independent packaging of cargo into SEVs with other proteins such as syntenin and heparanase stimulating this process (Stoorvogel, 2015).

### 1.4.3. Biological Role of SEVs

Upon discovery, SEVs were thought to be just another way the cell excretes junk. It was only in past decades that the true function and relevance of SEVs have been explored (Rokad et al., 2019). SEVs are crucial for intercellular communication - transporting proteins, lipids, and RNA between cells (Harischandra et al., 2017). SEVs can be taken up by neighbouring cells to provide autocrine and paracrine signalling or may travel further distances and play a role in endocrine signalling pathways (Zhang & Grizzle, 2014). The involvement of SEVs in cell-to-cell communication was first discovered by Dr. Graca Raposo who in 1996 showed that SEVs containing major histocompatibility complex class II molecules are released by B lymphoblastoid cells, inducing an antigen specific, major histocompatibility complex class II restricted T cell response (Raposo et al., 1996).

Possibly, the main area of SEV application is their use as disease biomarkers and therapeutic delivery agents. Unlike many therapeutic agents, SEVs can cross the blood brain barrier making

them an exciting alternative to traditional drug delivery systems (Iazifar et al., 2016). Furthermore, SEVs can be harvested from potentially any bodily sera and remain stable following isolation. After isolation, different extraction procedures may be implemented to study the protein and messenger RNA content of the SEVs. Traditionally, miRNA has been near impossible to quantify in most sera as they are highly unstable but SEVs appear to protect miRNA allowing for detection (Li et al., 2019). In recent years SEVs have been extensively studied for their roles in cancer progression brought about through oncogenic transformation, chemotherapeutic resistance, and increased cell survival (Bowers et al., 2020).

### 1.4.4. Isolation and Characterization

With interest growing in SEV research many different techniques have emerged to isolate SEVs. The most popular of these techniques include differential ultracentrifugation (dUC), sized based isolation, immunoaffinity capture, SEV precipitation, and microfluidics-based procedures. Despite new techniques emerging, dUC is still considered the gold standard in SEV isolation. Approximately 56% of published SEV studies utilize ultracentrifugation-based isolation methods, making it the most popular and well-defined procedure used today (Li et al., 2017). Risha et al. (2020) found that dUC provided the highest yield of SEV proteins analyzed by nano liquid chromatography-mass spectrometry (nano-LC-MS) given SEV size specificity over ultrafiltration and precipitation-based techniques. Alvarez et al. (2012) also compared isolation methods and found that ultracentrifugation-based techniques produced the highest protein SEV yield without implementing filtration or sucrose cushions. dUC involves several successive rounds of centrifugation to gradually sediment smaller from larger particles and was the isolation technique implemented in the present study. SEVs may be pelleted at forces at or greater than

100,000 g with previous lower force steps key to preventing co-pelleting of SEVs with other cells and large EVs (Li et al., 2017). Following pelleting at 100,000 g a final wash step in phosphate buffer saline (PBS) at 100,000 g is applied to remove any remaining free contaminating proteins and increase the purity of the final SEV pellet (Livshits et al., 2015).

Minimal information for studies of extracellular vesicles (MISEV) provides a series of reporting guidelines produced by leading scientist in the field of EV research. To adequately characterize the size distribution, morphology, and concentration of vesicles, the MISEV2018 recommends the use of two different techniques. Techniques allowing for the visualization of single vesicle morphology include electron microscopy, atomic force microscopy and super-resolution microscope. Other techniques, including nanoparticle tracking analysis (NTA), resistive pulse sensing or flow cytometry, may be implemented to determine vesicle size distribution and concentration (Théry et al., 2018).

## 1.5. Bladder-cancer derived SEVs

### 1.5.1. Invasion and Metastasis

SEVs derived from bladder cancer (BC) cells play a key role in cancer metastasis. Franzen et al. (2016) found that SEVs derived from two muscle-invasive bladder cancer cell lines induced early epithelial-to-mesenchymal transitional changes in primary urothelial cells treated for 4-6 hours. Additionally, urine SEVs isolated from BC patients enhance migration in primary urothelial cells (Franzen et al., 2016). SEVs may also have a role in establishing a pre-metastatic niche even after the surgical and chemotherapeutic intervention to remove tumours. Hiltbrunner

et al. (2020) reported that urinary SEVs derived from patients who had complete removal of macroscopic bladder tumours still housed malignant metabolic phenotypes, proposing the potential for cancer relapse and a reason for the high reoccurrence rates of BC. Understanding the mechanisms of BC metastasis is crucial for therapeutic intervention and controlling relapse. SEVs derived from high-grade BC cells (grade III and IV) can also promote the invasiveness of low-grade BC cells (grade II) as shown in a transwell assay. The same study also determined that high grade BC cell SEVs promoted angiogenesis and migration in human umbilical vein endothelial cells following 4-hour incubation (Beckham et al., 2014b). Yoshida et al. (2019) also found that SEVs derived from high-grade BC cells significantly increased invasive and proliferative properties of low-grade BC cells mediated by PI3K/AKT and FAK pathway upregulation.

### 1.5.2. SEV Bladder Cancer Biomarkers

SEVs have been widely explored for their application in the early identification of bladder cancer. Wang et al. (2020) published a review of the current proposed SEV biomarkers of bladder cancer. The review highlighted six studies that proposed a combined total of 16 bladder cancer-specific biomarkers found in both urine and cell media. Included in these biomarkers were TPP1, TMPRSS2, FOLR1, RALB, RAB35, TACSTD2, mucin-1, CEACAM-5, EPS8L2, moesin, TALDO1, EDIL-3, VIM, HDGF, CK2, and ANXA2. Moreover, five additional SEV purified proteins related to cancer were identified from HT1376 bladder cancer cells (Y. Wang et al., 2020). Welton et al., (2010) successfully verified soluble (hnRNPK and $\beta$-catenin) and membrane-associated (galectin-3, basigin, and CD73) proteins from HT1376 cells using western blot and flow cytometry techniques. In another study examining proteins in urine, nine other

proteins were found to be differentially expressed in the SEVs of bladder cancer patients (Smalley et al., 2008). A full list of SEV-derived proteins associated with bladder cancer is presented in **Table 1.1** which is adapted from the review conducted by Wang et al. (2020).

**Table 1.1.** Summary of studies examining SEV biomarkers of bladder cancer using a proteomics approach.

| Candidate Biomarker(s) | Sample(s) | Isolation Method | Proteomics Method | Results | Reference |
|---|---|---|---|---|---|
| TPP1, TMPRSS2, **FOLR1**, RALB, RAB35 | Urine/ureter: histologically downstaged BCa (n = 9) | dUC/F | Label-free | 1094 proteins identified; 40 significantly overexpressed in bladder urine; FOLR1 was validated by western blot. | (Hiltbrunner et al., 2020) |
| **TACSTD2** | Urine:<br>Discovery- BCa (n = 13), control (n = 9)<br>Verification - BCa (n = 28), control (n = 12)<br>Validation- BCa (n=140), control (n=81) | dUC | Dimethyl-labeling | 2,964 proteins identified; 24 were differentially expressed; TACSTD2 was validated by ELISA. | Chen et al., 2012 |
| **mucin-1, CEACAM-5, EPS8L2, moesin** | Urine: Bca (n = 10), controls (n = 10) | dUC | Label-free | 1,222 proteins identified; 56 proteins significantly increased in Bca; 4 validated by western blot. | Lee et al., 2018 |
| ANXA7, S100A4, HEXB, SND1, and **TALDO1** | Urine: BCa (n=6), control (n=6)<br>Cell media: MIBC (n = 51), normal urothelium (n = 79), and non-MIBC (n = 71) | dUC | Label-free | 719 proteins identified; 5 proteins significantly upregulated in MIBC and non-MIBC; TALDO1 validated by immunohistology chemistry in bladder tissues. | Silvers, Miyamoto, Messing, George, & Lee, 2017 |
| **EDIL-3** | Cell media: T24, TCC-SUP, and SVHUC1<br>Urine: BCa (n=12), controls (n=12) | dUC/F | Label-free | 453 proteins identified; EDIL-3 validated in BCa patient urine by western blot. | Beckham et al., 2014 |
| VIM, HDGF, CK2, ANXA2 | Cell media: isogenic metastatic BCa lines (SLT4 and FL3) and nonmetastatic cell line (T24) | dUC | iTRAQ | >1000 and >500 proteins identified in membrane and lumen fractions of exosome, respectively. | Jeppesen et al., 2014 |
| Nras, EPS8L1, **EPS8L2**, **Mucin 4**, EH Domain-containing Protein 4GsGTP, RAI3, resistin and G3BP | Urine: BCa (n=4), controls (n=5) | dUC | Label-free | 170 proteins identified with a spectral count >2. 9 were differentially expressed, 8 proteins were increased in Bca group while 1 was decreased (G3BP); EPS8L2 and Mucin 4 were validated by SDS-PAGE (n=2) | Smalley, Sheman, Nelson, & Theodorescu, 2008 |
| **Galectin-3, basigin, CD73, hnRNPK, $\beta$-catenin** | Cell media: BCa lines HT1376, HT1197, RT4, RT112, and T24. Main analysis was conducted using HT1376 cells.<br>Urine: BCa (n=3); controls (n=4) | dUC | Label-free | 353 proteins identified; 72 proteins novel to exosomes; Validation of 18 proteins by western blot. Only proteins related to BCa are reported. | Welton et al., 2010 |

BCa: Bladder Cancer; dUC: differential ultracentrifugation; UC/F: Ultracentrifugation/filtration; MICB: Muscle invasive bladder cancer; iTRAQ: Isobaric tags for relative and absolute quantification. **Bolded** proteins are those that were validated by a second targeted method.

## 1.6. Proteomics in SEV Research

Proteomics has become a facet of SEV exploratory research, with mass spectrometry being a foundational technique for the identification and characterization of SEV protein cargo. SEV proteomics has been used to study numerous diseases, including neurodegenerative, pulmonary, urological, and cardiovascular diseases, along with an array of cancers. A typical mass spectrometry-based proteomics workflow includes the isolation of SEVs from a biological fluid, extraction of SEV proteins using a detergent or non-detergent lysis buffer, and the separation of proteins and digestion prior to loading in the mass spectrometer. Proteomics is a particularly useful tool for non-targeted biomarker discovery as it enables the study of thousands of proteins simultaneously, providing information regarding the pathways and processes up and downregulated during disease (Mallia et al., 2020). A study employing label-free quantitative proteomics coupled with a novel machine learning method determined that four SEV proteins (ANXA5, VGF nerve growth factor inducible, glycoprotein MGA, and alpha-1 antichymotrypsin protein) could identify Alzheimer's Disease with 88% accuracy (Muraoka et al., 2020). Furthermore, it was found that elevated levels of ANAX5 were associated with the stage of disease severity and progression (Muraoka et al., 2020). Sundar et al. (2019) conducted a pilot study analyzing the plasma SEV proteome of smokers and individuals with chronic obstructive pulmonary disease and found several novel proteins including FN1, apolipoprotein D, and clusterin differentially enriched in their study groups. They concluded that SEVs were a rich source of novel biomarkers for the prognostic, diagnostic and therapeutic investigation of chronic obstructive pulmonary disease and the contribution of cigarette smoke exposure (Sundar et al., 2019). Proteomic investigation of urine SEVs collected from patients with renal cell carcinoma led to the development of a 10-protein panel that could accurately and reproducibly

differentiate renal cell carcinoma from control individuals (Raimondo et al., 2014). Ceruloplasmin and podocalyxin-like protein 1 were upregulated in renal cell carcinoma and showed high diagnostic potentials with area under the curve (AUC) values of 1. Proteins upregulated in renal cell carcinoma including dickkopf WNT signalling pathway inhibitor 4 (AUC = 0.979), matrix metallopeptidase 9 (AUC = 0.938), and extracellular matrix metallopeptidase inducer (AUC = 0.879) also had high diagnostic potential (Raimondo et al., 2014).

## 1.7. Rational and Research Objectives

Although arsenic is a legacy compound that we have been researching the effects of for decades, it is still regarded as the most significant chemical contaminant in drinking water sources globally (World Health Organization, 2018). Depending on geographical location, water sources, and proximity to industrial practices such as gold mining individuals may be at an elevated risk of the numerous adverse effects of arsenic exposure, including bladder cancer. For these groups, it is pivotal that their health and exposure is closely monitored in as minimally invasive a way as possible. An emerging technique in health monitoring and exposure science has been the study of SEVs. To determine the application of SEVs as biomarkers, it is important to first decipher the effect arsenic has on SEVs and the potential roles SEVs play during exposure. As discussed previously, SEVs are critical mediators in the tumour microenvironment and in the promotion of carcinogenesis (Franzen et al., 2016; Hiltbrunner et al., 2020; Beckham et al., 2014; Yoshida et al., 2019). The effect of arsenic exposure on SEV response has only been measured in a handful of studies all of which examined either bronchial epithelial, prostate, liver, or embryonic stem cell exposure with no studies detailing the response on any organs of the urinary tract (Bain et

al., 2016; Chen et al., 2017; Dai et al., 2018, 2019; Li et al., 2021; Ngalame et al., 2018; Xu et al., 2015). As urothelial cells line the urethra, bladder, ureters, and renal pelvis and as 95% of all bladder cancers begin in the uroepithelium, it is critical to decipher the SEV response in urothelial cells following arsenic exposure (Burger et al., 2017). This novel investigation can help lay the foundation for the study of SEVs in toxicology and provide insight into the still widely elusive mechanisms underlying arsenic induced bladder cancer.

Considering this gap of research, my master's thesis project sought to determine if SEVs are responsible for mediating toxic response signaling during arsenic exposure and if SEVs can be used as early biomarkers of urothelial injury. To address this question, it is vital to understand both the biological changes that occur in SEVs during arsenic exposure and the applications of SEVs as biomarkers for human health risk assessment. Specifically, I hypothesize first that the biology and protein packaging profile of urothelial SEVs are altered following arsenic exposure because of the induction of cell stress signaling pathways. I also hypothesize that urinary SEV proteins can be used as biomarkers of arsenic exposure because they are positively correlated with urinary arsenic concentrations in an exposed population.

To test these hypotheses, this thesis has the following specific objectives:

1. Characterize the effect of arsenic exposure on the number of total SEVs released to determine if cells respond by increasing intracellular signaling.
2. Assess the pattern of protein expression in SEVs released by arsenic-exposed cells to investigate whether they are core proteins involved in cancer-related pathways.

3. Investigate the changes in intracellular proteomics following arsenic exposure to determine how the packaged protein profiles differ between the SEVs and their parent cells.
4. Measure the SEV derived biomarkers identified in the *in vitro* study in the urine samples collected from an arsenic-exposed population and investigate the correlation with urinary arsenic concentrations to establish their applicability as novel biomarkers.

Objectives 1 and 2 are presented in Chapter 2. Objective 3 is presented in Chapter 3, and Objective 4 is presented in Chapter 4.

## 1.8 References


Alvarez, M. L., Khosroheidari, M., Kanchi Ravi, R., & Distefano, J. K. (2012). Comparison of protein, microRNA, and mRNA yields using different methods of urinary exosome isolation for the discovery of kidney disease biomarkers. *Kidney International*, *82*(9), 1024–1032. https://doi.org/10.1038/ki.2012.256

Ahmad, S. A., Khan, M. H., & Haque, M. (2018). Arsenic contamination in groundwater in Bangladesh: implications and challenges for healthcare policy. *Risk Management and Healthcare Policy*, *11*, 251. https://doi.org/10.2147/RMHP.S153188

Baastrup, R., Sørensen, M., Balstrøm, T., Frederiksen, K., Larsen, C. L., Tjønneland, A., Overvad, K., & Raaschou-Nielsen, O. (2008). Arsenic in drinking-water and risk for cancer in Denmark. *Environmental Health Perspectives*, *116*(2), 231–237. https://doi.org/10.1289/ehp.10623

Bagchi, S. (2007). Arsenic threat reaching global dimensions. *CMAJ*, *177*(11), 1344–1345. https://doi.org/10.1503/CMAJ.071456b

Bain, L. J., Liu, J., & League, R. E. (2016). Arsenic inhibits stem cell differentiation by altering the interplay between the Wnt3a and Notch signaling pathways. *Toxicology Reports*, *3*, 405–413. https://doi.org/10.1016/j.toxrep.2016.03.011

Bates, M. N., Rey, O. A., Biggs, M. L., Hopenhayn, C., Moore, L. E., Kalman, D., Steinmaus, C., & Smith, A. H. (2004). Case-Control Study of Bladder Cancer and Exposure to Arsenic in Argentina. *American Journal of Epidemiology*, *159*(4), 381–389. https://doi.org/10.1093/aje/kwh054

Beckham, C. J., Olsen, J., Yin, P., Wu, C., Ting, H., Hagen, F. K., Scosyrev, E., Messing, E. M., & Lee, Y. (2014). Bladder Cancer Exosomes Contain EDIL-3 / Del1 and Facilitate Cancer Progression. *Journal of Urology*, *192*(2), 583–592. https://doi.org/10.1016/j.juro.2014.02.035

Boffetta, P., & Borron, C. (2019). Low-Level Exposure to Arsenic in Drinking Water and Risk of Lung and Bladder Cancer: A Systematic Review and Dose-Response Meta-Analysis. *Dose-Response: A Publication of International Hormesis Society*, *17*(3), 1559325819863634–1559325819863634. https://doi.org/10.1177/1559325819863634

Bowers, E. C., Hassanin, A. A. I., & Ramos, K. S. (2020). Toxicology in Vitro In vitro models of exosome biology and toxicology: New frontiers in biomedical research. *Toxicology in Vitro*, *64*(October 2019), 104462. https://doi.org/10.1016/j.tiv.2019.02.016

Bozack, A. K., Hall, M. N., Liu, X., Ilievski, V., Lomax-Luu, A. M., Parvez, F., Siddique, A. B., Shahriar, H., Uddin, M. N., Islam, T., Graziano, J. H., & Gamble, M. V. (2019). Folic acid supplementation enhances arsenic methylation: results from a folic acid and creatine supplementation randomized controlled trial in Bangladesh. *The American Journal of Clinical Nutrition*, *109*(2), 380–391. https://doi.org/10.1093/ajcn/nqy148

Burger, M., Capoun, O., Cohen, D., Babjuk, M., Bo, A., Herna, V., Kaasinen, E., Palou, J., Roupre, M., Compe, E. M., Rhijn, B. W. G. Van, Shariat, S. F., Soukup, V., Sylvester, R. J., & Zigeuner, R. (2017). EAU Guidelines on Non – Muscle-invasive Urothelial Carcinoma of the Bladder : Update 2016. *European Urology*, *71*, 447–461. https://doi.org/10.1016/j.eururo.2016.05.041

Campion, S., Aubrecht, J., Boekelheide, K., Brewster, D. W., Vaidya, V. S., Anderson, L., Burt, D., Dere, E., Hwang, K., Pacheco, S., Saikumar, J., Schomaker, S., Sigman, M., & Goodsaid, F. (2013). The current status of biomarkers for predicting toxicity. *Expert Opinion on Drug Metabolism & Toxicology*, *9*(11), 1391–1408. https://doi.org/10.1517/17425255.2013.827170

Chen, C., Luo, F., Liu, X., Lu, L., Xu, H., & Yang, Q. (2017). *NF-kB-regulated exosomal miR-155 promotes the in fl ammation associated with arsenite carcinogenesis*. *388*. https://doi.org/10.1016/j.canlet.2016.11.027

Chen, C.-L., Chiou, H.-Y., Hsu, L.-I., Hsueh, Y.-M., Wu, M.-M., Wang, Y.-H., & Chen, C.-J. (2010). Arsenic in Drinking Water and Risk of Urinary Tract Cancer: A Follow-up Study from Northeastern Taiwan. *Cancer Epidemiology Biomarkers &Amp; Prevention*, *19*(1), 101 LP – 110. https://doi.org/10.1158/1055-9965.EPI-09-0333

Chen, S.-J., Yan, X.-J., & Chen, Z. (2013). Arsenic in Tissues, Organs, and Cells. *Encyclopedia of Metalloproteins*, 135–138. https://doi.org/10.1007/978-1-4614-1533-6_491

Chen, Y.-C., Su, H.-J. J., Guo, Y.-L. L., Hsueh, Y.-M., Smith, T. J., Ryan, L. M., Lee, M.-S., & Christiani, D. C. (2003). Arsenic methylation and bladder cancer risk in Taiwan. *Cancer Causes & Control*, *14*(4), 303–310. https://doi.org/10.1023/A:1023905900171

Chiou, H.-Y., Chiou, S.-T., Hsu, Y.-H., Chou, Y.-L., Tseng, C.-H., Wei, M.-L., & Chen, C.-J. (2001). Incidence of Transitional Cell Carcinoma and Arsenic in Drinking Water: A Follow-up Study of 8,102 Residents in an Arseniasis-endemic Area in Northeastern Taiwan. *American Journal of Epidemiology*, *153*(5), 411–418. https://doi.org/10.1093/aje/153.5.411

Chu, H.-A., & Crawford-Brown, D. (2007). Inorganic Arsenic in Drinking Water and Bladder Cancer: A Meta-Analysis for Dose-Response Assessment. *International Journal of Environmental Research and Public Health*, *4*(4), 340–341.

Chung, J. Y., Yu, S. do, & Hong, Y. S. (2014). Environmental Source of Arsenic Exposure. *Journal of Preventive Medicine and Public Health*, *47*(5), 253. https://doi.org/10.3961/JPMPH.14.036

Crenshaw, B. J., Gu, L., Sims, B., & Matthews, Q. L. (2018). Exosome Biogenesis and Biological Function in Response to Viral Infections. *The Open Virology Journal*, *12*(1), 134–148. https://doi.org/10.2174/1874357901812010134

Dai, X., Chen, C., Xue, J., Xiao, T., Mostofa, G., Wang, D., Chen, X., Xu, H., Sun, Q., Li, J., Wei, Y., & Chen, F. (2019). Exosomal MALAT1 derived from hepatic cells is involved in the activation of hepatic stellate cells via miRNA-26b in fi brosis induced by arsenite. *Toxicology Letters*, *316*(April), 73–84. https://doi.org/10.1016/j.toxlet.2019.09.008

Dai, X., Chen, C., Yang, Q., Xue, J., Chen, X., Sun, B., Luo, F., & Liu, X. (2018). Exosomal circRNA _ 100284 from arsenite- transformed cells, via microRNA-217 regulation of EZH2, is involved in the malignant transformation of human hepatic cells by accelerating the cell cycle and promoting cell proliferation. *Cell Death and Disease*, 1–14. https://doi.org/10.1038/s41419-018-0485-1

Elkkin, S.R., Lakoduk, A.M., Schmid, S. L. (2017). Endocytic Pathways and Endosomal Trafficking: A Primer. *Wien Med Wochenschr*, *166*(7–8), 196–204. https://doi.org/10.1007/s10354-016-0432-7.Endocytic

EPA. (2022, May 12). *Exposure Assessment Tools by Approaches - Exposure Reconstruction (Biomonitoring and Reverse Dosimetry)*. https://www.epa.gov/expobox/exposure-assessment-tools-approaches-exposure-reconstruction-biomonitoring-and-reverse

Fischer, J. M., Robbins, S. B., Al-Zoughool, M., Kannamkumarath, S. S., Stringer, S. L., Larson, J. S., Caruso, J. A., Talaska, G., Stambrook, P. J., & Stringer, J. R. (2005). Co-mutagenic activity of arsenic and benzo[a]pyrene in mouse skin. *Mutation Research/Genetic Toxicology and Environmental Mutagenesis*, *588*(1), 35–46. https://doi.org/https://doi.org/10.1016/j.mrgentox.2005.09.003

Flora, S. J. S. (2015). Arsenic: Chemistry, Occurrence, and Exposure. *Handbook of Arsenic Toxicology*, 1–49. https://doi.org/10.1016/B978-0-12-418688-0.00001-0

Franzen, C. A., Blackwell, R. H., Foreman, K. E., Kuo, P. C., Flanigan, R. C., & Gupta, G. N. (2016). Review Article Urinary Exosomes: The Potential for Biomarker Utility, Intercellular Signaling

and Therapeutics in Urological Malignancy. *Journal of Urology*, *195*(5), 1331–1339. https://doi.org/10.1016/j.juro.2015.08.115

Hall, M. N., & Gamble, M. V. (2012). Nutritional manipulation of one-carbon metabolism: effects on arsenic methylation and toxicity. *Journal of Toxicology*, *2012*, 595307. https://doi.org/10.1155/2012/595307

Harding, C., Stahl, P. (1983). Transferrin Recycling in Reticulocytes: pH and Iron Are Important Determinants of Ligand Binding and Processing. *Biochemical and Biophysical Research Communications*, *113*(2), 650–658.

Harischandra, D. S., Ghaisas, S., Rokad, D., & Kanthasamy, A. G. (2017). *Exosomes in Toxicology: Relevance to Chemical Exposure and Pathogenesis of Environmentally Linked Diseases*. *158*(1), 3–13. https://doi.org/10.1093/toxsci/kfx074

Hartwig, A., Asmuss, M., Ehleben, I., Herzer, U., Kostelac, D., Pelzer, A., Schwerdtle, T., & Bürkle, A. (2002). Interference by toxic metal ions with DNA repair processes and cell cycle control: molecular mechanisms. *Environmental Health Perspectives*, *110*, 797–799. https://doi.org/10.1289/ehp.02110s5797

Health Canada. (2022). *Arsenic - Canada.ca*. Retrieved February 7, 2022, from https://www.canada.ca/en/health-canada/services/food-nutrition/food-safety/chemical-contaminants/environmental-contaminants/arsenic.html

Hiltbrunner, S., Michael, M., Eldh, M., Rosenblatt, R., Holmström, B., Alamdari, F., Johansson, M., Veerman, R. E., Winqvist, O., Sherif, A., & Gabrielsson, S. (2020). Urinary Exosomes from Bladder Cancer Patients Show a Residual Cancer Phenotype despite Complete Pathological Downstaging. *Nature*, *10*, 1–10. https://doi.org/10.1038/s41598-020-62753-x

Howe, P., Hughes, M., Kenyon, E., Lewis, D. R., Moore, M., Ng, J., Aitio, A., & Becking, G. (2001). Environmental Health Criteria 224 ARSENIC AND ARSENIC COMPOUNDS Second edition. *World Health Organization Geneva*.

Huang, Y.-K., Pu, Y.-S., Chung, C.-J., Shiue, H.-S., Yang, M.-H., Chen, C.-J., & Hsueh, Y.-M. (2008). Plasma folate level, urinary arsenic methylation profiles, and urothelial carcinoma susceptibility. *Food and Chemical Toxicology*, *46*(3), 929–938. https://doi.org/https://doi.org/10.1016/j.fct.2007.10.017

IARC. (2004). *Arsenic and Arsenic Compounds*. https://monographs.iarc.who.int/wp-content/uploads/2018/06/mono100C-6.pdf

IARC. (2012). *Arsenic, Metals, Fibres, And Dusts: IARC Monographs on the Evaluation of Carcinogenic Risks to Humans*. https://www.ncbi.nlm.nih.gov/books/NBK304375/pdf/Bookshelf_NBK304375.pdf

Iazifar, M. I. R., Arhoodi, H. E. P. F., Hang, S. H. X. Z., Imak, J. A. N. Z., Ude, A. S. E., One, E. G. J. P., & Hao, W. E. Z. (2016). *Elucidation of Exosome Migration Across the Blood – Brain Barrier Model In Vitro*. *9*(4), 509–529. https://doi.org/10.1007/s12195-016-0458-3

Jadli, A. S., Ballasy, N., Edalat, P., & Patel, V. B. (2020). Inside(sight) of tiny communicator: exosome biogenesis, secretion, and uptake. *Molecular and Cellular Biochemistry*, *467*(1–2), 77–94. https://doi.org/10.1007/s11010-020-03703-z

Jha, A. N., Noditi, M., Nilsson, R., & Natarajan, A. T. (1992). Genotoxic effects of sodium arsenite on human cells. *Mutation Research*, *284*(2), 215–221. https://doi.org/10.1016/0027-5107(92)90005-M

Jomova, K., Jenisova, Z., Feszterova, M., Baros, S., Liska, J., Hudecova, D., Rhodes, C. J., & Valko, M. (2011). Arsenic: toxicity, oxidative stress and human disease. *Journal of Applied Toxicology*, *31*(2), 95–107. https://doi.org/10.1002/JAT.1649

Jones, L. B., Bell, C. R., Bibb, K. E., Gu, L., Coats, M. T., & Matthews, Q. L. (2018). Pathogens and their effect on exosome biogenesis and composition. *Biomedicines*, *6*(3). https://doi.org/10.3390/biomedicines6030079

Kitai, Y., Kawasaki, T., Sueyoshi, T., Kobiyama, K., Ishii, K. J., Zou, J., Akira, S., Matsuda, T., & Kawai, T. (2017). DNA-Containing Exosomes Derived from Cancer Cells Treated with Topotecan Activate a STING-Dependent Pathway and Reinforce Antitumor Immunity. *The Journal of Immunology*, *198*(4), 1649–1659. https://doi.org/10.4049/jimmunol.1601694

Koutros, S., Baris, D., Waddell, R., Beane Freeman, L. E., Colt, J. S., Schwenn, M., Johnson, A., Ward, M. H., Hosain, G. M. M., Moore, L. E., Stolzenberg-Solomon, R., Rothman, N., Karagas, M. R., & Silverman, D. T. (2018). Potential effect modifiers of the arsenic–bladder cancer risk relationship. *International Journal of Cancer*, *143*(11), 2640–2646. https://doi.org/https://doi.org/10.1002/ijc.31720

Kurttio, P., Pukkala, E., Kahelin, H., Auvinen, A., & Pekkanen, J. (1999). Arsenic concentrations in well water and risk of bladder and kidney cancer in Finland. *Environmental Health Perspectives*, *107*(9), 705–710. https://doi.org/10.1289/ehp.99107705

Lamm, S. H., Boroje, I. J., Ferdosi, H., & Ahn, J. (2021). A review of low-dose arsenic risks and human cancers. *Toxicology*, *456*, 152768. https://doi.org/https://doi.org/10.1016/j.tox.2021.152768

Lee-Chen, S. F., Gurr, J. R., Lin, I. B., & Jan, K. Y. (1993). Arsenite enhances DNA double-strand breaks and cell killing of methyl methanesulfonate-treated cells by inhibiting the excision of alkali-labile sites. *Mutation Research/DNA Repair*, *294*(1), 21–28. https://doi.org/10.1016/0921-8777(93)90054-K

Li, J., Xue, J., Ling, M., Sun, J., Xiao, T., Dai, X., Sun, Q., Cheng, C., Xia, H., Wei, Y., Chen, F., & Liu, Q. (2021). MicroRNA-15b in extracellular vesicles from arsenite-treated macrophages

promotes the progression of hepatocellular carcinomas by blocking the LATS1-mediated Hippo pathway. *Cancer Letters*, *497*(May 2020), 137–153. https://doi.org/10.1016/j.canlet.2020.10.023

Li, P., Kaslan, M., Lee, S. H., Yao, J., & Gao, Z. (2017). Progress in Exosome Isolation Techniques. *Theranostics*, *7*(3). https://doi.org/10.7150/thno.18133

Li, X., Corbett, A. L., Little, J. P., & Garnis, C. (2019). *Challenges and opportunities in exosome research — Perspectives from biology, engineering, and cancer therapy*. *011503*, 1–21. https://doi.org/10.1063/1.5087122

Lin, J., Li, J., Huang, B., Liu, J., Chen, X., Chen, X. M., Xu, Y. M., Huang, L. F., & Wang, X. Z. (2015). Exosomes: Novel Biomarkers for Clinical Diagnosis. *Scientific World Journal*, *2015*. https://doi.org/10.1155/2015/657086

Liu, L., Trimarchi, J. R., Navarro, P., Blasco, M. A., & Keefe, D. L. (2003). Oxidative Stress Contributes to Arsenic-induced Telomere Attrition, Chromosome Instability, and Apoptosis. *Journal of Biological Chemistry*, *278*(34), 31998–32004. https://doi.org/10.1074/JBC.M303553200

Liu, Y.-R., Silver, C., & Lee, Y.-F. (2015). Exosome as biomarkers and diagnostics in bladder cancer. *Cancer Research*, *75*(15 SUPPL. 1). https://doi.org/http://dx.doi.org/10.1158/1538-7445.AM2015-548

Livshits, M. A., Khomyakova, E., Evtushenko, E. G., & Laz, V. N. (2015). Isolation of exosomes by differential centrifugation: Theoretical analysis of a commonly used protocol. *Nature Publishing Group*, 1–14. https://doi.org/10.1038/srep17319

Luster, M. I., & Simeonova, P. P. (2004). Arsenic and urinary bladder cell proliferation. *Toxicology and Applied Pharmacology*, *198*(3), 419–423. https://doi.org/10.1016/J.TAAP.2003.07.017

Mallia, A., Gianazza, E., Zoanni, B., Brioschi, M., Barbieri, S. S., & Banfi, C. (2020). Proteomics of Extracellular Vesicles: Update on Their Composition, Biological Roles and Potential Use as Diagnostic Tools in Atherosclerotic Cardiovascular Diseases. *Diagnostics (Basel, Switzerland)*, *10*(10). https://doi.org/10.3390/DIAGNOSTICS10100843

Marsit, C. J., Karagas, M. R., Danaee, H., Liu, M., Andrew, A., Schned, A., Nelson, H. H., & Kelsey, K. T. (2006). Carcinogen exposure and gene promoter hypermethylation in bladder cancer. *Carcinogenesis*, *27*(1), 112–116. https://doi.org/10.1093/CARCIN/BGI172

Martinez, V. D., Vucic, E. A., Becker-Santos, D. D., Gil, L., & Lam, W. L. (2011). Arsenic Exposure and the Induction of Human Cancers. *Journal of Toxicology*, *2011*, 13. https://doi.org/10.1155/2011/431287

McGuigan, C. F., Hamula, C. L. A., Huang, S., Gabos, S., & Le, X. C. (2010). A review on arsenic concentrations in Canadian drinking water. *Environmental Reviews*, *18*(1), 291–308. https://doi.org/10.1139/A10-012

Meakin, C. J., Martin, E. M., & Fry, R. C. (2017). Epigenetic mechanisms underlying arsenic-induced toxicity. *Current Opinion in Toxicology*, *6*, 1–9. https://doi.org/10.1016/J.COTOX.2017.06.003

Meliker, J. R., Slotnick, M. J., & Avruskin, G. A. (2010). *Lifetime exposure to arsenic in drinking water and bladder cancer: a population-based case – control study in Michigan, USA*. 745–757. https://doi.org/10.1007/s10552-010-9503-z

Ming Tam, L., Price, N. E., & Wang, Y. (2020). Molecular Mechanisms of Arsenic-Induced Disruption of DNA Repair. *Chem. Res. Toxicol*, *2020*, 709–726. https://doi.org/10.1021/acs.chemrestox.9b00464

Mink, P. J., Alexander, D. D., Barraj, L. M., Kelsh, M. A., & Tsuji, J. S. (2008). Low-level arsenic exposure in drinking water and bladder cancer: A review and meta-analysis. *Regulatory Toxicology and Pharmacology*, *52*(3), 299–310. https://doi.org/https://doi.org/10.1016/j.yrtph.2008.08.010

Mohammed Abdul, K. S., Jayasinghe, S. S., Chandana, E. P. S., Jayasumana, C., & de Silva, P. M. C. S. (2015). Arsenic and human health effects: A review. *Environmental Toxicology and Pharmacology*, *40*(3), 828–846. https://doi.org/10.1016/J.ETAP.2015.09.016

Montermini, L., Meehan, B., Garnier, D., Lee, W. J., Lee, T. H., Guha, A., Al-Nedawi, K., & Rak, J. (2015). Inhibition of oncogenic epidermal growth factor receptor kinase triggers release of exosome-like extracellular vesicles and impacts their phosphoprotein and DNA content. *Journal of Biological Chemistry*, *290*(40), 24534–24546. https://doi.org/10.1074/jbc.M115.679217

Moore, L. E., Smith, A. H., Eng, C., Kalman, D., DeVries, S., Bhargava, V., Chew, K., Moore, D., Ferreccio, C., Rey, O. A., & Waldman, F. M. (2002). Arsenic-related chromosomal alterations in bladder cancer. *Journal of the National Cancer Institute*, *94*(22), 1688–1696. https://doi.org/10.1093/JNCI/94.22.1688

Mostafa, M. G., & Cherry, N. (2015). Arsenic in Drinking Water, Transition Cell Cancer and Chronic Cystitis in Rural Bangladesh. In *International Journal of Environmental Research and Public Health*, *12(11)*. https://doi.org/10.3390/ijerph121113739

Muraoka, S., DeLeo, A. M., Sethi, M. K., Yukawa-Takamatsu, K., Yang, Z., Ko, J., Hogan, J. D., Ruan, Z., You, Y., Wang, Y., Medalla, M., Ikezu, S., Chen, M., Xia, W., Gorantla, S., Gendelman, H. E., Issadore, D., Zaia, J., & Ikezu, T. (2020). Proteomic and biological profiling of extracellular vesicles from Alzheimer's disease human brain tissues. *Alzheimer's & Dementia*, *16*(6), 896–907. https://doi.org/10.1002/ALZ.12089

Naranmandura, H., Carew, M. W., Xu, S., Lee, J., Leslie, E. M., Weinfeld, M., & Le, X. C. (2011). Comparative Toxicity of Arsenic Metabolites in Human Bladder Cancer EJ-1 Cells. *Chem. Res. Toxicol*, *24*. https://doi.org/10.1021/tx200291p

National Research Council (US) Subcommittee on Arsenic in Drinking Water. (1999). Arsenic in Drinking Water. *National Academies Press*. https://www.ncbi.nlm.nih.gov/books/NBK230898/

Ngalame, N. N. O., Luz, A. L., Makia, N., & Tokar, E. J. (2018). Arsenic Alters Exosome Quantity and Cargo to Mediate Stem Cell Recruitment Into a Cancer Stem Cell-Like Phenotype. *Toxicological Sciences*, *165*(1), 40. https://doi.org/10.1093/TOXSCI/KFY176

Nordberg, G. F. (2010). Biomarkers of exposure, effects and susceptibility in humans and their application in studies of interactions among metals in China. *Toxicology Letters*, *192*(1), 45–49. https://doi.org/10.1016/J.TOXLET.2009.06.859

Pan, B. T., & Johnstone, R. M. (1983). Fate of the transferrin receptor during maturation of sheep reticulocytes in vitro: Selective externalization of the receptor. *Cell*, *33*(3), 967–978. https://doi.org/10.1016/0092-8674(83)90040-5

Patrick, L. (2003). Toxic Metals and Antioxidants: Part II. The Role of Antioxidants in Arsenic and Cadmium Toxicity. *Alternative Medicine Review*, 106–128.

Piper, R. C., & Katzmann, D. J. (2007). Biogenesis and Function of Multivesicular Bodies. *Annual Review of Cell and Developmental Biology*, *23*, 519-547. https://doi.org/10.1146/annurev.cellbio.23.090506.123319

Raimondo, F., Corbetta, S., Chinello, C., Pitto, M., & Magni, F. (2014). The urinary proteome and peptidome of renal cell carcinoma patients: A comparison of different techniques. *Expert Review of Proteomics*, *11*(4), 503–514. https://doi.org/http://dx.doi.org/10.1586/14789450.2014.926222

Raposo, G., Nijman, H. W., Stoorvogel, W., Leijendekker, R., Harding, C. V., Melief, C. J. M., & Geuze, H. J. (1996). B lymphocytes secrete antigen-presenting vesicles. *Journal of Experimental Medicine*, *183*(3), 1161–1172. https://doi.org/10.1084/jem.183.3.1161

Risha, Y., Minic, Z., Ghobadloo, S. M., & Berezovski, M. V. (2020). The proteomic analysis of breast cell line exosomes reveals disease patterns and potential biomarkers. *Scientific Reports*, 1–12. https://doi.org/10.1038/s41598-020-70393-4

Rokad, D., Jin, H., Anantharam, V., Kanthasamy, A., & Kanthasamy, A. G. (2019). Exosomes as Mediators of Chemical-Induced Toxicity Exosomes as Mediators of Chemical-Induced Toxicity. *Current Environmental Health Reports*, *6*, 73-79. https://doi.org/10.1007/s40572-019-00233-9

Rosen, B. P., & Liu, Z. (2009). Transport pathways for arsenic and selenium: a minireview. *Environment International*, *35*(3), 512–515. https://doi.org/10.1016/J.ENVINT.2008.07.023

Shao, K., Zhou, Z., Xun, P., & Cohen, S. M. (2021). Bayesian benchmark dose analysis for inorganic arsenic in drinking water associated with bladder and lung cancer using epidemiological data. *Toxicology*, *455*, 152752. https://doi.org/https://doi.org/10.1016/j.tox.2021.152752

Shen, H., Niu, Q., Xu, M., Rui, D., Xu, S., Feng, G., Ding, Y., Li, S., & Jing, M. (2016). Factors Affecting Arsenic Methylation in Arsenic-Exposed Humans: A Systematic Review and Meta-Analysis. *International Journal of Environmental Research and Public Health*, *13*(2), 205. https://doi.org/10.3390/ijerph13020205

Shen, S., Lee, J., Weinfeld, M., & Le, X. C. (2008). Attenuation of DNA damage-induced p53 expression by arsenic: A possible mechanism for arsenic co-carcinogenesis. *Molecular Carcinogenesis*, *47*(7), 508–518. https://doi.org/https://doi.org/10.1002/mc.20406

Shurtleff, M. J., Temoche-Diaz, M. M., Karfilis, K. V., Ri, S., & Schekman, R. (2016). Y-box protein 1 is required to sort microRNAs into exosomes in cells and in a cell-free reaction. *ELife*, *5*,1–23. https://doi.org/10.7554/eLife.19276

Shurtleff, M. J., Yao, J., Qin, Y., Nottingham, R. M., Temoche-Diaz, M. M., Schekman, R., & Lambowitz, A. M. (2017). Broad role for YBX1 in defining the small noncoding RNA composition of exosomes. *Proceedings of the National Academy of Sciences of the United States of America*, *114*(43), E8987–E8995. https://doi.org/10.1073/pnas.1712108114

Singh, A. A., Goel, R., & Kaur, T. (2011). Mechanisms pertaining to arsenic toxicity. *Toxicology International*, *18*(2).

Smalley, D. M., Sheman, N. E., Nelson, K., & Theodorescu, D. (2008). Isolation and Identification of Potential Urinary Microparticle Biomarkers of Bladder Cancer research articles. *Journal of Proteome Research*, 2088–2096. https://doi.org/10.1021/pr700775x

Smith, A. H., Marshall, G., Roh, T., Ferreccio, C., Liaw, J., & Steinmaus, C. (2018). Lung, Bladder, and Kidney Cancer Mortality 40 Years After Arsenic Exposure Reduction. *JNCI Journal of the National Cancer Institute*, *110*(3), 241. https://doi.org/10.1093/JNCI/DJX201

Soung, Y. H., Ford, S., Zhang, V., & Chung, J. (2017). Exosomes in Cancer Diagnostics. *Cancers*, *9*(8). https://doi.org/10.3390/cancers9010008

Steinmaus, C. M., Ferreccio, C., Romo, J. A., Yuan, Y., Cortes, S., Marshall, G., Moore, L. E., Balmes, J. R., Liaw, J., Golden, T., & Smith, A. H. (2013). Drinking Water Arsenic in Northern Chile: High Cancer Risks 40 Years after Exposure Cessation. *Cancer Epidemiology Biomarkers &Amp; Prevention*, *22*(4). https://doi.org/10.1158/1055-9965.EPI-12-1190

Steinmaus, C., Yuan, Y., Bates, M. N., & Smith, A. H. (2003). Case-Control Study of Bladder Cancer and Drinking Water Arsenic in the Western United States. *American Journal of Epidemiology*, *158*(12), 1193–1201. https://doi.org/10.1093/aje/kwg281

Stoorvogel, W. (2015). Resolving sorting mechanisms into exosomes. *Cell Research*, *25*, 531-532. https://doi.org/10.1038/cr.2015.39

Stuffers, S., Sem Wegner, C., Stenmark, H., & Brech, A. (2009). Multivesicular endosome biogenesis in the absence of ESCRTs. *Traffic*, *10*(7), 925–937. https://doi.org/10.1111/j.1600-0854.2009.00920.x

Sundar, I. K., Li, D., & Rahman, I. (2019). Proteomic Analysis of Plasma-Derived Extracellular Vesicles in Smokers and Patients with Chronic Obstructive Pulmonary Disease. *ACS Omega*, *4*(6), 10649–10661. https://doi.org/10.1021/ACSOMEGA.9B00966/SUPPL_FILE/AO9B00966_SI_001.ZIP

Tchounwou, P. B., Centeno, J. A., & Patlolla, A. K. (2004). Arsenic toxicity, mutagenesis, and carcinogenesis – a health risk assessment and management approach. *Molecular and Cellular Biochemistry*, *255*, 47–55.

Théry, C., Witwer, K. W., Aikawa, E., Alcaraz, M. J., Anderson, J. D., Andriantsitohaina, R., Antoniou, A., Arab, T., Archer, F., Atkin-Smith, G. K., Ayre, D. C., Bach, J. M., Bachurski, D., Baharvand, H., Balaj, L., Baldacchino, S., Bauer, N. N., Baxter, A. A., Bebawy, M., … Zuba-Surma, E. K. (2018). Minimal information for studies of extracellular vesicles 2018 (MISEV2018): a position statement of the International Society for Extracellular Vesicles and update of the MISEV2014 guidelines. *Journal of Extracellular Vesicles*, *7*(1). https://doi.org/10.1080/20013078.2018.1535750

Tsuji, J. S., Alexander, D. D., Perez, V., & Mink, P. J. (2014). Arsenic exposure and bladder cancer: Quantitative assessment of studies in human populations to detect risks at low doses. *Toxicology*, *317*, 17–30. https://doi.org/https://doi.org/10.1016/j.tox.2014.01.004

Villarroya-Beltri, C., Gutiérrez-Vázquez, C., Sánchez-Cabo, F., Pérez-Hernández, D., Vázquez, J., Martin-Cofreces, N., Martinez-Herrera, D. J., Pascual-Montano, A., Mittelbrunn, M., & Sánchez-Madrid, F. (2013). Sumoylated hnRNPA2B1 controls the sorting of miRNAs into exosomes through binding to specific motifs. *Nature Communications*, *4*, 1–10. https://doi.org/10.1038/ncomms3980

Wang, Y., Shi, T., Srivastava, S., Kagan, J., Liu, T., & Rodland, K. D. (2020). Proteomic Analysis of Exosomes for Discovery of Protein Biomarkers for Prostate and Bladder Cancer. *Cancers*, *12*.

Welton, J. L., Khanna, S., Giles, P. J., Brennan, P., Brewis, I. A., Staffurth, J., Mason, M. D., & Clayton, A. (2010). Proteomics Analysis of Bladder Cancer. *Molecular and Cellular Proteomics*, *9*, 1324–1338. https://doi.org/10.1074/mcp.M000063-MCP201

Wiencke, J. K., & Yager, J. W. (1992). Specificity of arsenite in potentiating cytogenetic damage induced by the DNA crosslinking agent diepoxybutane. *Environmental and Molecular Mutagenesis*, *19*(3), 195–200. https://doi.org/10.1002/EM.2850190303

World Health Organization (WHO). (2018). Arsenic. https://www.who.int/news-room/fact-sheets/detail/arsenic

Xu, Y., Luo, F., Liu, Y., Shi, L., & Lu, X. (2015). Exosomal miR - 21 derived from arsenite - transformed human bronchial epithelial cells promotes cell proliferation associated with arsenite carcinogenesis. *Archives of Toxicology*, 1071–1082. https://doi.org/10.1007/s00204-014-1291-x

Yoshida, K., Tsuda, M., Matsumoto, R., Semba, S., Wang, L., Sugino, H., Tanino, M., Kondo, T., Tanabe, K., & Tanaka, S. (2019). Exosomes containing ErbB2/CRK induce vascular growth in premetastatic niches and promote metastasis of bladder cancer. *Cancer Science*, *110*(7), 2119–2132. https://doi.org/10.1111/cas.14080

Yu, R. C., Hsu, K.-H., Chen, C.-J., & Froines, J. R. (2000). Arsenic Methylation Capacity and Skin Cancer. *Cancer Epidemiology Biomarkers*, *9*(11).

Zhang, H. G., & Grizzle, W. E. (2014). Exosomes: A Novel Pathway of Local and Distant Intercellular Communication that Facilitates the Growth and Metastasis of Neoplastic Lesions. *The American Journal of Pathology*, *184*(1), 28. https://doi.org/10.1016/J.AJPATH.2013.09.027

Zhang, Y., Liu, Y., Liu, H., & Tang, W. H. (2019). Exosomes: Biogenesis, biologic function and clinical potential. *Cell and Bioscience*, *9*(1), 1–18. https://doi.org/10.1186/s13578-019-0282-2

# Chapter 2: Investigating the role of SEVs in arsenic induced urothelial injury and cancer related pathways

Nicole Washuck[1], Yingxi Li[2], Zoran Minic[3], Emmanuel Yumvihoze[1], and Hing Man Chan[1]

[1]Department of Biology, University of Ottawa, Ottawa, Ontario, Canada

[2]Department of Chemistry and Biomolecular Sciences, University of Ottawa, Ottawa, Ontario, Canada

[3]John L. Holmes Mass Spectrometry Facility, University of Ottawa, Ottawa, Ontario, Canada

***Author Contributions***

Nicole Washuck: conceptualization, methodology, sample collection and preparation, data analysis, and manuscript preparation

Yingxi Li and Zoran Minic: sample preparation and mass spectrometry

Emmanuel Yumvihoze: chemical analysis

Hing Man Chan: conceptualization

## 2.1. Introduction

In recent years, small extracellular vesicles (SEVs) have been shown to be vital in intracellular communication and have been used in clinical studies as biomarkers of disease (Harischandra et al., 2017). Despite the importance of SEVs in cell signalling and the tumour microenvironment there are very few toxicology studies examining their role during chemical exposure. Of these studies, seven have examined the response of SEVs during arsenic exposure. Cumulatively it was found that SEVs released from cells following arsenic exposure are responsible for promoting a cancer-like phenotype, cell proliferation and can induce pro-inflammatory properties in recipient cells (Bain et al., 2016; Chen et al., 2017; Dai et al., 2018, 2019a; Li et al., 2021; Ngalame et al., 2018; Xu et al., 2015). Following chronic arsenic exposure Dai et al. (2018) found that human liver cells released circRNA_100284 in SEVs, which promoted malignant transformation of cells, accelerating the cell cycle, and promoting proliferation in healthy liver cells exposed to the SEVs. Similarly, Ngalame et al. (2018) found that the SEVs of arsenic transformed prostate epithelial cells are enriched with pro-oncogenic factors capable of recruiting stem cells to a cancer-like phenotype. Enhanced cell growth following exposure to SEVs derived from arsenic exposed cells was also noted in two other studies examining human liver and bronchial epithelial cells (Dai et al., 2019a; Xu et al., 2015). Furthermore, SEVs of arsenic transformed liver cells were found to transfer miR-55 to healthy cells, where miR-55 was then able to initiate immune responses (Chen et al., 2017). Overall, from the cited literature it is apparent that SEVs serve a variety of roles during arsenic exposure, but this relationship has only been assessed in a small number of cell types. The exact mechanisms by which arsenic may induce bladder cancer remain to be fully deciphered and the role SEVs play in cell signalling during exposure has never been assessed. SEVs may present a missing link in our understanding

of early response signalling that given chronic exposure can lead to the development of bladder cancer. With evidence that SEVs play a role in the adverse effects of arsenic exposure, and with the global need for early indicators of arsenic induced urological changes, we investigated whether arsenic could change the biology of SEVs released by exposed urothelial cells. To do this, we evaluated the proteomic changes in SEVs released from urothelial cells following a range of arsenic exposures as well as assessing the changes in size, concentration, and functionality of the SEVs released.

## 2.2. Methods

### 2.2.1. Cell Selection and Culturing

Urothelial cells were selected for analysis as urothelial carcinomas, also known as transitional cell carcinomas (TCC), account for approximately 90% of all bladder cancers (Welton et al., 2010). SVHUC1 human urothelial cells are derived from healthy ureter tissue from an 11 year old male that was immortalized with SV40 virus. SVHUC1 urothelial cells (ATCC® CRL-9520™) were selected for study as they have previously been used in the analysis of arsenic toxicity (Jou et al., 2019; X. Liu et al., 2012; Q. Zhou et al., 2018) and produced quantifiable numbers of SEVs (Yang et al., 2021; H. Zheng et al., 2021). In addition, T24 urothelial carcinoma cells (ATCC® HTB-4™) were selected as a positive control for carcinogenicity to compare the effects of arsenic exposure to. T24 cells were established from a high grade invasive 81 year old female bladder cancer patient and their SEV release and cargo have been widely studied (Jou et al., 2019; F. Lin et al., 2020; Whitehead et al., 2015). SVHUC1 cells were maintained in Kaighan's modification of Ham's F-12 medium (ATCC® 30-2004™) and T24

cells were maintained in McCoy's 5a medium modified (ATCC® 30-2007™). Both medias were supplemented with 10% Fetal Bovine Serum (Sigma-Aldrich, F1051). Cells were grown in 175 $cm^3$ tissue culture treated flasks (Montreal Biotech, MBI709001C) and were incubated at 37℃ with 5% $CO_2$. Cell media was changed every 3-4 days.

## 2.2.2. Arsenic Exposure

### *2.2.2.1. Cytotoxicity Testing*

To determine the optimal arsenic exposure concentrations that resulted in low cell death, cytotoxicity tests were conducted. Three separate passages of SVHUC1 cells were exposed to different concentrations of sodium arsenite (Sigma-Aldrich, S7400-100G) (400, 200, 100, 80, 40, 20, 10, 8, 4, 2, 1, 0.5 $\mu M$) for 48 hours. Cytotoxicity was assessed in four technical replicates of each concentration and 8 technical replicates of each SVHUC1 control. Cell viability was then assessed by incubating for another two hours with CellTiter 96® AQueous One Solution Cell Proliferation Assay and detecting absorbance at 490nm on the Cytation3 Cell Imaging Multimode Reader. The absorbance values for all four replicates were averaged and the background absorbance from the control wells were subtracted. The cell viability was then plotted as a percent of the control against the log concentration of arsenic in Rstudio using *drc* and *ggplot* packages and the dose response curves for each passage were fitted following a goodness of fit test with multiple models.

### *2.2.2.2. Experimental Exposure*

To reduce exposure variability between biological replicates primary (100,000 $\mu M$) and secondary (1,000 $\mu M$) stocks of sodium arsenite were made and kept for up to 6 and 3 months, respectfully. Primary stock was made by dissolving sodium arsenite in milliQ with 0.5%

hydrochloric acid (Fluka Analytical, 84415-500ML). The secondary stock was a dilution of the primary stock made in milliQ. The secondary stock was used to spike media prior to cell exposure. Flasks of SVHUC1 cells were exposed to 0, 1, 2, or 5 $\mu M$ sodium arsenite in EV depleted media for 48 hours. Exposures were repeated for three different biological replicates each with two 175cm$^3$ flask per treatment. A 2 mL sample of exposure media was kept at each exposure (n = 12) for quantification of arsenic content and speciation. All stock solutions and exposure media samples were stored at 4℃ in falcon tubes wrapped in tinfoil and double sealed in Ziplock bags to minimize oxidation.

#### *2.2.2.3. Arsenic Speciation Measurement by ICP-MS*

To report on the actual concentration of arsenic in each spiked media sample, cell media arsenic concentrations were analyzed using inductively coupled plasma mass spectrometry (ICP-MS) (770x ICP-MS, Agilent Technologies, Mississauga, ON). For arsenic speciation ($As^{III}$, $As^{V}$, MMA, DMA, and arsenobetaine (AsB)), samples were diluted in 10 m$M$ ammonium phosphate dibasic (Sigma, 37998-100G) prepared in milli-Q water and pH adjusted to 8.25 with ammonium hydroxide solution 28% (Sigma, 338818-100 mL). Arsenic species were measured with an Agilent 1200 Infinity Liquid Chromatography (LC) coupled to an Agilent 7700x ICP-MS (Agilent Technologies, Mississauga, ON). The limit of detection (LOD) for arsenic species was 0.005 $\mu g/L$ and concentrations under the LOD were replaced with half the LOD (Cheung et al., 2020).

### 2.2.3. SEV Isolation

Once cells reached 50-60% confluence, flasks were washed three times with PBS and incubated for 48 hours in EV free media containing the desired exposure of sodium arsenite. To prevent

background EV contamination from fetal bovine serum, EV free media was produced by diluting fetal bovine serum to 25% in media (McCoy's 5A or F-12) and ultra-centrifuging at 100,000 g for 21 hours (SW28 Ti rotor, Beckman Coulter). EV depleted fetal bovine serum in media was then filtered through 0.22 $\mu M$ sterile filters (Millipore, SLFG025LS) prior to use.

#### *2.2.3.1. Cell Media Differential Ultracentrifugation (dUC)*

Following 48-hour incubation, vesicle enriched media (30 mL) was harvested from flasks. Cells were washed once in 5 mL PBS which was then added to the media collections to ensure collection of all surface bound EVs. Media was centrifuged at 300 g for 10 minutes, then at 2,000 g for 20 minutes (SW2150, Heraeus Sepatech) prior to storage at -80C in 50 mL polypropylene conical centrifuge tubes (FroggaBio, TB50-25) for later SEV isolation. Vesicle enriched media was stored for a maximum of one month before being thawed overnight at 4℃ and subjected to differential centrifugation (dUC) (**Figure 2.1**). Previous 2,000 g centrifugation was repeated for 20 minutes, and pellets were discarded. The following centrifugation was carried out in a Beckman Coulter Optima XL-100K Ultracentrifuge at 4℃. The supernatant was centrifuged at 16,500 g for 30 minutes. Pellets were discarded and the supernatant was centrifuged at 100,000 g for 2 hours (SW28 Ti rotor, Beckman Coulter) to pellet SEVs. The SEV pellet was resuspended in 2.5 mL cold PBS following the 100,000 g spin. Resuspended SEVs from the two technical replicates within each biological replicate were then composited for the final wash spin. The collected SEVs were washed at 100,000 g for 1 hour (SWFF Ti rotor, Beckman Coulter) and resuspended in 120 $\mu L$ cold PBS for SEV analysis.

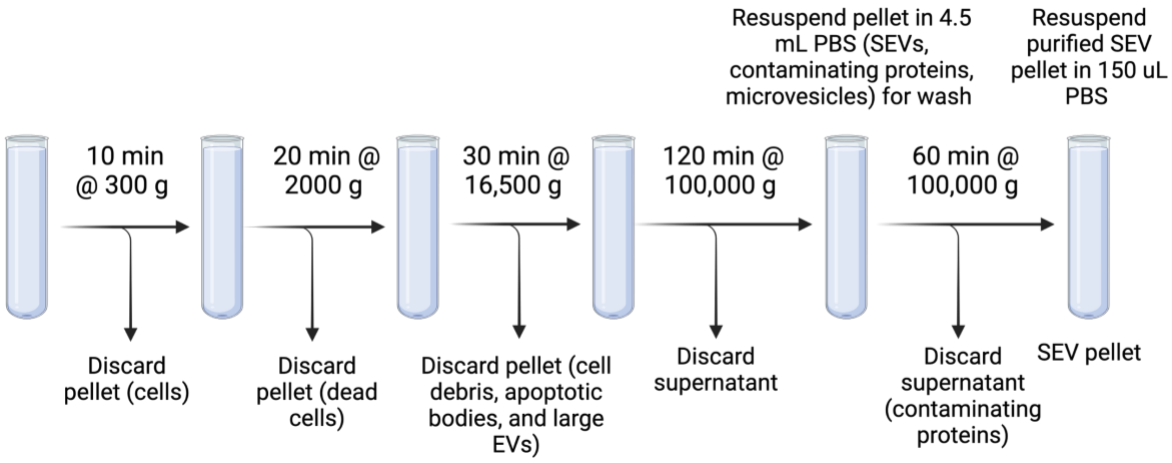


**Figure 2.1.** Method of differential ultracentrifugation for cell media SEV isolation. Created with BioRender.com.

## 2.2.4. Cell Counting

Cells were harvested and counted following each exposure to later quantify the number of SEVs released per cell in different treatment groups. Cells were digested in 0.25% trypsin-ethylenediaminetetraacetic acid (Gibco, 25200-056), and resuspended in 10 mL media for cell counting. A 10 $\mu L$ aliquot of cell suspension was then taken and mixed with 10 $\mu L$ trypan blue stain (Gibco, 15250-061) for dead cell staining. Alive and dead cells were then counted manually using a hemocytometer and the average of all four squares was used to report the total cells in each experimental flask.

## 2.2.5. SEV Characterization

### *2.2.5.1. Nanoparticle Tracking Analysis*

Nanoparticle tracking analysis was used to characterize the size and number of SEVs produced from each treatment. 2:1000 dilutions of samples in PBS were run through the ZetaView nanoparticle microscope PMS-110 (Particle Matrix) for determination of SEV concentration and

size distribution. For analysis the size detection range was set from 10-500 nm and the minimum brightness was set to 15. 102 nm polystyrene beads (Microtrac, 900383) were used to focus the instrument and sample size distribution was detected at 85 and 40 camera shutter speeds.

#### *2.2.5.2. Micro Bicinchoninic Acid Assay (microBCA)*

A Micro BCA Protein Assay Kit (Bio Basics SK3061) was used to measure the total protein content of SEV samples. 8 $\mu L$ of sample (unknown, bovine serum albumin (BSA) standard or PBS) was added to 2 $\mu L$ of radioimmunoprecipitation assay (RIPA) buffer (ThermoFischer Scientific, 89900) with dissolved Pierce protease inhibitor mini tablet (ThermoFischer Scientific, A32953) and sonicated three times at 3-minute intervals with intermediate incubation on ice for SEV membrane lysis (Lässer et al., 2012). The samples were then incubated at 60 ℃ for 1 hour. 2 $\mu L$ of sample was then added to Nanodrop 2000 Spectrophotometer (ThermoFischer Scientific, ND-2000) and absorbance was read at a wavelength of 560 nm. PBS was used as the reference buffer and BSA was used to produce the standard curves required for protein content determination. A new standard curve was constructed for each batch of samples analyzed. All samples were analyzed in triplicates and the average protein concentration was reported.

#### *2.2.5.3. Exo-check Antibody Array*

Exo-check antibody arrays (Systems Bioscience, EXORAY200B-4) were used to confirm the origin of SEV populations by detecting eight known SEV markers (CD63, CD81, ALIX, FLOT1, EpCam, ICAM1, ANXA5, and TSG101). Additionally, GM130 cis-Golgi marker was analyzed to determine the extent of cellular contamination in SEV samples. Briefly, 50 $\mu g$ of SEV proteins from T24 and SVHUC1 SEVs were extracted and quantified using the previous microBC method before being loaded onto gel membranes. Antibody staining was conducted in accordance to manufacture instructions (System Biosciences, 2021). Advansta WesternBright

Sirius HRP Substrate (Advansta, K12043-C20) was used to develop the blots. Imaging was done on the UVP ChemStudio PLUS Imaging System, Analytik Jena, with CCD camera and automatic exposure.

### 2.2.6. SEV Cell Proliferation Assay

To determine if SEVs from cancer or arsenic exposed cells mediate cell proliferation, untreated SVHUC1 cells were exposed to SEVs for 48 hours. Three passages of SVHUC1 cells were plated on 96 well plates and incubated overnight to adhere. Cells were then treated with either 2 $\mu L$ of PBS, SEVs isolated from untreated SVHUC1 cells, 5 $\mu M$ treated SVHUC1 cells, or T24 cells. Cells were then incubated for 48 hours. Four technical replicates of each treatment and eight technical replicates of the PBS control were run. Cell proliferation was then assessed using the same methods as the previously conducted cytotoxicity testing. Data were uploaded into R studio and a two-sided students T-Test was run to determine significance between the SEV treatments and the PBS control.

### 2.2.7. In-solution Digestion

For proteomic analysis 100 $\mu L$ of each SEV sample was lysed in solubilization buffer containing 8 M urea, 100 mM HEPES, 10% glycerol, 1uM dithiothreitol, and 0.5% n-dodecyl $\beta$-D-maltoside. 4 $\mu L$ of TCEP was added to reduce samples which were then incubated at 25℃ for 45 minutes on a 400 RPM shaker. Samples were then alkylated by adding 4 $\mu L$ iodoacetamide and incubating again at 25℃ for 50 minutes on a 400 RPM shaker covered with tinfoil. Lastly, proteins were digested by adding 1.5 $\mu L$ of 0.3 $\mu g/\mu L$ trypsin/LysC solution (Trypsin/LyC

Protease mix, ThermoFischer Scientific A41007) to each sample and incubating at 25℃ for 24 hours on a 400 RPM shaker. 1.5 $\mu L$ of formic acid was then added to each sample to quench trypsin and tubes were vortexed at 10,000 g for 30 seconds. Samples were desalted using C18 TopTip (Glygen Corp, TT2C18) columns as per manufactures instructions. Columns were washed three times with 70% acetonitrile in 0.1% formic acid (ThermoFischer Scientific, 85174) and another three times with water in 0.1% formic acid (Fischer Scientific, LS1181). 100 $\mu L$ of sample was then slowly added to each column using a syringe. Columns containing sample were then washed three times with water in 0.1% formic acid. Columns were then transferred to a clean microfuge tube and 50 $\mu L$ of 70% acetonitrile in 0.1% formic acid was added to each column to elute bound peptides. This process was repeated three times to ensure all peptides were eluted. Microfuge tubes containing peptides were then transferred to a SpeedVac centrifuge and run for 2 hours to evaporate remaining acetonitrile solvent. Samples were then ready for analysis by Nano-LC-MS/MS.

### 2.2.8. Nano-LC-MS/MS

Prepared samples were analyzed by an Orbitrap Fusion Mass Spectrometer (Thermo Fischer Scientific) coupled to a Ultimate3000 RLSCnano System (Dionex, Thermo Fischer Scientific). Peptides were separated on a packed column (Polymicro Technology) measuring 15 cm x 70 $\mu$m ID, LunaC18(2), 3$\mu$m, 100 Å (Phenomenex) using a water/acetonitrile/0.1% formic acid gradient. Samples were loaded onto the packed column at a flow rate of 0.30 $\mu$l/min for 105 minutes. For the first 7 minutes peptides were separated using 2% acetonitrile, followed by 70 minutes of a linear gradient from 3 to 38% acetonitrile and 3 minutes from 38-98% acetonitrile, and lastly a 10-minute wash at 2% acetonitrile. Eluted peptides were then sprayed into a mass

spectrometer using positive electrospray ionization at a spray voltage of 2.1 kV and an ion source temperature of 250℃. A resolution of 60 000 was used to obtain full-scan MS spectra and precursor ions were filtered based upon monoisotopic precursor selection, dynamic exclusion (30 s with a ± 10 s ppm window), and charge state (+2 to +7). Automatic gain control setting was set to 1 x $10^4$ for MS/MS and 5 x $10^5$ for Fourier transform MS. Collision-induced dissociation was used to perform fragmentation in the linear ion trap. Finally, precursors were fragmented with a normalized collision energy of 35% using a 2 m/z isolation window.

### 2.2.9. Data Processing and Statistical Analysis

Mass spectrometry raw files were analyzed in MaxQuant for protein identification. Peptides were searched against the UniProt FASTA Human Proteome Database using the integrated Andromeda search engine (Cox et al., 2011). Trypsin protease was set as the type of digestion enzymes used, allowing a maximum of 2 missed cleavage sites. Carbamidomethyl was set as a fixed modification and oxidation and N-terminal acetylation were set as variable modifications. Proteins had a first search peptide tolerance of 20 ppm and a main search peptide tolerance of 10 ppm. A reverse sequence database integrated into MaxQuant was used to determine the false discovery rate (FDR). FDR was set to 1% for peptides with a minimum of 7 amino acids for identification. A contaminants database provided by the Andromeda search engine was used to label and later filter out common contaminants. Label-free protein quantification (LFQ) values were obtained using only unique peptides for analysis. Subsequent data analysis was conducted using LFQ intensities.

### 2.2.10. Bioinformatics Analysis

The protein group file from the MaxQuant output was uploaded to R studio (Version 1.4.1103 © 2009-2021 "Wax Begonia") for bioinformatics. All differential expression analysis was completed using the Bioconductor package DEP 1.17.0 and visualizations were rendered with the ggplot2 package (Smits, 2021). Proteins that matched the contaminates database, were the result of reverse identifications, or were only identified by site were filtered out. Next, proteins were filtered based upon valid values with proteins present in two of three replicates in at least one sample group included in analysis. All remaining proteins were normalized by variance stabilizing normalization to reduce protein samples variance nondependent from their mean intensities and scale samples using parametric transformations and maximum likelihood estimations (Välikangas et al., 2018). Multiple imputation techniques including no imputation, manual imputation, minimum probability imputation, quantile regression imputation of left centered data, and k-nearest neighbor imputation were tested to determine which imputation technique best fit the data based upon missing values, intensity distributions, and differentially expressed protein before and after imputation. Following imputation, differentially expressed proteins were determined based upon a log-fold change of at least 1.5 and an FDR adjusted p-value of 0.05. Gene identifiers, log-fold change, and p-values of all identified proteins were then uploaded to the Qiagen Ingenuity Pathway Analysis (IPA) software for identification of enriched pathways and biological processes. The resulting IPA canonical pathway analysis data was visualized in R studio using the ggplot2 package.

### 2.2.11 Enzyme Linked Immunosorbent Assay Biomarker Validation

Following proteomic investigation and biomarker selection of Transforming Growth Factor Beta Receptor 1 (TGFBR1) and Ribonuclease Inhibitor 1 (RNH1), cell exposures were repeated to harvest another set of SEV samples for biomarker validation. SEV samples were analyzed for TGFBR1(Antibodies-online, ABIN6970804) and RNH1 (ExpressBio, XPEH1611) using Sandwich Enzyme Linked Immunosorbent Assay (ELISA) kits. Prior to analysis SEV samples were mixed with 10% NP-40 buffer (ThermoFischer Scientific, FN0021) and sonicated three times at 3-minute intervals with intermediate incubation on ice for SEV membrane lysis as outlined by Lässer et al., 2012. Preliminarily experiments were conducted to optimize SEV lysis and protein extraction using various concentrations of NP-40 buffer. Samples were analyzed according to the manufacturer's instructions and absorbance was read at a wavelength of 450 nm using a Biotek Cytation 3 imaging reader (BioTek Instrument, Inc.). The lower limit of detection of each kit was 31.25 pg/mL and 0.313 pg/mL for TGFBR1 and RNH1, respectfully. All effect biomarker concentration were converted to $\mu g/L$ for analysis. CurveExpert Professional Version 2.7.3 was used to plot the standard curves of both RNH1 and TGFBR1 as per manufactures recommendations. All possible linear and non-linear regressions were run and the model providing the highest $R^2$ value was selected for each standard curve.

#### *2.2.11.1 Statistical Analysis*

Statistical analysis was performed using R studio (Version 1.4.1103 © 2009-2021 "Wax Begonia"). Association between effect (TGFBR1 and RNH1) and exposure biomarkers were assessed using Welch's t-test. For statistical significance, $\alpha < 0.05$ was used. Box plot analysis was used to assess the differences in effect biomarker expression in SEV samples.

## 2.3. Results

### 2.3.1. Cytotoxicity Tests

The 48-hour cytotoxicity data were similar between all three biological replicates indicating high reproducibility and similar sensitivity between cells of different passages (**Figure 2.2**). A five-parameter log logistic model best fit the data for each passage and the resulting average effective concentration for reducing cell viability by 5, 10, 20, and 50 percent were determined to be 3.2, 4.3, 6.3, and 14.6 $\mu M$ respectfully. Cell proliferation began to decrease at concentrations above 2 $\mu M$ NaAsO2. Based on this data, concentrations of 1, 2 and 5 $\mu M$ were selected for cell dosing in proteomics experiments as these concentrations showed little to no cytotoxicity given acute exposure.

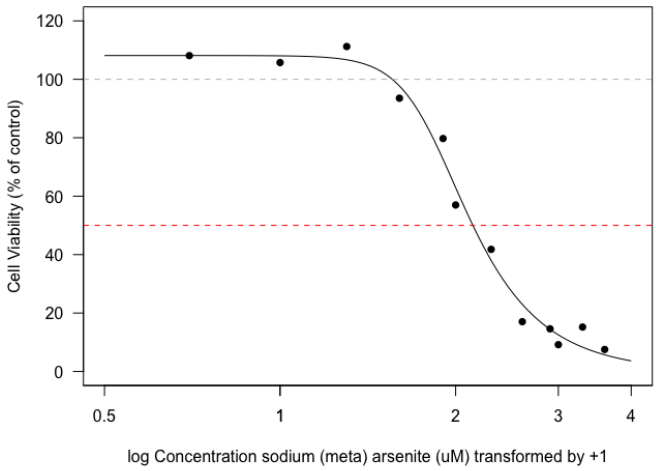


**Figure 2.2.** MTS viability assay of SVHUC-1 urothelial cells exposed to sodium (meta) arsenic (NaAsO2) for 48 hours fitted to a five-parameter log logistics model (biological replicates (n=3), technical replicates (n=4)) with the red line indicating 50% cell viability.

### 2.3.2. Measured Arsenic Exposure Concentrations

The measured concentrations of arsenic determined by ICP-MS were close to the expected concentrations based upon initial dilutions (**Table 2.1**). Less than 6% of arsenic at all concentrations had undergone oxidation to arsenate, meaning that at least 94% of cell exposure was to arsenite.

**Table 2.1.** Measured exposure concentrations of inorganic arsenic in cell media samples.

| **Exposure Group** | **Expected Arsenite Concentration (ug/L)** | **Measured Concentration (ug/L)** | |
|---|---|---|---|
| | | Arsenite ($As^{III}$) | Arsenate ($As^{V}$) |
| **Control** | 0.00 | $0.093 \pm 0.132$ | $0.113 \pm 0.007$ |
| **1 $\mu M$ NaAsO2** | 75.00 | $67.586 \pm 9.764$ | $3.952 \pm 0.524$ |
| **2 $\mu M$ NaAsO2** | 150.00 | $125.408 \pm 10.940$ | $6.971 \pm 0.100$ |
| **5 $\mu M$ NaAsO2** | 375.00 | $304.900 \pm 14.424$ | $14.851 \pm 0.959$ |

### 2.3.3. Nanoparticle Tracking Analysis

Based on an average of three biological replicates T24 SEVs had a median diameter of 110 nm and SVHUC1 SEVs had a median diameter of 90 nm (**Figure 2.3 (A)**). As the size definition of SEVs is between 50-200 nm the EVs harvested from both cell types fit the definition of SEVs (Théry et al., 2018). The mean concentration of SEVs ranged between $1.0 \times 10^9$ to $7.1 \times 10^9$ particles per mL. The concentration of SEVs released per cell was not significantly increased following exposure but was nearly 4 folds higher when comparing T24 SEV concentration to the SVHUC1 control concentration (**Figure 2.3 (B)**).

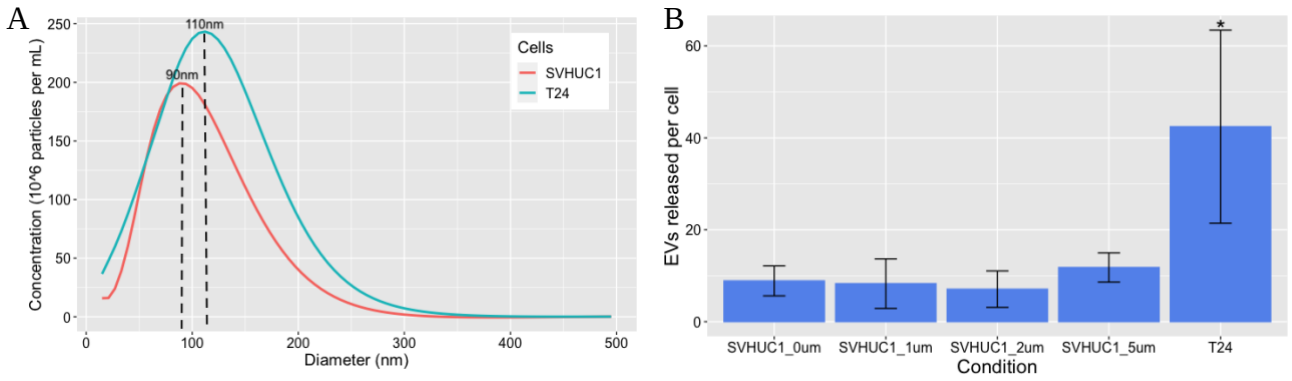


**Figure 2.3.** Nanoparticle tracking analysis results of SEV size and concentration characterization (A) and SEV concentration standardized to the number of cells in each condition (B) (n=3 biological replicates).

## 2.3.4. Exo-check Antibody Array

The results from the Exo-check antibody array analysis can be compared between SEV samples to determine the relative abundance of endosomal proteins but cannot be compared within each blot. Different amounts of protein antibody were used to prepare blots and thus the band intensity between proteins of a given blot is not relevant. Both blots showed the identification of the two positive control bands and no sign of a blank band (**Figure 2.4**). Both blots also showed evidence of cellular contamination indicated by the presence of Golgi matrix protein 130 (GM130). Overall, T24 SEVs showed higher amounts of most endosomal proteins including Flotillin-1 (FLOT1), Intercellular adhesion molecule 1 (ICAM), cluster of differentiation 81 (CD81), tumor susceptibility gene 101 (TSG101), and Annexin A5 (ANXA5). ALG-2-interacting protein X (ALIX) was the only protein marker to show higher abundance in SVHUC1 SEVs with epithelial cellular adhesion molecule (EpCAM) and cluster of differentiation 63 (CD63) showing low abundance in both SEV blots.

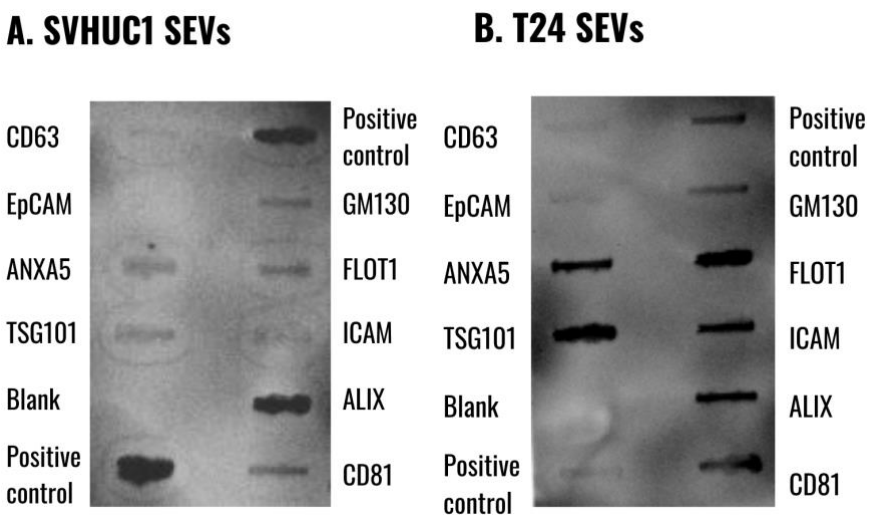


**Figure 2.4.** Exo-check array analysis of SVHUC1 SEVs (A) and T24 SEVs (B) for 8 endosomal proteins (CD63, EpCAM, ANXA5, TSG101, FLOT1, ICAM, ALIX, and CD81) and one cell contamination protein (GM130).

## 2.3.5. Protein Concentration

For the BCA analysis all standard curves had $R^2$ values greater than 0.995 and the average protein concentration and standard deviation is listed in (**Table 2.2**). Overall, SEVs had low protein abundances with relatively high variance between the samples collected. Due to the low protein abundance the entirety of each sample was used for mass spectrometry loading.

**Table 2.2.** micro-BCA analysis of the total protein concentration in cell SEV samples.

| Sample | Average protein in SEVs ($\mu$g/ul) |
|---|---|
| **T24** | $0.0381 \pm 0.0174$ |
| **SVHUC1- Control** | $0.0179 \pm 0.0102$ |
| **SVHUC1- 1 $\mu M$ $NaAsO_2$** | $0.0194 \pm 0.0085$ |
| **SVHUC1- 2 $\mu M$ $NaAsO_2$** | $0.0112 \pm 0.0050$ |
| **SVHUC1- 5 $\mu M$ $NaAsO_2$** | $0.0408 \pm 0.0211$ |

## 2.3.6. SEV Proteomics

### *2.3.6.1. Protein Identification*

A total of 2679 protein identifications were made in MaxQuant and were uploaded to R studio for further filtering. 2443 proteins remained following filtering based upon the contaminants database, reverse identification, and proteins only identified by sites. Following filtering based on proteins present in at least 2 out of 3 replicates in at least one condition 1408 proteins remained for variance stabilizing normalization. From the missing values distribution (**Appendix Figure 2.1**) it is apparent that proteins were missing not at random (MNAR) and that there is a left shift in the missing values (**Appendix Figure 2.2**). Therefore, values needed to be imputated by a left censored imputation method such as quantile regression imputation of left-censored data, minimum probability, or manual imputation. Minimum probability imputation was selected as the differential protein expression pattern was similar between all possible left-censored imputation methods. Principal component analysis (PCA) of the top 500 variable proteins (**Figure 2.5**) displayed clear grouping of the highest exposure groups (5 $\mu M$) and the T24 SEV proteins with similar protein expression in the control, 1 $\mu M$, and 2 $\mu M$ exposure groups. From this analysis it showed that 44.2% of the variance was attributed to PC1, which is closely associated with cell type, and 12.4% was attributed to PC2, which is associated with arsenic exposure.

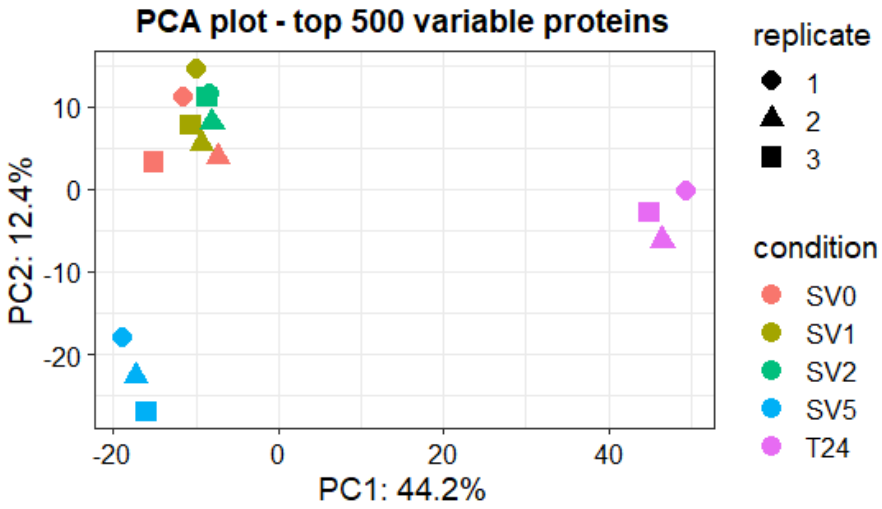


**Figure 2.5.** Unsupervised principal component analysis of the top 500 variable proteins in SEV samples. SV0 = control group, SV1 = 1$\mu M$ $NaAsO_2$ group, SV2 = 2$\mu M$ $NaAsO_2$ group, SV5 = 5$\mu M$ $NaAsO_2$ group, T24 = T24 group.

***2.3.6.2. Statistical Analysis***

Differential expression was assessed based upon significance (adjusted p-value <0.05) and fold change (FC>1.5 or FC<-1.5) which resulted in the identification of 109 differentially expressed proteins (DEPs). The heat map of the DEPs (**Figure 2.6**) corroborated the results of the PCA, showing clear grouping of T24 SEV proteins and of SEV proteins in 5 $\mu M$ arsenite exposure group. From the heatmap there is also clear grouping of the control with similar expression in the 1 $\mu M$ and 2 $\mu M$ exposure groups. Volcano plots displayed DEPs in each condition compared to the control with the most when comparing T24 SEV proteins (74) followed by the 5 $\mu M$ arsenic exposure (34), 2 $\mu M$ arsenic exposure (5), and 1 $\mu M$ arsenic exposure (4) (**Figure 2.7 A-D**). A full list of the up and downregulated DEPs is available in the **Appendix Table 2.1** and **2.2**.

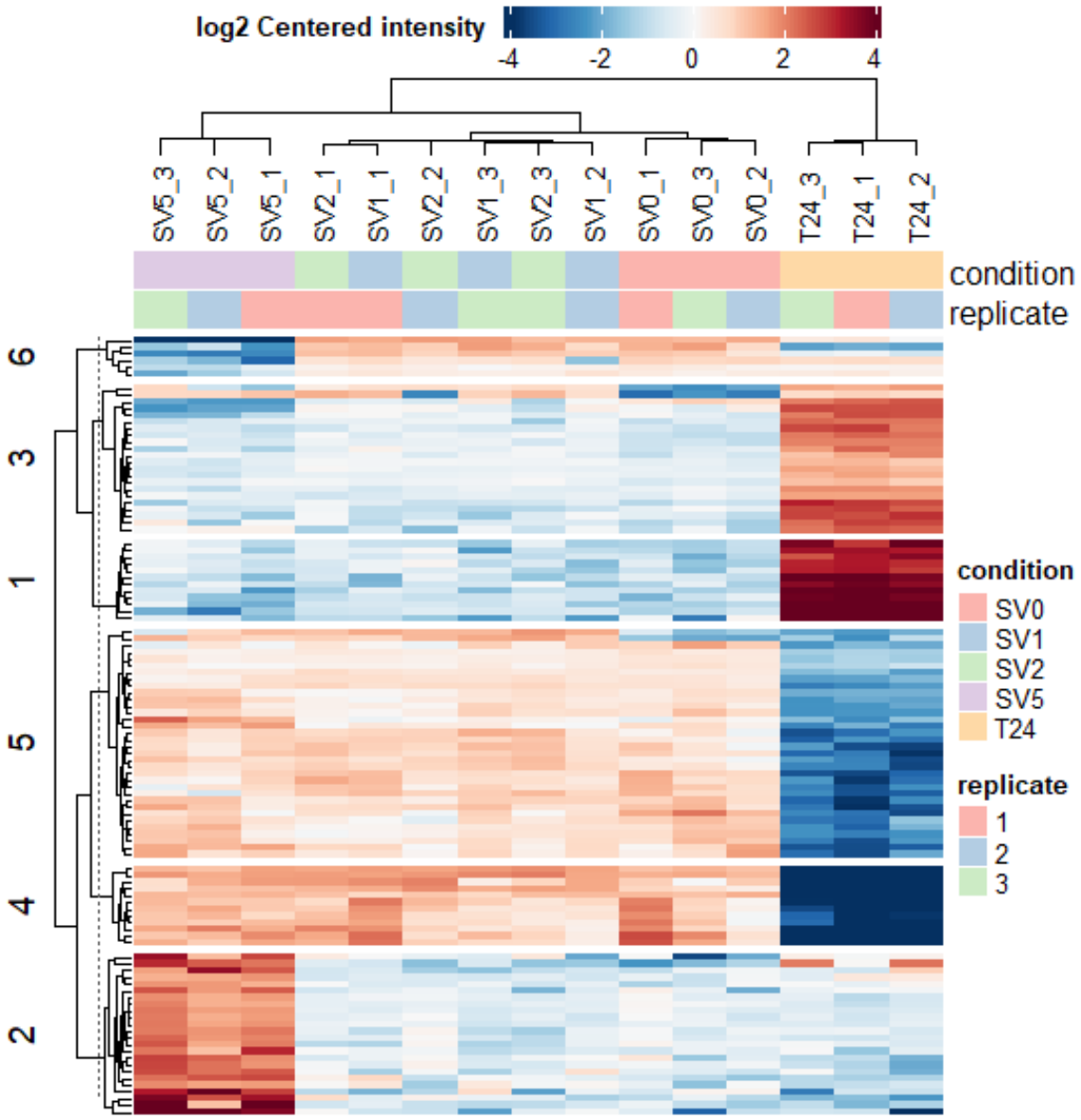


**Figure 2.6.** Heatmap of the 109 differentially expressed proteins (LFC ≥1.5, p-value ≤ 0.05) in SEV samples with hierarchal clustering of condition replicates and proteins. SV0 = control group, SV1 = 1$\mu M$ $NaAsO_2$ group, SV2 = 2$\mu M$ $NaAsO_2$ group, SV5 = 5$\mu M$ $NaAsO_2$ group, T24 = T24 group.

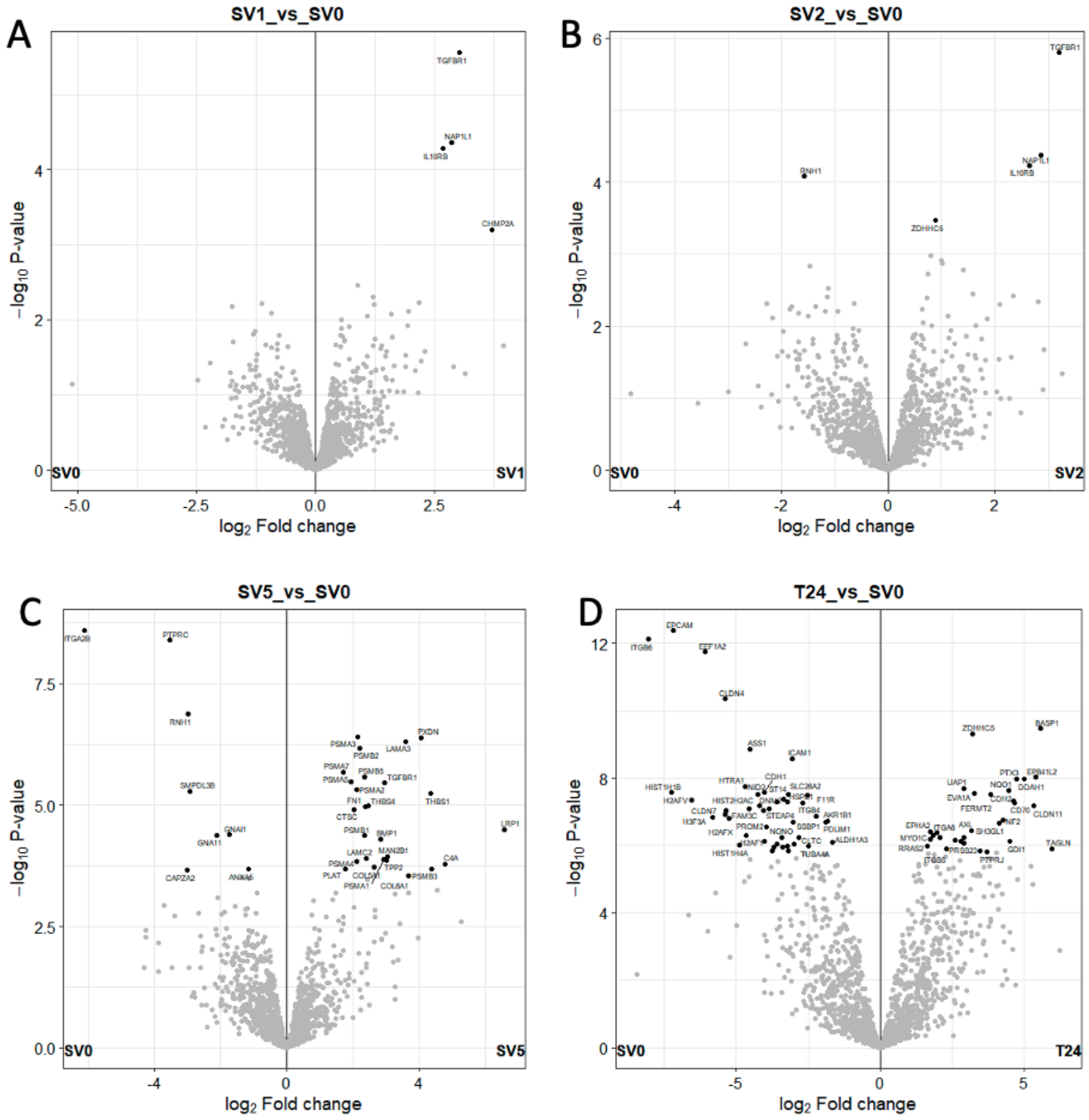


**Figure 2.7.** Volcano plot detailing the differentially expressed proteins (LFC ≥1.5, p-value ≤ 0.05) following 1 $\mu M$ arsenic exposure (A), 2 $\mu M$ arsenic exposure (B), 5 $\mu M$ arsenic exposure (C), and T24 SEVs (D) compared to the SVHUC1 SEV control group.

#### *2.3.6.3. Pathway Analysis of Identified Proteins*

Despite the proteins differentially expressed in T24 urothelial carcinoma SEVs and SEVs collected following arsenic exposure not being the same we wanted to determine if there were similar pathways being up and downregulated in each condition. IPA was used to visualize enriched pathways and biological processes within the 5 $\mu m$ exposure and T24 experimental groups. Pathway analysis could not be conducted for the 1 and 2 $\mu m$ groups as there were not enough proteins differentially expressed. The top pathways and functional annotations were plotted for each group using the R studio ggplot package and the graphical summaries were extracted directly from the IPA platform.

**Canonical Pathway Analysis**

Canonical pathway analysis was conducted in the Ingenuity Knowledge Base and returned three measures of association (1) a p-value of the Fischer's exact test, (2) a ratio of the number of differentially expressed genes in our sample that matched with the pathway divided by the total number of genes in that pathway, and (3) z-score. Z-score indicates the predicted pathway activation (z-score >0) or inactivation (z-score <0). The higher the ratio, the greater the association of genes in our sample to the Ingenuity Knowledge Base. Additionally, the count refers to the total number of differentially expressed genes in our sample that belong to a given pathway. Since z-score could only be determined for a limited number of canonical pathways the present analysis is based on p-value significantly expressed pathways (p-value $\leq 0.05$). The resulting canonical pathway analysis can be found in **Figure 2.8** for arsenic exposure SEVs and **Figure 2.9** for T24 SEVs. In SEVs derived from the 5 $\mu m$ exposure there was an upregulation of 10 proteasomal subunit proteins (PSMA1, PSMA2, PSMA3, PSMA4, PSMA5, PSMA7, PSMB1, PSMB2, PSMB3, and PSMB5), which resulted in the enrichment of canonical pathways

involved in protein ubiquitination and degradation; FAT10 signaling pathway, BAG2 signaling pathway, inhibition of AU-rich elements-mediated messenger RNA degradation pathway, Huntington's disease signaling, and protein ubiquitination pathway. Other enriched pathways of note include those related to wound healing and fibrosis signaling. The differentially expressed proteins related to these pathways include extracellular matrix (ECM) and scaffold proteins including collagen proteins (COL5A1 and COL6A1), fibronectin (FN1), laminin proteins (LAMA3 and LAMC2), and transforming growth factor beta receptor 1 (TGFBR1). Lastly, the cancer related pathways associated with arsenic exposed SEV proteins included molecular mechanisms of cancer and colorectal cancer metastasis signaling. The proteins associated with cancer pathways include guanine nucleotide-binding protein G subunit alpha-1 and 11 (GNAI1 and GNA11), integrin subunit alpha 2b (ITGA2B), LDL receptor related protein 1 (LRP1), and TGFBR1. The main conical pathways enriched in T24 SEVs included those responsible for cancer metastasis and cancer cell signaling. The proteins associated with these pathways were typical biomarkers of cancer including integrin proteins (ITGA6, ITGB4, ITGB5, and ITGB6) and Kirsten rat sarcoma viral proteins (KRAS and RRAS2). Sertoli cell-sertoli cell junction signaling was the pathway with the greatest number of matching proteins including members of the claudin family of proteins (CDH1, CLDN11, CLDN4, and CLDN7).

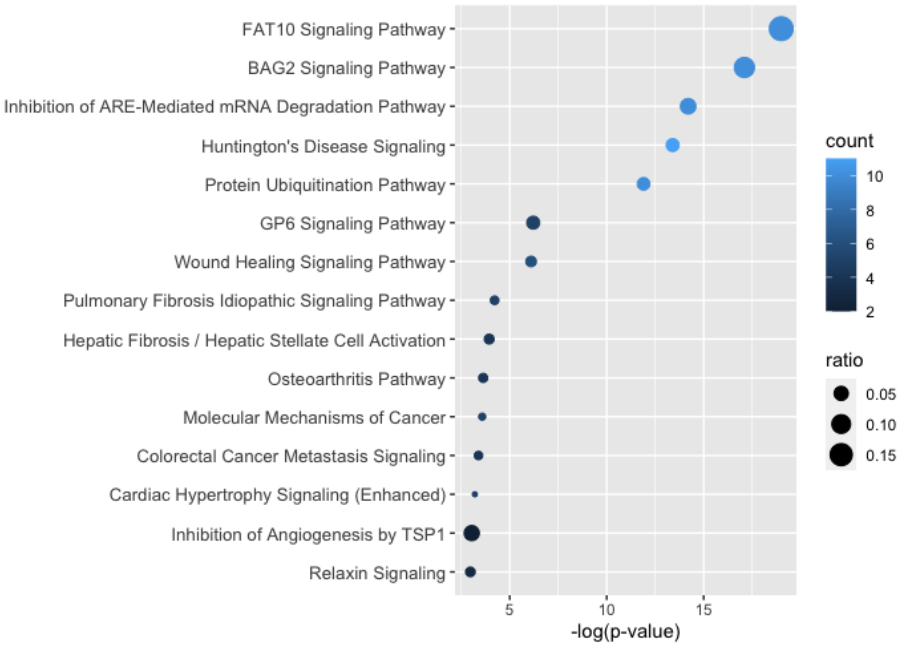


**Figure 2.8.** Canonical pathway analysis of the top 15 pathways significantly (p-value $\leq$ 0.05) associated with 5$\mu$m arsenic exposure SEVs.

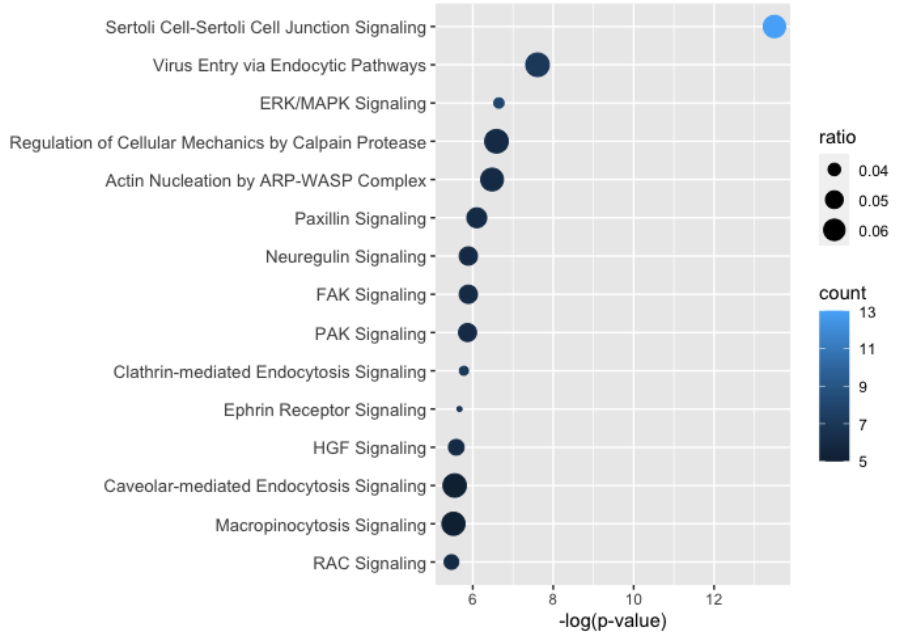


**Figure 2.9.** Canonical pathway analysis of the top 15 pathways significantly (p-value $\leq$ 0.05) associated with T24 SEVs.

**Disease and Functional Annotations**

Next, the disease and functional annotations of the DEPs were analyzed. The z-score as well as the log p-value for each annotation was determined in IPA and plotted to see which functions were up and downregulated. IPA's z-score is used to indicate a predicted inhibition (z-score $\leq 0$) or activation (z-score $\geq 0$) of a disease or function. Typically, a z-score $\geq 2$ or $\leq -2$ and a p-value $< 0.05$ (i.e., -log10 >1.3) reflects significant activation or inhibition (St-Pierre et al., 2013). Here we show all the functional annotations with z-scores $\geq 2$, all of which have p-values $\leq 0.05$. The resulting disease and functional annotations can be found in **Figure 2.10** for arsenic exposure SEVs and **Figure 2.11** for T24 SEVs.

The results of this analysis reveal that arsenic exposure SEVs may serve a functional role in increasing cell survival, migration, and viability and decreasing cell death based on the functions predicted to be activated. 18 of the 34 DEPs were associated with inhibition of necrosis. Additionally, proteasomal subunit genes and others including Laminin subunit alpha 3 (LAMA3), TGFBR1, and thrombospondin 1 (THBS1) that are associated with the inhibition of cancer cell death including malignant and non-malignant tumors and osteosarcoma cells were enriched. Over half of the DEPs were associated with the activation of cell viability, survival, migration, and invasion all of which are early hallmarks of carcinogenesis. The functional and disease annotations with a significant z-score for T24 DEPs showed more advanced stages of functional categories related to carcinogenesis. Two of the highest-ranking z-scores belonged to the invasion of cancer cell lines, this aligns with T24 cells being characterized as a highly invasive and high-grade transitional cell carcinoma line. Over 20 of the DEPs were related to activation of solid tumor or pulmonary metastasis, which is interesting as T24 cells are not

known to have metastatic potential (Jou et al., 2019). There was also activation of several advanced cancers including malignant solid tumor, lung cancer, and extracranial solid tumor. The functional and disease annotations that were predicted to decrease mainly related to inflammation as well as protein metabolism. DEPs derived from arsenic exposed SEVs showed similar activation of invasion and migration when compared to T24 DEPs.

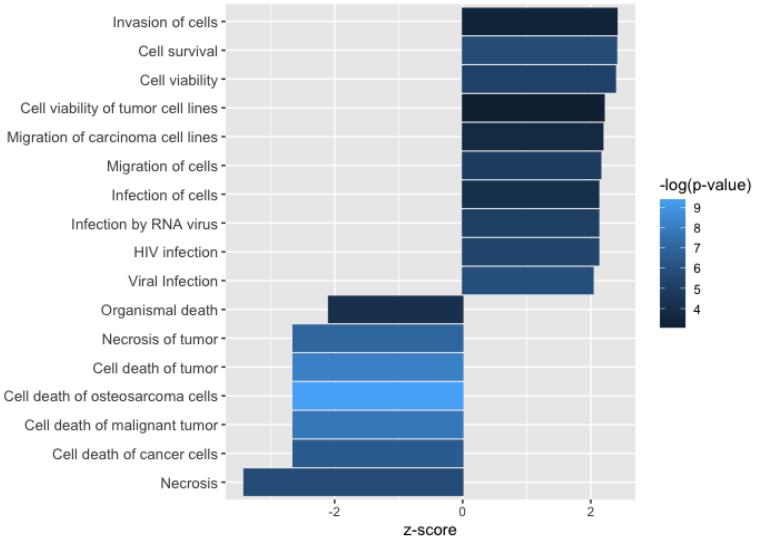


**Figure 2.10.** Analysis of the significant diseases and functions (p-value $\leq$ 0.05) predicted to be activated (z-score $\geq$ 2) or inactivated (z-score $\leq$ -2) in the 5$\mu$m arsenic exposure SEVs.

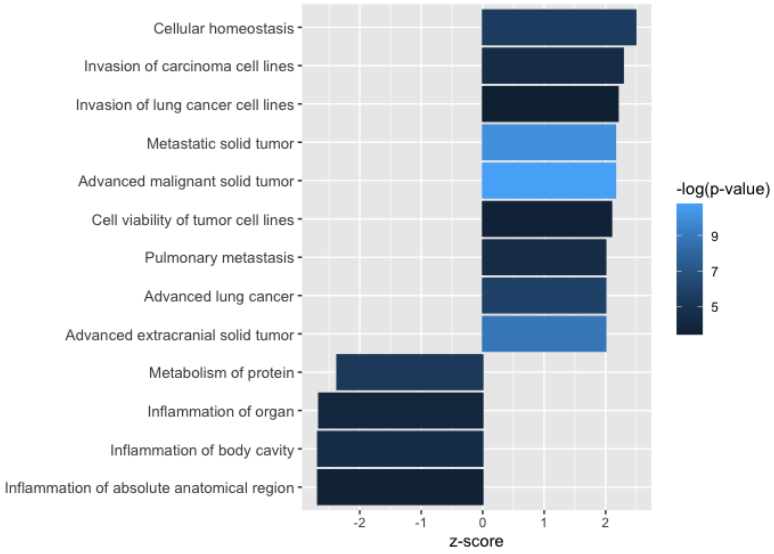

**Figure 2.11.** Analysis of the significant diseases and functions (p-value $\leq$ 0.05) predicted to be activated (z-score $\geq$ 2) or inactivated (z-score $\leq$ -2) in the T24 SEVs.

#### *2.3.6.4. SEV Biomarker Selection*

We selected candidates for biomarkers of the effect of arsenic exposure based on the following criteria: 1) magnitude of changes upon exposure, 2) involvement of the proteins in multiple key pathways, and 3) predicted function in urological disease. For the candidate SEV biomarker selection, all proteins with significant expression in the highest or multiple exposure groups were considered. Those proteins that followed a dose-response relationship or had significant expression in multiple exposure groups were selected as potential SEV protein biomarkers leaving four upregulated (LRP1, PSMB3, PXDN, TFGBR1) and four downregulated (GNAI1, GNA11, SMPDL3B, and RNH1) protein candidates. Proteins from this list were closer examined to determine their predicted function, previous reports in urological disease or function and any previous links to arsenic exposure (**Appendix Table 2.3**). Ultimately, TGFBR1 and RNH1 were selected for further biomarker validation as these proteins were significantly altered in multiple exposure groups and had functional importance in renal disease and arsenic exposure.

### 2.3.7 SEV Proliferation Assay

Based upon the results of the pathway analysis, the ability of SEVs derived from 5 $\mu m$ arsenic exposed cells and T24 cells to increase proliferation rates in recipient cells was assessed. Following 48-hours of SEV exposure there were no significant differences in proliferation rates observed when comparing SEVs derived from arsenic exposed or T24 cells to SEVs derived from unexposed SVHUC1 cells (**Figure 2.12**). There were however significantly increased

proliferation rates when comparing treatment of cells with SEVs compared to treatment with PBS alone, displaying the biological activity of SEVs in recipient cells.

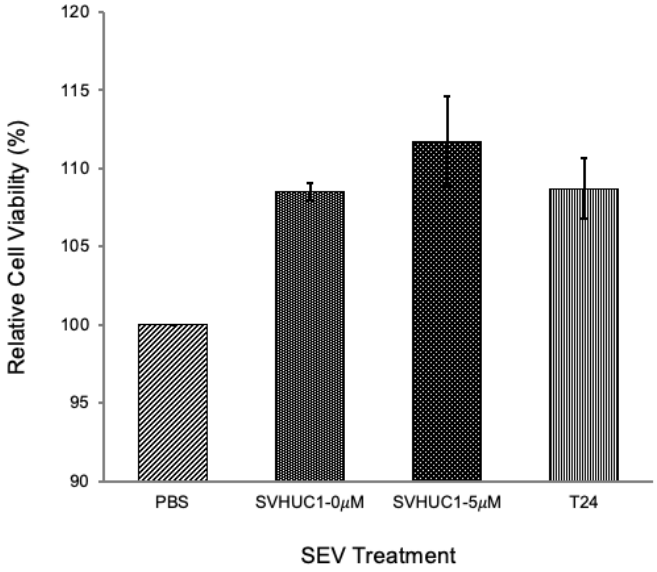


**Figure 2.12.** Bar chart of cell viability measured using an MTS proliferation assay following exposure to SEVs derived from arsenic exposed, T24, or control cells with PBS as a negative control.

## 2.3.8. Biomarker Validation

### *2.3.8.1. Protein Content*

Differences in total protein concentration between cell lines and exposure groups showed that overall biomarker concentrations needed to be normalized to total protein concentrations (**Table 2.3**).

**Table 2.3.** Micro-BCA analysis of the total protein concentration in cell SEV samples for biomarker validation.

| Sample | Average protein in SEVs ($\mu g/\mu l$) |
|---|---|
| **SVHUC1- Control** | $0.044 \pm 0.013$ |
| **SVHUC1- 1 $\mu M$ $NaAsO_2$** | $0.053 \pm 0.006$ |
| **SVHUC1- 2 $\mu M$ $NaAsO_2$** | $0.038 \pm 0.022$ |
| **SVHUC1- 5 $\mu M$ $NaAsO_2$** | $0.052 \pm 0.014$ |
| **T24** | $0.089 \pm 0.014$ |

#### *2.3.8.2. TGFBR1 Validation*

The standard curve plotted for TGFBR1 best fit a Rational model ($R^2 = 0.9998$) and thus this model was used to determine the concentration of TGFBR1 in each sample based on measured absorbance values (**Appendix Figure 2.3**).

**Protein Normalization**

TGFBR1 concentration was normalized based on the total protein concentration determined by microBCA. TGFBR1 concentration was first converted to $\mu g/L$ and then divided by the total SEV protein concentration resulting in TGFBR1($\mu g$) per protein ($g$).

**Box Plot**

The boxplot analysis of TGFBR1 in the exposure groups does not show a clear association of increased TGFBR1 expression with increased arsenic exposure (**Figure 2.13**). Furthermore, TGFBR1 was not expected to be elevated in the T24 group compared to the control.

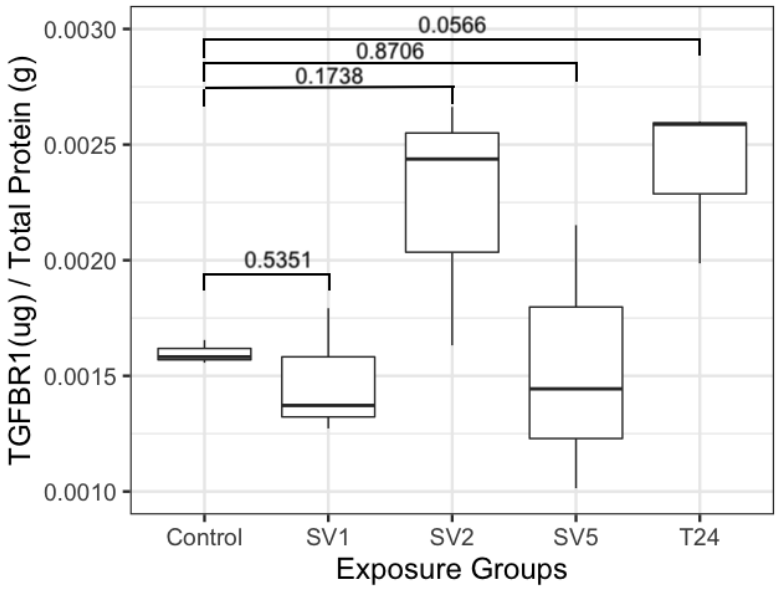


**Figure 2.13.** Box plot analysis of TGFBR1 concentrations normalized to total protein concentration in cell media SEV samples with Welch's t-test results.

### *2.3.8.3. RNH1 Validation*

The standard curve plotted for RNH1 best fit a Rational model ($R^2$ = 0.9999) and thus, this model was used to determine the concentration of RNH1 in each sample based on measured absorbance values (**Appendix Figure 2.4**).

**Protein Normalization**

RNH1 concentration was normalized based on the total protein concentration determined by microBCA. RNH1 concentration was first converted to $\mu g/L$ and then divided by the total SEV protein concentration resulting in RNH1 ($\mu g$) per protein ($g$).

**Box Plot**

The expected results based on the previous proteomics analysis were a down regulation of RNH1 following arsenic exposure and an upregulation in T24 SEVs compared to the control group. RNH1 had greater expression in T24 SEVs as expected but did not show higher expression in the

control in comparison to arsenic exposure groups (**Figure 2.14**). Compared to TGFBR1, RNH1 had an overall lower concentration in all samples.

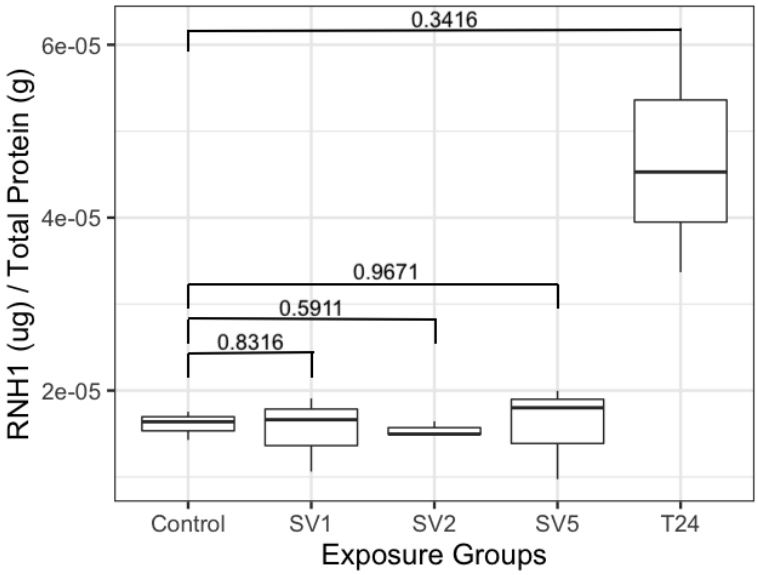


**Figure 2.14.** Box plot analysis of RNH1 concentrations normalized to total protein concentration in cell media SEV samples with Welch's t-test results.

## 2.4. Discussion

### 2.4.1 SEV Characterization

This is the first study that measured the SEV response following arsenic exposure in urothelial cells or any cells of the urinary tract. Based on the SEV characterization it was confirmed that the main extracellular vesicles examined belonged to those commonly termed "exosomes". The average SEV size fell well within the 50-200 nm definition set by the international society of extracellular vesicles (Théry et al., 2018). Based upon previous literature detailing SEV response during cell stress we expected to see an increase in the number of SEVs released per cell following arsenic exposure (Alharbi et al., 2021; Atienzar-Aroca et al., 2016; Bala et al., 2022; He et al., 2022). However, in the present investigation there was no significant increase in the

number of SEVs released per cell in any of the exposure conditions which addresses our first research objective. It is possible that to see changes in the number of SEVs produced, chronic exposure is necessary or potentially the effect of arsenic on SEV response is observed only in the SEV cargo rather than the number of SEVs produced. There was a nearly 4-fold increase in the SEVs secreted from T24 urothelial carcinoma cells versus SVHUC1 urothelial cells. It has been widely reported that cancer cells secrete higher numbers of SEVs to aid in the tumor microenvironment and enhance migration and invasion (Bebelman et al., 2021). SEVs were further characterized using an antibody array for eight proteins commonly associated with the endosomal pathway (CD63, EpCAM, ANXA5, TSG101, FLOT1, ICAM, ALIX, and CD81) and one protein that is indicative of cellular contamination (GM130). The same amount of protein was loaded for both cell types and the results show that T24 SEVs had an overall higher concentration of most of the protein markers except for ALIX, which had higher expression in SVHUC1 SEVs. Overall, this analysis provides further evidence that the EVs examined in this experiment were those SEVs (commonly referred to as 'exosomes') of endosomal origin.

### 2.4.2 SEV Proteomics Analysis

Based on the visualization of the various conditions by unsupervised principal component analysis and heatmap hierarchal clustering it is evident that there is grouping between conditions and minimal variability between condition replicates. This analysis revealed that the 5 $\mu m$ condition and T24 SEVs were responsible for the main differences observed in protein expression. The hierarchal clustering indicated that expression of the DEPs were similar between the 1 $\mu m$ and 2 $\mu m$ arsenic exposure conditions. Looking at the overlap in DEPs, there were similarities when comparing between arsenic exposure groups but not when comparing these

groups with T24 DEPs. T24 cells are derived from a high grade and invasive urothelial carcinoma and therefore the proteins expressed will be indicative of late-stage carcinogenesis (Peng et al., 2006). In contrast, acute arsenic exposure was hypothesized to result in differential pathway expression indicating early hallmarks of carcinogenesis. Future studies examining SEV protein expression in early-stage urothelial carcinoma would also be useful in comparing with the present arsenic induced DEPs.

## 2.4.3 SEV Canonical Pathway Analysis

### *2.4.3.1 Protein degradation pathways*

When examining the canonical pathways enriched following arsenic exposure, SEVs showed the upregulation of 10 proteasomal subunit proteins that were enriched in pathways related to protein ubiquitination and degradation. The proteasomal subunit is responsible for the degradation of intracellular proteins and maintenance of normal cell function and aberrations in the proteasome are linked to several diseases (Kors, 2019). Protein quality control is critical to cell survival and arsenic has previously been reported to alter the balance between protein folding and degradation (Bomberger et al., 2012). Specifically trivalent inorganic arsenic has been shown to bind to cystine residues in proteins and inhibit spontaneous oxidative protein folding through the formation of disulfide bonds (Jacobson et al., 2012; Ramadan et al., 2009). Furthermore, oxidative refolding can be disrupted by arsenic induced depletion of glutathione which binds to arsenic and decreases its interaction with cysteine sulfhydryl groups found in proteins (Tam & Wang, 2020). The results of the proteomics analysis suggest that protein degradation signaling during arsenic exposure may be trafficked through SEVs.

#### *2.4.3.2 Fibrosis and wound healing pathways*

Other canonical pathways that were enriched in exposure SEVs include those for fibrosis and wound healing. Arsenic has previously been linked as an environmental factor in the development of kidney and lung fibrosis (Assad et al., 2018; Chang & Singh, 2019; W. Wang et al., 2021). In a study by Chang & Singh (2019), arsenic induced fibrotic changes including the expression of markers of fibrosis such as collagen 1, fibronectin, and transforming growth factor beta in kidney epithelial cells. Similar upregulation of collagen proteins, fibronectin and TGFBR1 was noted in the SEVs released from arsenic exposed cells in our present study. TGFBR1, which can mediate fibrosis by promoting ECM deposition and accelerating pro-fibrotic responses was significantly upregulated in all three of our arsenic exposure groups (Walton et al., 2017). These results indicate that SEVs may serve a functional role in promoting fibrosis during exposure.

#### *2.4.3.3 Cancer pathways*

Cancer related pathways were enriched in both exposure and T24 SEVs, which addresses the second objective leading this chapter's research. The two SEV groups showed enrichment of pathways for metastasis and cancer cell signalling with differences in the specific pathway expression. T24 SEVs showed enrichment of pathways responsible for cancer metastasis and cancer cell signalling that was related to the enrichment of integrin and claudin family proteins. Previous studies have found that cancer derived SEV integrins may promote cell detachment, migration, and may drive the selection of metastatic sites. Additionally, different integrins may be specific to the type of cancer, serving as prospective biomarkers (Hurwitz & Meckes, 2019; Paolillo & Schinelli, 2017). Furthermore, the claudin family of proteins is integral to the tight junctions of epithelial cells and loss of cell-to-cell adhesion is central to the metastatic potential

of cancer cells (Dhawan et al., 2010). Because of this, claudin proteins are regularly associated with numerous cancers including bladder cancer and have been proposed as molecular biomarkers of metastasis (Székely et al., 2011).

#### *2.4.3.4 Comparative pathway analysis*

The top canonical pathways presented in figures 2.8 and 2.9 were not directly comparable between arsenic exposed SEV and T24 SEV proteins. However, when looking at the top 50 conical pathways there were 10 overlapping between these groups, including wound healing signaling, pulmonary fibrosis idiopathic signaling, osteoarthritis, molecular mechanisms of cancer, cardiac hypertrophy signaling (enhanced), hepatic fibrosis signaling, ephrin receptor signaling, Rho GDP-dissociation inhibitor signaling, signaling by Rho Family GTPases, and Phosphatase and tensin homolog signaling. This analysis may highlight interesting comparisons; however as these were not the pathways with the greatest enrichment and the significant proteins were not the same between conditions there is uncertainty surrounding the direct comparison of these pathways.

### 2.4.4. SEV Functional and Disease Annotations

The functional and disease analysis showed that SEVs derived from arsenic exposed cells had significant (z-score $\geq$ 2, p-value $\leq$ 0.05) activation of cell survival, viability, invasion, migration, and infection and significant (z-score $\leq$ -2, p-value $\leq$ 0.05) inactivation of cell death and necrosis. These functions also happen to be hallmarks of early carcinogenesis. The six major hallmarks of cancer include sustaining proliferative signalling, evading growth suppressors, activating invasion and metastasis, enabling replicative immortality, inducing angiogenesis, and resisting cell death (Hanahan & Weinberg, 2011). This functional analysis highlights that SEVs

may serve a role in arsenic induced carcinogenesis, further supporting out second objective, but chronic studies are necessary to confirm this relationship and cell transition. Moreover, from the small pool of literature surrounding arsenic exposure and SEV response, two other publications note the role SEVs had on increased cell growth and proliferation following arsenic exposure in human bronchial epithelial and liver cell models (Dai et al., 2018; Xu et al., 2015). Indeed, DEPs derived from arsenic exposed SEVs showed similar activation of functions involved in invasion and migration when compared to T24 DEPs. However, the functions and diseases activated in T24 DEPs were more closely related to advanced cancer, whereas 5 $\mu$M exposure DEP functions were similar to the beginning stages of carcinogenesis including migration, cell survival and invasion. These findings suggest that SEVs derived from both arsenic exposed cells and T24 cells may mediate invasion and cell growth. Unique to the T24 SEV functionas was the inactivation of inflammation. Inflammation is closely related to cancer. Chronic bladder inflammation may result in cancer formation and inversely inflammatory cells such as natural killer, CD4(+), and CD8(+) cells may effectively eliminate cancer cells (Aggarwal & Gakis, 2014). In the case of T24 cells the administration of macrophages was shown to inhibit cancer cell growth and thus a decrease in inflammatory signaling may be beneficial to cell survival (Dufresne et al., 2011).

### 2.4.5 SEV Proliferation Assay

Despite the significant activation of pathways responsible for proliferation and cell viability the *in vitro* proliferation assay did not indicate any significant increase in proliferation in SEV exposed cells from the arsenic exposure or T24 group. It is possible that a 48-hour exposure with SEVs was not long enough to allow for changes in gene expression required to observe increased

proliferation in recipient cells. Other studies have noted that SEVs from arsenite transformed cells can elect a malignant transformation and inflammatory responses in unexposed cells who take up their SEVs (Dai et al., 2018; Chen et al. 2016). Through co-culturing or subsequent SEV collection and exposure as was done in the present study this method allows for the functional assessment of SEVs that get released into systemic circulation. Further studies to understand the functional importance of SEVs released following arsenic exposure would be valuable to help decipher the mechanisms of arsenic induced carcinogenesis particularly as it affects various organs in the body.

### 2.4.6. SEV Biomarker Candidates

Finally, out of the 109 DEPs those that followed a dose-response relationship in expression or that were significantly altered in multiple exposure groups were identified. This led to eight proposed biomarkers of exposure. Of the proposed biomarkers, those downregulated following arsenic exposure included G protein subunit alpha I1 (GNAI1), G protein subunit alpha 11 (GNA11), Sphingomyelin Phosphodiesterase Acid-Like 3b (SMPDL3B), and ribonuclease inhibitor 1 (RNH1). Of the proposed biomarkers those upregulated included transforming growth factor beta receptor 1 (TGFBR1), peroxidasin (PDXN), proteasome 20S subunit beta 3 (PSMB3), and LDL receptor related protein 1 (LRP1). Additional investigation of these eight biomarkers would be valuable to further decipher their relationship to arsenic exposure. Based on their biological applicability and significant expression in multiple exposure groups TGFBR1 and RNH1 were considered as the most promising biomarkers of urothelial injury during arsenic exposure. TGFBR1 was significantly upregulated in all three arsenic exposure groups. TGFBR1 is a kinase receptor located in the plasma membrane which transmits signals that can trigger

responses for cell proliferation, movement, and apoptosis. TGFBR1 relies on the attachment of transforming growth factor beta (TGF-$\beta$) for activation. Multiple studies have noted that arsenic is involved with the regulation of the TGF-$\beta$ system (J. Dai et al., 2019a; Okamura et al., 2020; Y. Wang et al., 2019). Upregulation of TGFBR1 and other components of the TBF-$\beta$ system were previously noted in tumor tissues from an arsenic exposed group of mice (Okamura et al., 2020). RNH1 was significantly downregulated following a dose response in both the 2 $\mu m$ and 5 $\mu m$ exposure groups. During homeostasis RNH1 is found in the nucleus promoting RNA transcription. Under cell stress RHN1 can translocate to the cytosol and cleave transfer RNA into fragments, inhibiting protein synthesis. Downregulation of RNH1 was reported to increase cell proliferation, migration and invasion and enhance tumorigenesis and metastasis in T24 bladder cancer cells (Xiong et al., 2014). Multiple reports also detailed that the stress of arsenic exposure may result in RHN1 translocating to different cell compartments which is likely mediated through the production of reactive oxygen species (Mishra & Dubey, 2006; Pizzo et al., 2013; Saikia et al., 2012).

### 2.4.7. Biomarker Analysis

The analysis of TGFBR1 by ELISA as a biomarker of exposure did not show the expected increase in all arsenic treatments. The reason for the discrepancy between proteomic and ELISA results may be due to the capacity of analyzing only soluble TGFBR1 with the ELISA kit. The ELISA TGFBR1 conjugated antibody is only cable of binding with the TGFBR1 antigen in its solubilized form rather than when it is embedded in the plasma membrane. If not all TGFBR1 was solubilized during SEV lysis with NP-40 buffer then it is possible that a proportion of TGFBR1 could not be detected with the ELISA. Preliminary experiments were conducted to

optimize the membrane lysis method for the highest total protein yield but the results of this method on individual protein quantification could not be determined at that time. A potential future direction of this analysis would be to employ flow cytometry for membrane bound TGFBR1 detection. RNH1 was also further investigated by ELISA with predicted downregulation during exposure. The results of the ELISA showed low expression of RNH1 in all SVHUC1 samples with elevated expression in T24 SEVs as predicted. The expression in SVHUC1 exposure samples did not however reflect the proteomic results with no clear trend in decreased expression in higher exposure groups.

## 2.5 Conclusion

The research objectives for this chapter were to 1) characterize the effect of arsenic exposure on the number of total SEVs released to determine if cells respond by increasing intracellular signaling and 2) assess the pattern of protein expression in SEVs released by arsenic exposed cells to look for core proteins reported in cancer related pathways. Based on the results of this study it appears that cells do not respond to arsenic by increasing the rate of SEV excretion at least not following acute exposure as was presently tested. As T24 carcinoma cells showed significantly more SEVs released, it is possible that chronically exposing cells to arsenic may also have this affect as arsenite transformed cells have been shown to present cancer like phenotypes (Ngalame et al., 2018). Besides increasing the sheer volume of SEVs produced, we tested if arsenic exposure impacts the cargo that is packaged into SEVs which we hypothesized to play a key role in toxic response signalling. The results of this study showed that arsenic impacts SEV cargo and alters the functional pathways expressed in SEVs. The differential pathways and functions we observed indicate that SEVs released from arsenic exposed cells may

promote cell survival, viability, and migration, while decreasing cell death and necrosis. This analysis is of particular importance as these functions are some of the major early hallmarks of carcinogenesis.

The results of this chapter's work led to the identification of eight proposed biomarkers of exposure including an upregulation of LRP1, PSMB3, PXDN, and TFGBR1 and a downregulation of GNAI1, GNA11, SMPDL3B, and RNH1. TGFBR1 and RNH1 were further examined with ELISA to validate their presence in SEV samples. Both TGFBR1 and RNH1 were detectable in all SEV samples. However, analysis of TGFBR1 and RNH1 with ELISA did not clearly corroborate the results of the previous SEV proteomics analysis. Differences in protein solubilization and sample collection may explain this discrepancy and future analysis using different techniques such as flow cytometry is required to better validate differential expression in all exposure groups.

Overall, this chapter's results add to the growing body of evidence indicating that SEVs are crucial in toxic response signalling. Our work suggests that there are several potential SEV biomarkers that should be further investigated to assess the early urological effects of arsenic exposure.

## 2.6 References

Aggarwal, B. B., & Gakis, G. (2014). The Role of Inflammation in Bladder Cancer. *Advances in Experimental Medicine and Biology*, *816,* 183–196. https://doi.org/10.1007/978-3-0348-0837-8_8

Alharbi, M. G., Lee, S. H., Abdelazim, A. M., Saadeldin, I. M., & Abomughaid, M. M. (2021). Role of Extracellular Vesicles in Compromising Cellular Resilience to Environmental Stressors. *BioMed Research International*. https://doi.org/10.1155/2021/9912281

Assad, N., Sood, A., Campen, M. J., & Zychowski, K. E. (2018). Metals-induced pulmonary fibrosis. *Current Environmental Health Reports*, *5*(4), 486. https://doi.org/10.1007/S40572-018-0219-7

Atienzar-Aroca, S., Flores-Bellver, M., Serrano-Heras, G., Martinez-Gil, N., Barcia, J. M., Aparicio, S., Perez-Cremades, D., Garcia-Verdugo, J. M., Diaz-Llopis, M., Romero, F. J., & Sancho-Pelluz, J. (2016). Oxidative stress in retinal pigment epithelium cells increases exosome secretion and promotes angiogenesis in endothelial cells. *Journal of Cellular and Molecular Medicine*, *20*(8), 1457. https://doi.org/10.1111/JCMM.12834

Bain, L. J., Liu, J., & League, R. E. (2016). Arsenic inhibits stem cell differentiation by altering the interplay between the Wnt3a and Notch signaling pathways. *Toxicology Reports*, *3*, 405–413. https://doi.org/10.1016/j.toxrep.2016.03.011

Bebelman, M. P., Janssen, E., Pegtel, D. M., & Crudden, C. (2021). The forces driving cancer extracellular vesicle secretion. *Neoplasia*, *23*(1), 149. https://doi.org/10.1016/J.NEO.2020.11.011

Bomberger, J. M., Coutermarsh, B. A., Barnaby, R. L., & Stanton, B. A. (2012). Arsenic Promotes Ubiquitinylation and Lysosomal Degradation of Cystic Fibrosis Transmembrane Conductance Regulator (CFTR) Chloride Channels in Human Airway Epithelial Cells. *The Journal of Biological Chemistry*, *287*(21), 17130. https://doi.org/10.1074/JBC.M111.338855

Chang, Y. W., & Singh, K. P. (2019). Arsenic induces fibrogenic changes in human kidney epithelial cells potentially through epigenetic alterations in DNA methylation. *Journal of Cellular Physiology*, *234*(4), 4713–4725. https://doi.org/10.1002/JCP.27244

Chen, C., Luo, F., Liu, X., Lu, L., Xu, H., & Yang, Q. (2017). *NF-kB-regulated exosomal miR-155 promotes the inflammation associated with arsenite carcinogenesis*. *388*. https://doi.org/10.1016/j.canlet.2016.11.027

Cheung, J. S. J., Hu, X. F., Parajuli, R. P., Rosol, R., Torng, A., Mohapatra, A., Lye, E., & Chan, H. M. (2020). Health risk assessment of arsenic exposure among the residents in Ndilǫ, Dettah, and Yellowknife, Northwest Territories, Canada. *International Journal of Hygiene and Environmental Health*, *230*, 113623. https://doi.org/10.1016/J.IJHEH.2020.113623

Cox, J., Neuhauser, N., Michalski, A., Scheltema, R. A., Olsen, J. v, & Mann, M. (2011). Andromeda: A Peptide Search Engine Integrated into the MaxQuant Environment. *J. Proteome Res*, *10*, 20. https://doi.org/10.1021/pr101065j

Dai, J., Xu, M., Zhang, X., Niu, Q., Hu, Y., Li, Y., & Li, S. (2019b). Bi-directional regulation of TGF-β/Smad pathway by arsenic: A systemic review and meta-analysis of in vivo and in vitro studies. *Life Sciences*, *220*, 92–105. https://doi.org/10.1016/J.LFS.2019.01.042

Dai, X., Chen, C., Xue, J., Xiao, T., Mostofa, G., Wang, D., Chen, X., Xu, H., Sun, Q., Li, J., Wei, Y., & Chen, F. (2019a). Exosomal MALAT1 derived from hepatic cells is involved in the activation

of hepatic stellate cells via miRNA-26b in fibrosis induced by arsenite. *Toxicology Letters*, *316*, 73–84. https://doi.org/10.1016/j.toxlet.2019.09.008

Dai, X., Chen, C., Yang, Q., Xue, J., Chen, X., Sun, B., Luo, F., & Liu, X. (2018). Exosomal circRNA _ 100284 from arsenite- transformed cells, via microRNA-217 regulation of EZH2, is involved in the malignant transformation of human hepatic cells by accelerating the cell cycle and promoting cell proliferation. *Cell Death and Disease*, 1–14. https://doi.org/10.1038/s41419-018-0485-1

Dhawan, P., Singh, A. B., & Sharma, A. (2010). Claudin Family of Proteins and Cancer: An Overview. *Journal of Oncology*, *2010*, 11. https://doi.org/10.1155/2010/541957

Dufresne, M., Dumas, G., Asselin, É., Carrier, C., Pouliot, M., & Reyes-Moreno, C. (2011). Pro-inflammatory type-1 and anti-inflammatory type-2 macrophages differentially modulate cell survival and invasion of human bladder carcinoma T24 cells. *Molecular Immunology*, *48*(12–13), 1556–1567. https://doi.org/10.1016/J.MOLIMM.2011.04.022

Hanahan, D., & Weinberg, R. A. (2011). Hallmarks of cancer: The next generation. *Cell*, *144*(5), 646–674. https://doi.org/10.1016/J.CELL.2011.02.013/ATTACHMENT/3F528E16-8B3C-4D8D-8DE5-43E0C98D8475/MMC1.PDF

Harischandra, D. S., Ghaisas, S., Rokad, D., & Kanthasamy, A. G. (2017). *Exosomes in Toxicology: Relevance to Chemical Exposure and Pathogenesis of Environmentally Linked Diseases*. *158*(1), 3–13. https://doi.org/10.1093/toxsci/kfx074

He, G., Peng, X., Wei, S., Yang, S., Li, X., Huang, M., Tang, S., Jin, H., Liu, J., Zhang, S., Zheng, H., Fan, Q., Liu, J., Yang, L., & Li, H. (2022). Exosomes in the hypoxic TME: from release, uptake and biofunctions to clinical applications. *Molecular Cancer*, *21*(1), 1–22. https://doi.org/10.1186/S12943-021-01440-5

Hurwitz, S. N., & Meckes, D. G. (2019). Extracellular Vesicle Integrins Distinguish Unique Cancers. *Proteomes*, *7*(2). https://doi.org/10.3390/PROTEOMES7020014

Jacobson, T., Navarrete, C., Sharma, S. K., Sideri, T. C., Ibstedt, S., Priya, S., Grant, C. M., Christen, P., Goloubinoff, P., & Tamá, M. J. (2012). Arsenite interferes with protein folding and triggers formation of protein aggregates in yeast. *Journal of Cell Science*, *125*(21), 5073–5083. https://doi.org/10.1242/JCS.107029

Jou, Y. C., Wang, S. C., Dai, Y. C., Chen, S. Y., Shen, C. H., Lee, Y. R., Chen, L. C., & Liu, Y. W. (2019). Gene expression and DNA methylation regulation of arsenic in mouse bladder tissues and in human urothelial cells. *Oncology Reports*, *42*(3), 1005–1016. https://doi.org/10.3892/OR.2019.7235

Kors, S. (2019). Regulation of Proteasome Activity by (Post-)transcriptional Mechanisms. *Frontiers in Molecular Biosciences*, *6*, 48. https://doi.org/10.3389/FMOLB.2019.00048/BIBTEX

Lässer, C., Eldh, M., & Lötvall, J. (2012). Isolation and Characterization of RNA-Containing Exosomes. *Journal of Visualized Experiments*, *59*, 1–6. https://doi.org/10.3791/3037

Li, J., Xue, J., Ling, M., Sun, J., Xiao, T., Dai, X., Sun, Q., Cheng, C., Xia, H., Wei, Y., Chen, F., & Liu, Q. (2021). MicroRNA-15b in extracellular vesicles from arsenite-treated macrophages promotes the progression of hepatocellular carcinomas by blocking the LATS1-mediated Hippo pathway. *Cancer Letters*, *497*, 137–153. https://doi.org/10.1016/j.canlet.2020.10.023

Lin, F., Yin, H. bin, Li, X. Y., Zhu, G. M., He, W. Y., & Gou, X. (2020). Bladder cancer cell-secreted exosomal miR-21 activates the PI3K/AKT pathway in macrophages to promote cancer progression. *International Journal of Oncology*, *56*(1), 151–164. https://doi.org/10.3892/IJO.2019.4933

Liu, X., Huang, Y., Hung, W., Chen, W., & Yu, H. (2012). Sodium arsenite-induced abnormalities in expressions of Caveolin-1, eNOS, IKK b, and COX-2 in SV-40 immortalized human uroepithelial cells and in urothelial carcinomas. *Toxicology in Vitro*, *26*(7), 1098–1105. https://doi.org/10.1016/j.tiv.2012.07.003

Mishra, S., & Dubey, R. S. (2006). Inhibition of ribonuclease and protease activities in arsenic exposed rice seedlings: role of proline as enzyme protectant. *Journal of Plant Physiology*, *163*(9), 927–936. https://doi.org/10.1016/J.JPLPH.2005.08.003

Ngalame, N. N. O., Luz, A. L., Makia, N., & Tokar, E. J. (2018). Arsenic Alters Exosome Quantity and Cargo to Mediate Stem Cell Recruitment Into a Cancer Stem Cell-Like Phenotype. *Toxicological Sciences*, *165*(1), 40. https://doi.org/10.1093/TOXSCI/KFY176

Okamura, K., Suzuki, T., & Nohara, K. (2020). Gestational arsenite exposure augments hepatic tumors of C3H mice by promoting senescence in F1 and F2 offspring via different pathways. *Toxicology and Applied Pharmacology*, *408*, 115259. https://doi.org/10.1016/J.TAAP.2020.115259

Paolillo, M., & Schinelli, S. (2017). Integrins and Exosomes, a Dangerous Liaison in Cancer Progression. *Cancers*, *9*(8). https://doi.org/10.3390/CANCERS9080095

Peng, C. C., Chen, K. C., Peng, R. Y., Su, C. H., & Hsieh-Li, H. M. (2006). Human urinary bladder cancer T24 cells are susceptible to the Antrodia camphorata extracts. *Cancer Letters*, *243*(1), 109–119. https://doi.org/10.1016/J.CANLET.2005.11.021

Pizzo, E., Sarcinelli, C., Sheng, J., Fusco, S., Formiggini, F., Netti, P., Yu, W., D'Alessio, G., & Hu, G. F. (2013). Ribonuclease/angiogenin inhibitor 1 regulates stressinduced subcellular localization of angiogenin to control growth and survival. *Journal of Cell Science*, *126*(18), 4308–4319. https://doi.org/10.1242/JCS.134551/-/DC1

Ramadan, D., Rancy, P. C., Nagarkar, R. P., Schneider, J. P., & Thorpe, C. (2009). Arsenic (III) species inhibit oxidative protein folding in vitro. *Biochemistry*, *48*(2), 424–432. https://doi.org/10.1021/BI801988X

Saikia, M., Krokowski, D., Guan, B. J., Ivanov, P., Parisien, M., Hu, G. F., Anderson, P., Pan, T., & Hatzoglou, M. (2012). Genome-wide identification and quantitative analysis of cleaved tRNA fragments induced by cellular stress. *The Journal of Biological Chemistry*, *287*(51), 42708–42725. https://doi.org/10.1074/JBC.M112.371799

Smits, A. (2021, November 21). *Introduction to DEP*. https://bioconductor.org/packages/devel/bioc/vignettes/DEP/inst/doc/DEP.html

St-Pierre, C., Brochu, S., Vanegas, J. R., Dumont-Lagacé, M., Lemieux, S., & Perreault, C. (2013). Transcriptome sequencing of neonatal thymic epithelial cells. *Scientific Reports 2013 3:1*, *3*(1), 1–10. https://doi.org/10.1038/srep01860

System Biosciences. (2021). *Exo-Check Exosome Antibody Arrays*.

Székely, E., Törzsök, P., Riesz, P., Korompay, A., Fintha, A., Székely, T., Lotz, G., Nyirády, P., Romics, I., Tímár, J., Schaff, Z., & Kiss, A. (2011). Expression of Claudins and Their Prognostic Significance in Noninvasive Urothelial Neoplasms of the Human Urinary Bladder. *Journal of Histochemistry and Cytochemistry*, *59*(10), 932. https://doi.org/10.1369/0022155411418829

Tam, L. M., & Wang, Y. (2020). Arsenic Exposure and Compromised Protein Quality Control. *Chemical Research in Toxicology*, *33*(7), 1594. https://doi.org/10.1021/ACS.CHEMRESTOX.0C00107

Théry, C., Witwer, K. W., Aikawa, E., Alcaraz, M. J., Anderson, J. D., Andriantsitohaina, R., Antoniou, A., Arab, T., Archer, F., Atkin-Smith, G. K., Ayre, D. C., Bach, J. M., Bachurski, D., Baharvand, H., Balaj, L., Baldacchino, S., Bauer, N. N., Baxter, A. A., Bebawy, M., … Zuba-Surma, E. K. (2018). Minimal information for studies of extracellular vesicles 2018 (MISEV2018): a position statement of the International Society for Extracellular Vesicles and update of the MISEV2014 guidelines. *Journal of Extracellular Vesicles*, *7*(1). https://doi.org/10.1080/20013078.2018.1535750

Välikangas, T., Suomi, T., & Elo, L. L. (2018). A systematic evaluation of normalization methods in quantitative label-free proteomics. *Briefings in Bioinformatics*, *19*(1), 1. https://doi.org/10.1093/BIB/BBW095

Walton, K. L., Johnson, K. E., & Harrison, C. A. (2017). Targeting TGF-β mediated SMAD signaling for the prevention of fibrosis. *Frontiers in Pharmacology*, *8*, 461. https://doi.org/10.3389/FPHAR.2017.00461/BIBTEX

Wang, W., Zheng, F., & Zhang, A. (2021). Arsenic-induced lung inflammation and fibrosis in a rat model: Contribution of the HMGB1/RAGE, PI3K/AKT, and TGF-β1/SMAD pathways. *Toxicology and Applied Pharmacology*, *432*. https://doi.org/10.1016/J.TAAP.2021.115757

Wang, Y., Liu, Y., Liu, S., & Wu, B. (2019). Influence of Iron on Cytotoxicity and Gene Expression Profiles Induced by Arsenic in HepG2 Cells. *International Journal of Environmental Research and Public Health*, *16*(22). https://doi.org/10.3390/IJERPH16224484

Welton, J. L., Khanna, S., Giles, P. J., Brennan, P., Brewis, I. A., Staffurth, J., Mason, M. D., & Clayton, A. (2010). Proteomics Analysis of Bladder Cancer. *Molecular and Cellular Proteomics*, *9*, 1324–1338. https://doi.org/10.1074/mcp.M000063-MCP201

Whitehead, B., Wu, L. P., Hvam, M. L., Aslan, H., Dong, M., DyrskjØt, L., Ostenfeld, M. S., Moghimi, S. M., & Howard, K. A. (2015). Tumour exosomes display differential mechanical and complement activation properties dependent on malignant state: implications in endothelial leakiness. *Journal of Extracellular Vesicles*, *4*(1). https://doi.org/10.3402/JEV.V4.29685

Xiong, D., Liou, Y., Shu, J., Li, D., Zhang, L., & Chen, J. (2014). Down-regulating ribonuclease inhibitor enhances metastasis of bladder cancer cells through regulating epithelial-mesenchymal transition and ILK signaling pathway. *Experimental and Molecular Pathology*, *96*(3), 411–421. https://doi.org/10.1016/J.YEXMP.2014.04.012

Xu, Y., Luo, F., Liu, Y., Shi, L., & Lu, X. (2015). Exosomal miR - 21 derived from arsenite - transformed human bronchial epithelial cells promotes cell proliferation associated with arsenite carcinogenesis. *Archives of Toxicology*, 1071–1082. https://doi.org/10.1007/s00204-014-1291-x

Yang, H., Qu, H., Huang, H., Mu, Z., Mao, M., Xie, Q., Wang, K., & Hu, B. (2021). Exosomes-mediated transfer of long noncoding RNA LINC01133 represses bladder cancer progression via regulating the Wnt signaling pathway. *Cell Biology International*, *45*(7), 1510–1522. https://doi.org/10.1002/CBIN.11590

Zheng, H., Chen, C., Luo, Y., Yu, M., He, W., An, M., Gao, B., Kong, Y., Ya, Y., Lin, Y., Li, Y., Xie, K., Huang, J., Lin, T., & Tianxin Lin, C. (2021). Tumor-derived exosomal BCYRN1 activates WNT5A/VEGF-C/VEGFR3 feedforward loop to drive lymphatic metastasis of bladder cancer. *Clinical and Translational Medicine*, *11*(7) https://doi.org/10.1002/ctm2.497

Zhou, Q., Jin, P., Liu, J., Wang, F., & Xi, S. (2018). HER2 and Src co-regulate proliferation, migration, and transformation by downstream signaling pathways in arsenite-treated human uroepithelial cells. *Metallomics*, *10*. https://doi.org/10.1039/c8mt00131f

# Chapter 3: Deciphering the pathways of arsenic induced urothelial injury using comparative proteomics analysis

Nicole Washuck[1], Yingxi Li[2], Zoran Minic[3], and Laurie H.M. Chan[1]

[1]Department of Biology, University of Ottawa, Ottawa, Ontario, Canada

[2]Department of Chemistry and Biomolecular Sciences, University of Ottawa, Ottawa, Ontario, Canada

[3]John L. Holmes Mass Spectrometry Facility, University of Ottawa, Ottawa, Ontario, Canada

***Author Contributions***

Nicole Washuck: conceptualization, methodology, sample collection and preparation, data analysis, and manuscript preparation

Yingxi Li and Zoran Minic: sample preparation and mass spectrometry

Hing Man Chan: conceptualization

## 3.1. Introduction

Proteomics is a powerful tool in the assessment of the key molecular events underlining chemical toxicity. Non-targeted proteomics of cells allows for the assessment of hundreds of pathways simultaneously occurring in cells during exposure. Recent evaluation of arsenic exposed bladder cells has unearthed new insight into the mechanisms of arsenic toxicity (Chen et al., 2020). Both acute and chronic arsenic exposure in urothelial carcinoma T24 cells were found to alter the biological pathways involved in cytoskeleton remodeling, oxidative stress, and immune response (Chen et al., 2020). Another proteomics investigation done in partnership with the United States Environmental Protection Agency found that proteins differentially expressed following arsenic exposure in UROtsa human bladder cells were involved in antigen presentation, protein folding, apoptosis regulation, metal ion binding, oxidative stress, and biopolymer metabolism (Ortiz et al., 2007). Non-targeted proteomics also has the potential to reveal new therapeutic interventions in arsenic induced bladder carcinogenesis. In a study by Chen et al., 2010, nucleophosmim was proposed to be a key mediator of arsenic related bladder cancer as it was expressed in all uroepithelial cell lines examined following arsenic exposure and was associated with cell proliferation, anti-apoptosis, and migration. The study also found that soy isoflavones were capable of inhibiting nucleophosmim and potentially supressing the arsenic related tumorigenesis (Chen et al., 2010).

SEVs contain a subset of the proteins and other genetic cargo of their parent cells that are packaged during endosomal biogenesis. It has been hypothesized that specific mechanisms exist to aid in the deliberate packaging of cargo important in cellular communication, however, these mechanisms or evidence of deliberate packaging are still elusive (Shurtleff et al., 2017; Shurtleff

et al., 2016). The minimal information for studies of extracellular vesicles 2018 (MISEV2018), which sets the global standards for SEV research, recommended the investigation of paired cell and EV samples, when possible, to better understand the functional role of extracellular vesicles (Théry et al., 2018). This paired investigation enables researchers to untangle which cargo is selectively packaged into extracellular vesicles and may point towards cargo that serve a particularly important role in cell communication.

In this study we investigated the proteomic changes in urothelial cells following arsenic exposure and determined the relationship between the differentially expressed protein profiles in the SEV samples and those in the cultured cells. We hypothesize that the differentially expressed protein profiles in the SEV samples would be different to those in the cultured cells because proteins involved in cell communication pathways will be selectively excreted in the SEVs.

## 3.2. Methods

The methods and data produced for SEV isolation and proteomic investigation were previously described in chapter 2.

### 3.2.1. Cell Lysate Collection and Storage

Paired cell samples were collected at the same time as SEV enriched cell media for further investigation in this chapter's research. Samples consisted of three biological replicates for each exposure and control group. Following dissociation by 0.25% trypsin-ethylenediaminetetraacetic acid (Gibco, 25200-056) and cell counting, the remaining cells were pelleted at 800 x g for 6 minutes and resuspended in PBS for a final wash. Sample aliquots were then centrifuged again at 800 x g for 6 minutes and the remaining PBS was aspirated out. Cell pellets were stored at -80c

prior to lysis and proteomics. For cell lysis, pellets were resuspended in 1 mL radioimmunoprecipitation assay (RIPA) buffer (ThermoFischer Scientific, 89900) with dissolved Pierce protease inhibitor mini tablet (ThermoFischer Scientific, A32953) and probe sonicated for three 30 second intervals and placed on ice for 30 seconds between sonication. Lysate was then centrifuged at 20,000 x g for 30 minutes at 4℃ to pellet any cell debris. The resulting supernatant was used for protein content determination and proteomics analysis.

### 3.2.2. Bicinchoninic Acid Assay (BCA)

Pierce BCA Protein Assay Kit (Thermo Fischer, 23227) was used to measure the total protein in cell lysate to standardize the amount of protein loading for mass spectrometry. 10 $\mu L$ of cell lysate was used for protein content determination prior to freezing. The lysate and standard curve samples were incubated at 60℃ for 30 minutes and absorbance was read at 560 nm using the Nanodrop 2000 Spectrophotometer (ThermoFischer, ND-2000). PBS was used as the reference buffer and BSA was used to produce the standard curves required for protein content determination. A new standard curve was constructed for each batch of samples analyzed. All samples were analyzed in triplicates and the average protein concentration was reported.

### 3.2.3. In-solution Digestion

For proteomic analysis 50 $\mu$g of cell lysate was diluted to 120 $\mu L$ in PBS and lysed in solubilization buffer containing 8 M urea, 100 mM HEPES, 10% glycerol, 1 $\mu M$ dithiothreitol, and 0.5% n-dodecyl $\beta$-D-maltoside. 4 $\mu L$ of TCEP was added to reduce samples which were then incubated at 25℃ for 45 minutes on a 400 RPM shaker. Samples were then alkylated by

adding 4 $\mu L$ iodoacetamide and incubating again at 25℃ for 50 minutes on a 400 RPM shaker covered with tinfoil. Lastly, proteins were digested by adding 1.5 $\mu L$ of 0.3 $\mu g/\mu L$ trypsin/LysC solution (Trypsin/LyC Protease mix, ThermoFischer Scientific, A41007) to each sample and incubating at 25℃ for 24 hours on a 400 RPM shaker. 1.5 $\mu L$ of formic acid was then added to each sample to quench trypsin and tubes were vortexed at 10,000 g for 30 seconds. Samples were desalted using C18 TopTip (Glygen Corp, TT2C18) columns as per manufactures instructions. Columns were washed three times with 70% acetonitrile in 0.1% formic acid (ThermoFischer Scientific, 85174) and another three times with water in 0.1% formic acid (Fischer Scientific, LS1181). 100 $\mu L$ of sample was then slowly added to each column using syringe. Columns containing sample were then washed three times with water in 0.1% formic acid. Columns were then transferred to a clean microfuge tube and 50 $\mu L$ of 70% acetonitrile in 0.1% formic acid was added to each column to elute bound peptides. This process was repeated three times to ensure all peptides were eluted. Microfuge tubes containing peptides were then transferred to SpeedVac centrifuge and ran for 2 hours to evaporate remaining acetonitrile solvent. Samples were then ready for analysis by Nano-LC-MS/MS.

### 3.2.4. Nano-LC-MS/MS

Prepared samples were analyzed by an Orbitrap Fusion Mass Spectrometer (Thermo Fischer Scientific) coupled to a Ultimate3000 RLSCnano System (Dionex, Thermo Fischer Scientific). Peptides were separated on a packed column (Polymicro Technology) measuring 15 cm x 70 $\mu$m ID, LunaC18(2), 3$\mu$m, 100 Å (Phenomenex) using a water/acetonitrile/0.1% formic acid gradient. Samples were loaded onto the packed column at a flow rate of 0.30 $\mu$l/min for 105 minutes. For the first 7 minutes peptides were separated using 2% acetonitrile, followed by 70

minutes of a linear gradient from 3 to 38% acetonitrile and 3 minutes from 38-98% acetonitrile, lastly a 10-minute wash at 2% acetonitrile. Eluted peptides were then sprayed into a mass spectrometer using positive electrospray ionization at a spray voltage of 2.1 kV and an ion source temperature of 250 ℃. A resolution of 60 000 was used to obtain full-scan MS spectra and precursor ions were filtered based upon monoisotopic precursor selection, dynamic exclusion (30 s with a $\pm$ 10 s ppm window), and charge state (+2 to +7). Automatic gain control setting was set to 1 x $10^4$ for MS/MS and 5 x $10^5$ for Fourier transform MS. Collision-induced dissociation was used to perform fragmentation in the linear ion trap. Finally, precursors were fragmented with a normalized collision energy of 35% using a 2 m/z isolation window.

### 3.2.5. Data Processing and Statistical Analysis

Mass spectrometry raw files were analyzed in MaxQuant for protein identification. Peptides were searched against the UniProt FASTA Human Proteome Database using the integrated Andromeda search engine (Cox et al., 2011). Trypsin protease was set as the type of digestion enzymes used, allowing a maximum of 2 missed cleavage sites. Carbamidomethyl was set as a fixed modification and oxidation and N-terminal acetylation were set as variable modifications. Proteins had a first search peptide tolerance of 20 ppm and a main search peptide tolerance of 10 ppm. A reverse sequence database integrated into MaxQuant was used to determine the false discovery rate (FDR). FDR was set to 1% for peptides with a minimum of 7 amino acids for identification. A contaminates database provided by the Andromeda search engine was used to label and later filter out common contaminates. Label-free protein quantification (LFQ) values were obtained using only unique peptides for analysis. Subsequent data analysis was conducted using LFQ intensities.

### 3.2.6. Bioinformatics Analysis

The protein group file from the MaxQuant output was uploaded to R studio (Version 1.4.1103 © 2009-2021 “Wax Begonia”) for bioinformatics. All differential expression analysis was completed using the Bioconductor package DEP 1.17.0 and visualizations were rendered with the ggplot2 package (Smits, 2021). Proteins that matched the contaminates database, were the result of reverse identifications or were only identified by site were filtered out. Next, proteins were filtered based upon valid values with proteins present in all replicates in at least one sample group included in analysis. All remaining proteins were normalized by variance stabilizing normalization to reduce protein sample variance nondependent from their mean intensities and scale samples using parametric transformations and maximum likelihood estimations (Välikangas et al., 2018). Multiple imputation techniques including no imputation, manual imputation, minimum probability imputation, quantile regression imputation of left centered data, and k-nearest neighbor imputation were tested to determine which imputation technique best fit the data based upon missing values, intensity distributions, and differentially expressed protein before and after imputation. Following imputation, differentially expressed proteins were determined based upon a log-fold change of at least 1.5. Gene identifiers and log-fold change of all identified proteins were then uploaded to the Qiagen Ingenuity Pathway Analysis (IPA) software for identification of enriched pathways and biological processes. The resulting IPA canonical pathway analysis data was visualized in R studio using the ggplot2 package.

## 3.3. Results

### 3.3.1. Protein Concentration

The total protein concentration was determined for each cell lysate sample (**Table 3.1**). Based on this determination appropriate volumes of sample were used to load 50 $\mu g$ of protein for filter assisted sample preparation prior to mass spectrometry proteomic analysis.

**Table 3.1.** Average protein concentration in cell lysate samples (n=3 replicates).

| Sample | Average protein in cell lysate ($\mu g/mL$) |
|---|---|
| **T24** | 1422.667 $\pm$ 102.188 |
| **SVHUC1- Control** | 1434.667 $\pm$ 347.080 |
| **SVHUC1- 1 $\mu M$ NaAsO2** | 1374.000 $\pm$ 312.069 |
| **SVHUC1- 2 $\mu M$ NaAsO2** | 1340.333 $\pm$ 485.371 |
| **SVHUC1- 5 $\mu M$ NaAsO2** | 1410.333 $\pm$ 297.821 |

### 3.3.2. Proteomics

#### *3.3.2.1. Protein Identification*

A total of 3943 protein identifications were made in MaxQuant and were uploaded to R studio for further filtering. 3820 proteins remained following filtering based upon the contaminates database, reverse identification, and proteins only identified by site. Following filtering based on proteins present in at least 2/3 replicates in at least one condition 2061 proteins remained for variance stabilizing normalization. A heatmap of the missing values (**Appendix Figure 3.1**) and plot of the total number of proteins per sample (**Appendix Figure 3.2**) showed that replicates from passage 6 SVHUC1 cells had a high number of missing values. Furthermore, unsupervised principal component analysis (**Appendix Figure 3.3**) showed that the protein variance in

passage 6 samples was a main factor driving difference in protein expression and accounted for 17.6% of protein differences. A potential reason for this variation is that passage 6 samples were run a month later than the other samples due to supply shortages and as such were displaying major batch variance and decreased protein yields. We decided to exclude these samples from the analysis. An additional control was added for a total of n=3 in control and T24 groups and n=2 in arsenic exposure groups. To account for the higher variability of reduced replicates, we made the filtering more conservative by allowing proteins to pass only if they were present in all replicates in at least one sample condition. This resulted in 1923 proteins being included in the analysis. Following filtering, the missing value distribution appeared to have proteins missing not at random (MNAR) with clustering within exposure groups (**Appendix Figure 3.4**). The data also showed a left shift in the missing values meaning those missing proteins were attributed to low intensity proteins (**Appendix Figure 3.5**). Based on this information multiple left censored imputation techniques including minimum probability imputation, manual imputation, and quantile regression imputation of left censored data were ran. Minimum probability imputation was selected as it was the method used in the previous SEV proteomics analysis and as similar DEPs were displayed in all three possible imputations.

#### *3.3.2.2. Statistical Analysis*

Due to the limited sample size in arsenic treatment groups (n=2 per treatment group) and unequal sample sizes between treatment, control and T24 groups (n = 3 per control and T24 group), p-values could not be determined, and the differential expression analysis was based upon proteins displaying log2 fold changes >1.5 or <-1.5. A total of 470 proteins matched this criterion. Principal component analysis of the top 500 variable proteins showed grouping between arsenic

exposures (PC2: 8.5%) with the most variance (PC1: 48.5%) being attributed to differences between the two cell lines (SVHUC1 vs T24 proteins) (**Figure 3.1**).

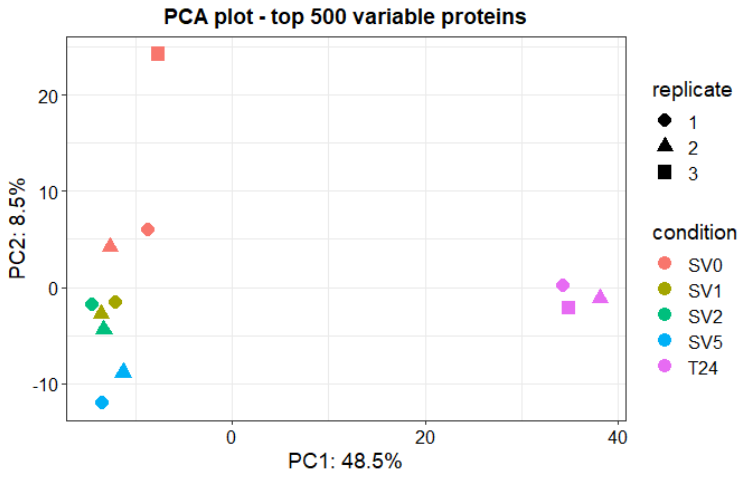


**Figure 3.1.** Unsupervised principal component analysis of the top 500 variable cell lysate proteins. SV0 = control group, SV1 = 1$\mu M$ $NaAsO_2$ group, SV2 = 2$\mu M$ $NaAsO_2$ group, SV5 = 5$\mu M$ $NaAsO_2$ group, T24 = T24 group.

### *3.3.2.2. Pathway Analysis of Identified Proteins*

**Canonical Pathway Analysis**

Canonical pathway analysis was conducted in the Ingenuity Knowledge Base and the calculated p-values of the Fischer's exact test were used to assemble a heatmap of pathways expressed in all cell lysate samples (**Figure 3.2**). Few pathways had calculatable z scores and therefore the pathway analysis can only be based on significant pathway expression (p-value <0.05 or -log(p-value) >1.3) not activation state. Individual plots of the top p-value significant canonical pathways along with ratios (# genes in a condition matching a pathway / total number of genes in the pathway) can be found in the **Appendix Figures 3.6-3.9**. From the heatmap analysis pathways involved in xenobiotic metabolism, protein ubiquitination, oxidative phosphorylation,

and mitochondrial dysfunction are expressed in all samples. These pathways were also all significantly altered in T24 cell lysate samples along with the strong change in mismatch and nucleotide excision repair pathways.

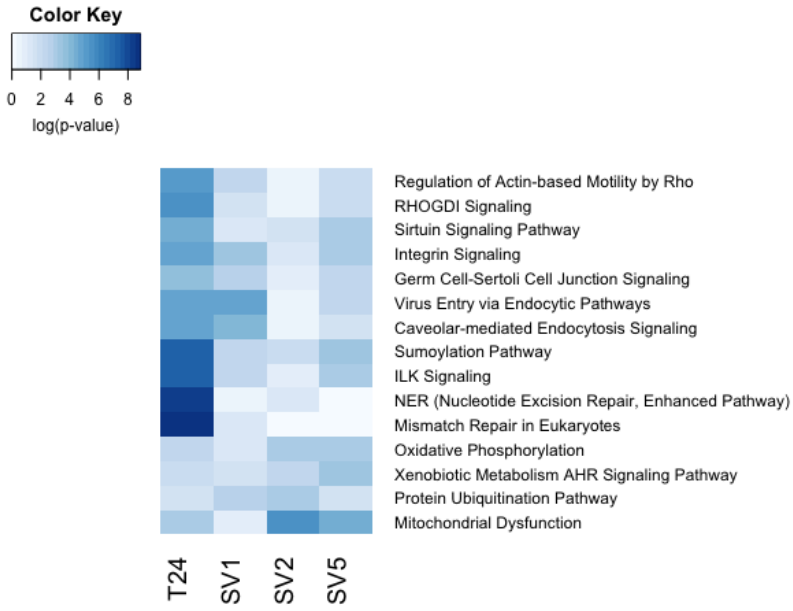


**Figure 3.2.** Heatmap of the top comparable canonical pathways altered in all cell lysate conditions versus the control based on p-value.

**Disease and Functional Annotations**

Disease and functional annotations along with their calculated p-values and z-scores were determined in IPA for each exposure group (SV1, SV2, and SV5) along with T24 samples. Z-score is used to indicate the predicted activation (z-score > 0) or inhibition (z-score < 0) of a disease or function. A z-score >2 or <-2 and a p-value <0.05 (i.e., -log10 >1.3) reflects significant activation or inhibition (St-Pierre et al., 2013). Full illustrations of all functions and diseases with calculatable z-scores for each condition can be found in the appendix (**Appendix Figures 3.10-3.13**). For the 1-$\mu$m arsenic exposure group the significantly activated diseases and functions included non-hematologic malignant solid tumor, frequency of tumor, incidence of

tumor, formation of solid tumor, and proliferation of fibroblast cell lines (**Appendix Figure 3.10**). For the 2-$\mu$m exposure group there was significant activation of cell viability of nervous tissue cell lines, survival of stem cell lines, cell viability of tumor cell lines and cell viability with significant inhibition of organismal death (**Appendix Figure 3.11**). For the 5-$\mu$m exposure group there was significant proliferation of prostate cancer cell lines, infection of kidney cell lines and internalization of tumor cell lines (**Appendix Figure 3.12**). Finally, for the T24 group there was significant activation of extrapancreatic malignant tumor, extracranial solid tumor, abdominal neoplasm, intraabdominal organ tumor, organismal death, incidence of tumor, development of malignant tumor, digestive organ tumor, gastrointestinal tumor, development of digestive organ tumor, benign lesion, hepatobiliary neoplasm, and abnormality of skin morphology. The T24 groups also showed significant inactivation of cell death of cervical cancer cell lines and replication of virus (**Appendix Figure 3.13**).

To compare each condition, a heatmap of all diseases and functions with calculatable z-scores shared amongst the four conditions was plotted (**Figure 3.3**). Similar activation of genes involved in solid and malignant tumor formation was present across exposure conditions and urothelial carcinoma (T24) cells. Furthermore, this analysis displayed similar trends in inactivation of genes involved in organismal death and necrosis in arsenic exposure groups.

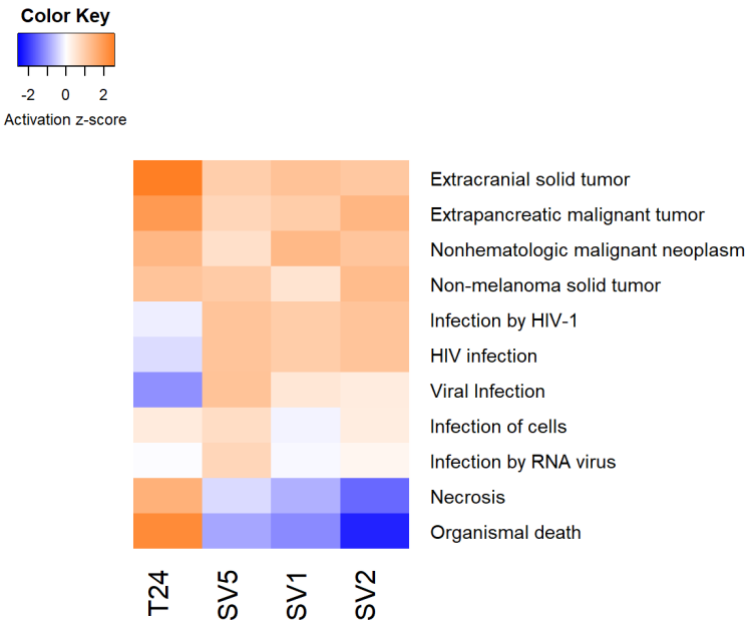


**Figure 3.3.** Heatmap of the top diseases and functions with calculatable z-scores in all cell lysate conditions based upon z-score.

### *3.3.2.3. Comparative SEV and Cell Lysate Proteomics*

**Overlap in protein identification**

To directly compare the proteins detected in the paired SEV and cell lysate samples following filtering, a venn diagram was constructed (**Figure 3.4**). Not all proteins present in the SEVs were detected in cell lysate samples. It would be expected that SEVs provide a snapshot of the pathways and processes occurring in cells and thus that cells would contain all SEV proteins. To determine the cause of these 535 missing SEV proteins, the origin of these proteins was determined by uploading a list into David 6.8, which can provide functional and compartmental data for gene list uploads (Huang et al., 2009; Sherman et al., 2022). From cell compartment analysis, it was determined that the top enriched compartments were plasma membrane, extracellular exosomes, integral component of the plasma membrane, cytosol, cytoplasm,

membrane, integral component of the plasma membrane, extracellular region, extracellular space, and cell surface localized proteins (**Appendix Table 3.1**). These results showed that the missing proteins are those related to the plasma membrane and cell surface and as SEVs are largely made up of their lipid membrane this accounted for a high number of SEV proteins. Some of the missing proteins may have been localized in the cytosol and cytoplasm however these proteins were also present in membrane associated compartment. Most likely these proteins were lost during the proteolytic cleavage of membrane proteins caused by trypsin, resulting in a low number of membrane-associated proteins in cell lysate samples.

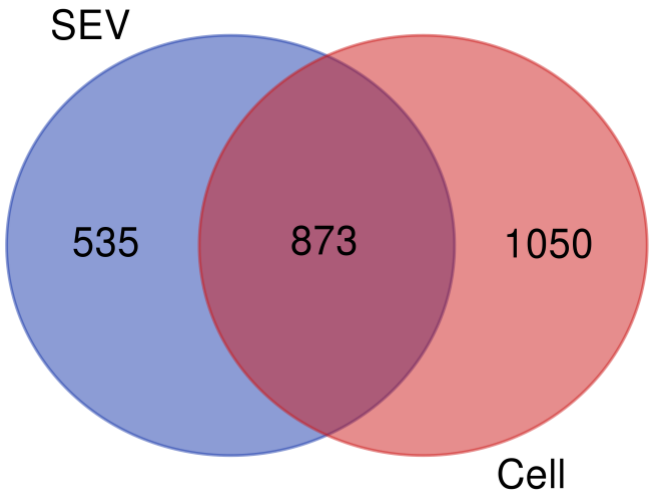


**Figure 3.4.** Venn diagram comparing the total proteins identified in paired SEV and Cell lysate samples.

**Comparison of IPA results**

Heatmaps for the 5 $\mu M$ exposure (**Figure 3.5**) and for T24 cells (**Figure 3.6**) were constructed using IPA data for comparative analysis of diseases and functions with calculatable z-scores shared between cell lysate and SEV samples. The comparative analysis of the 5 $\mu M$ arsenic exposure shows similar trends in the activation of infection, viability, and solid tumors and the

inactivation of organismal death and necrosis in both cell lysate and SEV samples. The comparative analysis of T24 cells had a greater number of diseases and functions to compare and showed a greater divergence in activation states between cell lysate and SEV samples. T24 cell lysate and SEV samples showed similar trends in the activation of metastasis, invasion, and cell death related functions. The major functions differing between samples were related to cell infection, viability, and other tumor specific functions.

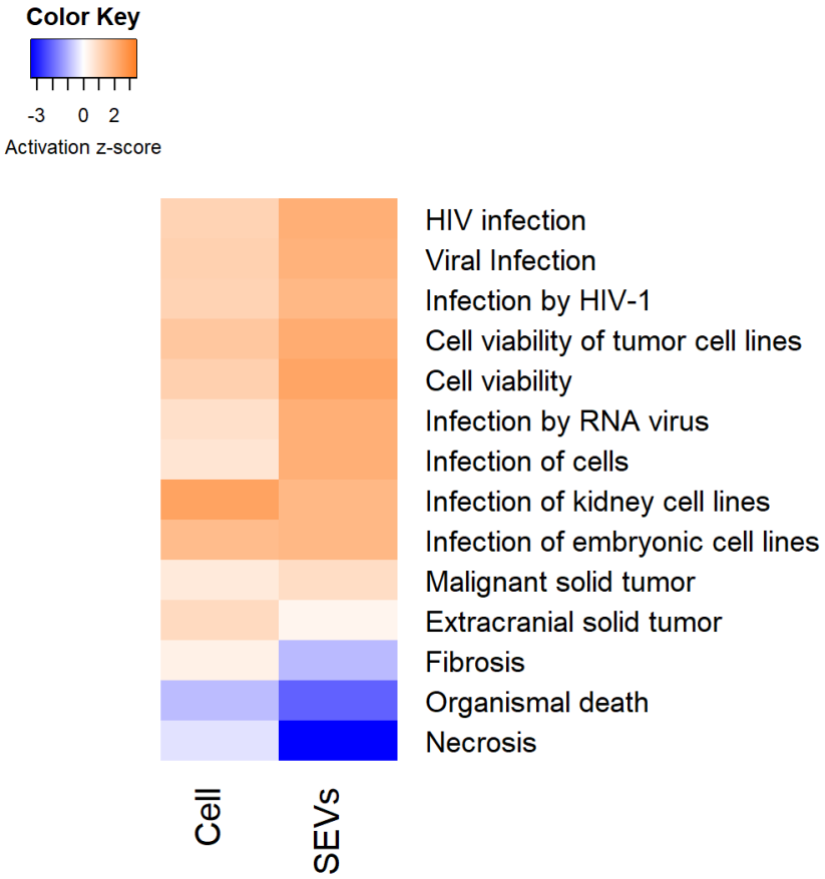


**Figure 3.5.** Heatmap of the top diseases and functions with calculatable z-scores in paired 5 $\mu M$ arsenic exposure SVHUC1 cell lysate and SEV samples


**Figure 3.6.** Heatmap of the top diseases and functions with calculatable z-scores in paired T24 cell lysate and SEV samples.

## 3.4. Discussion

### 3.4.1. Proteomics Analysis

The analysis of paired cell and SEV samples is not commonly done but has the potential to show the differential packaging of SEV cargo and assess how representative SEVs are of their parent cells. Based on the revised unsupervised principal component analysis there was obvious grouping within conditions and similar proportions of variance attributed to arsenic exposure groups (8.5%) and different cell lines (48.5%) as was apparent in the previous SEV assessment. Comparing the principal component analysis there was greater variation observed between the 1 and 2 $\mu M$ exposure groups and the control group than was present in the previous SEV analysis. As cell lysate samples contained a great number of proteins than SEVs (1923 vs 1408), there were more potential opportunities to assess variance between samples.

### 3.4.2. Canonical Pathway Analysis

The results of the cell lysate canonical analysis revealed expression of pathways typically related to arsenic exposure, including xenobiotic metabolism, protein ubiquitination, oxidative phosphorylation, and mitochondrial dysfunction expressed in all samples. One of the major toxic effects of arsenic is the inhibition of mitochondrial enzymes and uncoupling of oxidative phosphorylation caused by oxidative stress and the binding of arsenic with important thiol groups (Ming Tam et al., 2020). As discussed in the previous chapter, protein misfolding resulting in increased protein ubiquitination is another common effect of exposure as arsenic can bind with important cysteine thiol groups of proteins inhibiting spontaneous oxidative protein folding (Jacobson et al., 2012; Ramadan et al., 2009). Proteasomal changes were evident in both

cell lysate and SEV samples. However other hallmarks of arsenic exposure, including oxidative stress and xenobiotic metabolism were not apparent in the previous SEV analysis.

### 3.4.3. Function and Disease Annotations

For the analysis of each exposure group there were a variety of diseases and functions predicted to be significantly activated and inactivated. Though the exact diseases and functions varied the overall trends were in the activation of tumour formation, cell viability, proliferation, and infection with an inactivation of organismal death observed following arsenic exposure. These once again represent many of the hallmarks of cancer that may indicate early changes in cells capable of leading to cancer (Hanahan & Weinberg, 2011). The results of the heat map constructed of all diseases and functions with calculatable z-scores in all groups showed similarities between arsenic exposure and T24 cells. All three exposure groups and the T24 positive control for carcinogenicity detail an activation of four disease groups responsible for malignant and solid tumors. Contrastingly, functions related to infection were activated in exposure groups and inactivated in T24 cells and functions related to cell death were inactivated in exposure groups but activated in T24 cells.

### 3.4.4. SEV and Cell Lysate Comparative Analysis

Comparative analysis of diseases and functions activation in the 5 $\mu M$ exposure cell and SEV samples showed many similarities to one another. From those diseases and functions with calculable z-scores all showed similar activation and inactivation states between SEV and cell samples with the activation of infection, viability, and solid tumors and the inactivation of organismal death and necrosis. This direct comparability indicates that following exposure SEVs

may be used to determine the functional and disease changes occurring in their parent cells. The study of SEVs over cell samples is preferred in human health biomonitoring as cells are invasive to collect and often require surgical biopsies, whereas SEVs can be harvested from a wide variety of biological samples such as blood and urine (Smalley et al., 2008; Panfoli, 2017). The results of the T24 comparative functional analysis showed greater variance between cell and SEV samples, which may complicate the direct extrapolation of SEVs to cell samples. There was similar activation of many cancer related functions between SEV and cell lysate samples including metastasis, cell movement, solid tumor, and cell death. However, major differences arose in the predicted activation of cell viability, infection, and other cancer and non-cancer related diseases. Without any overarching trend in the diseases and functions altered between T24 cell and SEV samples it is hard to say whether the differences can be attributed to the selective packaging of SEV cargo or are the result of protein loss following chemical cell dissociation. To discern the potential reasons for the observed functional differences it would be beneficial to compare SEV samples with cells that have been physically detached or are free in suspension rather than adherent to prevent any protein loss.

## 3.5 Conclusion

The research objective in chapter three was to investigate the changes in intracellular proteomics following arsenic exposure to determine how different SEVs are from their parent cells. The results of this investigation showed that cell lysate analysis captured many of the expected changes following arsenic exposure that SEVs did not, including functions related to oxidate damage, mitochondrial function, and xenobiotic metabolism. Furthermore, this deviation was also observed in many of the non-cancer related diseases expressed in T24 cells. These

differences in expression between paired samples may be explained by the differential packaging of protein cargo into SEVs for the purpose of intracellular communication. Additionally, SEVs house mainly membrane associated proteins which may have been lost in the present cell lysate analysis. The differential packaging of cargo into SEVs is still widely understudied and further analysis may provide a more concrete explanation as to why select pathways in SEVs and cell lysate samples diverge. Despite some differences, all the diseases and functions with calculatable z-scores in both arsenic SEV and cell lysate samples showed similar trends in activation. The cell lysate analysis corroborated the previous predicted activation of functions responsible for cell survival, viability, and migration and inactivation of cell death and necrosis following arsenic exposure. These results indicate that the diseases and functions of SEVs from arsenic exposed cells appear to be representative of the changes occurring in their parent cells. The present comparative analysis is not commonly done in the study of SEVs and a paired sampling technique has never been examined in SEVs released following chemical exposure. This study highlighted the importance of examining both SEVs and their origin cells when possible to obtain a more encompassing view of the effects of chemical exposure and provide a basis for the functionality of SEVs in toxic responses.

## 3.6 References

Chen, S. H., Wang, Y. W., Hsu, J. L., Chang, H. Y., Wang, C. Y., Shen, P. T., Chiang, C. W., Chuang, J. J., Tsai, H. W., Gu, P. W., Chang, F. C., Liu, H. S., & Chow, N. H. (2010). Nucleophosmin in the pathogenesis of arsenic-related bladder carcinogenesis revealed by quantitative proteomics. *Toxicology and Applied Pharmacology*, *242*(2), 126–135. https://doi.org/10.1016/J.TAAP.2009.09.016

Chen, Y. T., Ou Yang, W. T., Juang, H. H., Chen, C. L., Chen, H. W., Tsui, K. H., Chang, Y. H., Tsai, C. H., Hsueh, C., & Liao, W. C. (2020). Proteomic characterization of arsenic and cadmium exposure in bladder cells. *Rapid Communications in Mass Spectrometry*, *34*. https://doi.org/10.1002/RCM.8578

Cox, J., Neuhauser, N., Michalski, A., Scheltema, R. A., Olsen, J. v, & Mann, M. (2011). Andromeda: A Peptide Search Engine Integrated into the MaxQuant Environment. *J. Proteome Res*, *10*, 20. https://doi.org/10.1021/pr101065j

Hanahan, D., & Weinberg, R. A. (2011). Hallmarks of cancer: The next generation. *Cell*, *144*(5), 646–674. https://doi.org/10.1016/J.CELL.2011.02.013/ATTACHMENT/3F528E16-8B3C-4D8D-8DE5-43E0C98D8475/MMC1.PDF

Huang, D. W., Sherman, B. T., & Lempicki, R. A. (2009). Systematic and integrative analysis of large gene lists using DAVID bioinformatics resources. *Nature Protocols*, *4*(1), 44–57. https://doi.org/10.1038/NPROT.2008.211

Jacobson, T., Navarrete, C., Sharma, S. K., Sideri, T. C., Ibstedt, S., Priya, S., Grant, C. M., Christen, P., Goloubinoff, P., & Tamá, M. J. (2012). Arsenite interferes with protein folding and triggers formation of protein aggregates in yeast. *Journal of Cell Science*, *125*, 5073–5083. https://doi.org/10.1242/JCS.107029

Kreimer, Simion, Ivanov, A. (2018). Rapid Isolation of Extracellular Vesicles from Blood Plasma with Size-Exclusion Chromatography Followed by Mass Spectrometry-Based Proteomic Profiling. *Methods in Molecular Biology*, 295–302. https://doi.org/10.1007/978-1-4939-7253-1

Ming Tam, L., Price, N. E., & Wang, Y. (2020). Molecular Mechanisms of Arsenic-Induced Disruption of DNA Repair. *Cite This: Chem. Res. Toxicol*, *2020*, 709–726. https://doi.org/10.1021/acs.chemrestox.9b00464

Ortiz, P. A., Wallace, K., & Winnik, W. (2007). Proteomic profiling of cultured human bladder cells after trivalent arsenical exposures. *The FASEB Journal*, *21*(6), A1003–A1003. https://doi.org/10.1096/FASEBJ.21.6.A1003

Panfoli, I. (2017). Cancer exosomes in urine: A promising biomarker source. *Translational Cancer Research*, *6*, 1389–1393. https://doi.org/http://dx.doi.org/10.21037/tcr.2017.10.17

Ramadan, D., Rancy, P. C., Nagarkar, R. P., Schneider, J. P., & Thorpe, C. (2009). Arsenic(III) species inhibit oxidative protein folding in vitro. *Biochemistry*, *48*(2), 424–432. https://doi.org/10.1021/BI801988X

Sherman, B. T., Hao, M., Qiu, J., Jiao, X., Baseler, M. W., Lane, H. C., Imamichi, T., & Chang, W. (2022). DAVID: a web server for functional enrichment analysis and functional annotation of gene lists (2021 update). *Nucleic Acids Research*. https://doi.org/10.1093/NAR/GKAC194

Shurtleff, M. J., Temoche-Diaz, M. M., Karfilis, K. V., Ri, S., & Schekman, R. (2016). Y-box protein 1 is required to sort microRNAs into exosomes in cells and in a cell-free reaction. *ELife*, *5*,1–23. https://doi.org/10.7554/eLife.19276

Shurtleff, M. J., Yao, J., Qin, Y., Nottingham, R. M., Temoche-Diaz, M. M., Schekman, R., & Lambowitz, A. M. (2017). Broad role for YBX1 in defining the small noncoding RNA

composition of exosomes. *Proceedings of the National Academy of Sciences of the United States of America*, *114*(43), 8987–8995. https://doi.org/10.1073/pnas.1712108114

Smits, A. (2021, November 21). *Introduction to DEP*. https://bioconductor.org/packages/devel/bioc/vignettes/DEP/inst/doc/DEP.html

St-Pierre, C., Brochu, S., Vanegas, J. R., Dumont-Lagacé, M., Lemieux, S., & Perreault, C. (2013). Transcriptome sequencing of neonatal thymic epithelial cells. *Scientific Reports*, *3*(1), 1–10. https://doi.org/10.1038/srep01860

Théry, C., Witwer, K. W., Aikawa, E., Alcaraz, M. J., Anderson, J. D., Andriantsitohaina, R., Antoniou, A., Arab, T., Archer, F., Atkin-Smith, G. K., Ayre, D. C., Bach, J. M., Bachurski, D., Baharvand, H., Balaj, L., Baldacchino, S., Bauer, N. N., Baxter, A. A., Bebawy, M., … Zuba-Surma, E. K. (2018). Minimal information for studies of extracellular vesicles 2018 (MISEV2018): a position statement of the International Society for Extracellular Vesicles and update of the MISEV2014 guidelines. *Journal of Extracellular Vesicles*, *7*(1). https://doi.org/10.1080/20013078.2018.1535750

Välikangas, T., Suomi, T., & Elo, L. L. (2018). A systematic evaluation of normalization methods in quantitative label-free proteomics. *Briefings in Bioinformatics*, *19*(1), 1. https://doi.org/10.1093/BIB/BBW095

# Chapter 4: Investigation of TGFBR1 and RNH1 as urinary SEV biomarkers of arsenic exposure

Nicole Washuck[1], Janet Cheung[1], Emmanuel Yumvihoze[1], and Laurie H.M. Chan[1]

[1]Department of Biology, University of Ottawa, Ottawa, Ontario, Canada

### *Author Contributions*

Nicole Washuck: conceptualization, methodology, sample collection and preparation, data analysis, and manuscript preparation

Janet Cheung: creatinine analysis

Emmanuel Yumvihoze: chemical analysis

Hing Man Chan: conceptualization

## 4.1. Introduction

Biomarkers are an essential staple in human health risk assessment. A biomarker of exposure relates to the direct measurement of chemicals in biological samples such as blood and urine to characterize human exposure. A biomarker of effect may include the quantification of other molecules in biological samples typically related to physiological processes that are predicted to be altered by chemical exposure or related to a disease outcome (Lowry, 1995). Urine provides an ideal source for the quantification of these biomarkers as it is minimally invasive to collect and released in high volumes. Urine is also an ideal source for SEVs that are secreted directly from the urinary bladder epithelial lining and is readily examined for effect biomarkers of urological diseases. Urinary SEVs have been reported to be stable in samples stored at -80C for up to four years showing minimal changes in SEV concentration, morphology, and RNA yield (Barreiro et al., 2021). The high stability of SEVs is mainly attributed to their lipid membrane which protects the encased molecules from degradation (Boukouris & Mathivanan, 2015).

Arsenic is one of the ten chemicals of major public health concern set by the World Health Organization resulting in global efforts to monitor high risk populations and reduce exposure (WHO, 2018). Despite the widely studied epidemiological effects of arsenic exposure there are still a lack of biomarkers of effect capable of indicating adverse health risks. Based upon the previous assessment of SEV proteins following urothelial cell arsenic exposure, an increase of SEV transforming growth factor beta receptor 1 (TGFBR1) and a decrease of ribonuclease inhibitor 1 (RNH1) have been proposed as novel effect biomarkers. These two biomarkers were selected based upon their significant up and downregulation in multiple exposure groups and based upon their biological relevance in cancer.

TGFBR1 is a transmembrane serine/threonine kinase receptor for the transforming growth factor beta (TGF-$\beta$) superfamily of signaling ligands. TGFBR1 forms a heterodimeric complex with TGFB2 that binds TGF-$\beta$ proteins which include the suppressor of mothers against decapentaplegic (SMAD) family of proteins (Lin et al., 2017). TGF-$\beta$ family proteins have been shown to regulate the generation and function of different types of immune cells as well as serving roles in cell differentiation and the health of tissues (Batlle & Massagué, 2019; de Caestecker et al., 2000; Vargas & Varga, 2002). Together this has led to the use of TGF-$\beta$ associated proteins as biomarkers of fibrosis and cancer. In a recent meta-analysis, the TGF-$\beta$/Smad pathway was examined for its bidirectional regulation during arsenic exposure. This analysis of 47 articles found that low dose arsenic exposure activates the TGF-$\beta$/Smad pathway and induced fibrosis whereas, high-dose arsenic exposure may inhibit this pathway (J. Dai et al., 2019b).

RNH1/angiogenin inhibitor 1 is a cytosolic protein that is induced by angiogenin to protect RNA against invading ribonucleases and oxidative damage. During homeostasis, angiogenin is found in the nucleus promoting ribosomal RNA transcription. Under cell stress, angiogenin will translocate to the cytosol and cleave transfer RNA into fragments, inhibiting protein synthesis (Sarangdhar & Allam, 2021). When localized in the cytosol, RNH1 has been shown to inhibit angiogenin, protecting against tumor-induced angiogenesis and growth (J. X. Chen et al., 2005). RNH1 overexpression in bladder cancer cells inhibited the epithelial-to-mesenchymal transition reducing cancer cell growth and invasion (Yao et al., 2013). Furthermore, RNH1 has been shown to be downregulated in colorectal cancer and overexpression is indicative of a good prognosis

(Y. Tang et al., 2015). These relationships have resulted in decreased levels of RNH1 being a suspected prognostic marker for urological cancers. There are currently no human studies detailing the relationship between arsenic exposure and RNH1 expression.

The aim of this study is to evaluate SEV derived TGFBR1 and RNH1 as prospective biomarkers of effect related to urinary arsenic levels and other chemicals of potential concern (cadmium and lead). Given the biological importance of these proteins and the proven regulation of TGFBR1 by arsenic, this study has the potential to discover novel minimally invasive biomarkers of adverse health effects related to arsenic exposure.

## 4.2. Methods

### 4.2.1. Ethics

This study is approved by the Health Sciences and Sciences Research Ethics Board of the University of Ottawa (http://research.uottawa.ca/ethics/reb) and the Aurora College Research Ethics Committee. In addition, the study has been granted a Scientific Research License from the Aurora Research Institute in Northwest Territories. Individual Participation in the study was voluntary and based on informed written consent following an oral and written explanation of each project component.

### 4.2.2. Study Area and Population

The samples used in this study were collected in Yellowknife, Northwest Territories, Canada. In Yellowknife there is a high geological presence of arsenopyrite and a legacy of arsenic contamination left behind by regional mining activities including Giant and Con Mine (Cheung

et al., 2020). Giant Mine which was once the largest gold mine in Canada closed in 2004 and during its 50 years of operation produced 237,000 tonnes of arsenic trioxide waste which is now being stored in underground chambers. Despite the mines closure, there are still concerns of chemical contamination originating from historical aerial deposition and ground water runoff (Chan et al., 2020). The Yellowknife Health Effects Monitoring Program (YKHEMP) was established in 2017 to assess the impact Giant Mine and remediation efforts have on the residents of Dettah, Ndilǫ, and Yellowknife including members of the Yellowknife Dene First Nation (YKDFN) and North Slave Métis Alliance (NSMA). A total of 2037 individuals aged 3-79 participated in the baseline study. Recruitment of the baseline cohort occurred over two sampling waves; the first wave was from September-December 2017, and the second wave was from April to June 2018. A more complete breakdown of the study cohort is published in the YKHEMP Cohort Profile (Chan et al., 2020).

### 4.2.3. Urine Sample Collection and Storage

Participants were asked to refrain from consuming shellfish and fish for a minimum of 2 days prior to urine collection. Seafood is a common dietary source of arsenic exposure that has been documented to spike urine arsenic level readings resulting in exaggerated exposure levels (Cheung et al., 2020). Additionally, participants were asked to provide first morning void (first urine upon waking) samples for analysis. Urine samples collected from 2017 and 2018 sampling years were refrigerated and shipped to the University of Ottawa where they were then aliquoted for respective analysis. 10 mL of urine collected from each participant was set aside for future SEV research and has been stored at -80C since 2017 or 2018.

### 4.2.4. Participant Sample Selection

A total of 2037 individuals participated in the YKHEMP in wave 1 (2017) and wave 2 (2018) sample collection periods. Of these participants, 1966 provided urine samples. Participants in Indigenous groups, including the Yellowknife Dene First Nations (YKDFN) (n = 194) and North Slave Metis Alliance (NSMA) (n = 46) and participants greater then 55 years of age or less than 35 years of age were (n = 1064) were excluded from this analysis. Out of the remaining 662 participants, 95 were excluded for having urinary arsenobetaine (AsB) concentrations greater than 10 $\mu g/L$ as these participants were suspected to have elevated urinary arsenic attributed to fish and shellfish consumption prior to sample collection. Next participants who actively smoke (n = 100), are pregnant (n = 11), or who have or have had cancer (n = 16) were excluded from analysis leaving 440 eligible study participants. The remaining participants were divided into three quartiles based in total inorganic urinary arsenic levels. 12 participants from each quartile (Q1: <25%, Q2:>25 and <75%, and Q3:>75%) were randomly selected matching individual sex (i.e., 6 male and 6 female) and wave 1 or wave 2 sample collection dates (i.e., 6 from wave 1 and 6 from wave 2) for a total of 36 participants. A full breakdown of inclusion and exclusion criteria is available in **Figure 4.1**.

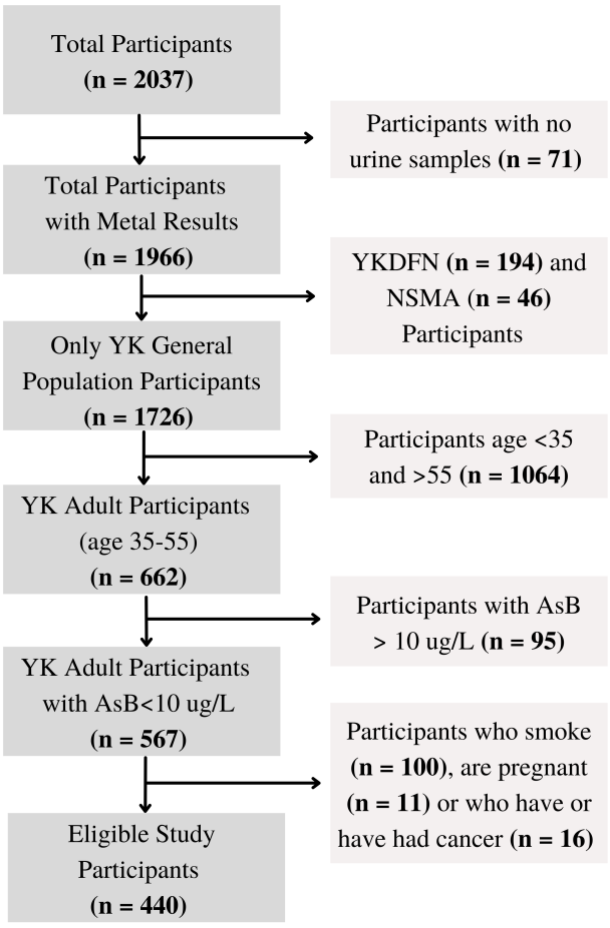


**Figure 4.1.** Participant exclusion flow chart for the selection of eligible study participants.

## 4.2.5 Laboratory Analysis

Laboratory analysis of chemicals and urine creatinine was completed upon sample collection in the 2017 and 2018 sampling waves. 10 mL aliquots of urine samples were stored at -80c until ELISA biomarker analysis.

### *4.2.5.1. Urinary Analysis of Arsenic and Other Metals*

The chemical analysis was performed at the University of Ottawa in the Laboratory for the Analysis of Natural and Synthetic Environmental Toxicants. Total arsenic and other metals including Cadmium (Cd) and Lead (Pb) were measured using inductively coupled plasma mass

spectrometry (ICP-MS) (7700x ICP-MS, Agilent Technologies, Mississauga, ON). An Agilent ASX-500 was used as an ICP-MS autosampler. Urine arsenic species including arsenite ($As^{III}$), arsenate ($As^{V}$), monomethylarsonic acid (MMA), dimethylarsenic acid (DMA), and arsenobetaine (AsB) were analyzed by inductively coupled plasma mass spectrometry (ICP-MS) (7700x ICP-MS, Agilent Technologies, Mississauga, ON) coupled to liquid chromatography (LC). For chromatographic separation of $As^{III}$, $As^{V}$, MMA, DMA, urine samples were diluted in 10 $mM$ ammonium phosphate dibasic (Sigma, 37998-100G) prepared in Milli-Q water and pH adjusted to 8.25 with ammonium hydroxide solution 28% (Sigma, 338818-100mL). Arsenic species were measured with an Agilent 1200 Infinity Liquid Chromatography (LC) coupled to an Agilent 7700x ICP-MS (Agilent Technologies, Mississauga, ON). The injection volume was 100 $\mu L$ and the mobile phase was delivered at 1 mL/min. The limit of detection (LOD) for was 0.005 $\mu g/L$ for arsenic species, 0.001 $\mu g/L$ for total arsenic, 0.007 $\mu g/L$ for cadmium, 0.02 $\mu g/L$ for lead. Concentrations under the LOD were replaced with half the LOD (Cheung et al., 2020).

#### *4.2.5.2. Creatinine Analysis*

Creatinine had previously been analyzed for all YKHEMP participants as a biomarker of kidney function and as an indicator of hydration and urine dilution. For this analysis urine samples were diluted 10 times in ultrapure water and measured using a urinary creatinine detection kit (Thermo Fisher Scientific, EIACUN). Absorbance was measured at a wavelength of 500 nm using a Biotek Cytation 3 imaging reader (BioTek Instrument, Inc.). The lower limit of detection for creatinine analysis was 0.3 $mg/dL$. Urinary concentrations of arsenic species ($As^{III}$, $As^{V}$, MMA, DMA, arsenobetaine), other metals (Cd and Pb), and protein biomarkers (TGFBR1 and RNH1) are displayed with and without creatinine adjustment.

#### *4.2.5.3. Biomarker Analysis*

Isolated SEVs from adult participant urine samples (n=36) were analyzed for TGFBR1 (Antibodies-online, ABIN6970804) and RNH1 (ExpressBio, XPEH1611) using sandwich enzyme linked immunosorbent assay (ELISA) kits. Prior to analysis, SEV samples were mixed with 10% NP-40 buffer (ThermoFischer Scientific, FN0021) and sonicated three times at 3-minute intervals with intermediate incubation on ice for SEV membrane lysis as outlined by Lässer et al., 2012. Preliminarily experiments were conducted to optimize SEV lysis and protein extraction using various concentrations of NP-40 buffer. Samples were analyzed according to the manufacturer's instructions and absorbance was read at a wavelength of 450 nm using a Biotek Cytation 3 imaging reader (BioTek Instrument, Inc.). The lower limit of detection of each kit was 31.25 $pg/mL$ and 0.313 $pg/mL$ for TGFBR1 and RNH1, respectfully. All effect biomarker concentrations were converted to $\mu g/L$ for analysis. CurveExpert Professional Version 2.7.3 was used to plot the standard curves of both RNH1 and TGFBR1 as per manufacture's recommendations. All possible linear and non-linear regressions were run and the model providing the highest $R^2$ value was selected for each standard curve.

### 4.2.6. Urine SEV Isolation

Ten milliliters of frozen urine sample were thawed overnight at 4℃. All successive centrifuging was completed in a Beckman Coulter Optima XL-100K Ultracentrifuge at 4℃ (SWFF Ti rotor, Beckman Coulter) (**Figure 4.2**). Samples were first centrifuged at 3,000 g for 10 minutes. Pellets were discarded and the supernatant was centrifuged at 17,000 g for 20 minutes. Next, pellets were discarded, and the supernatant was centrifuged at 200,000 g for 1 hour to pellet SEVs. Supernatant was discarded and SEVs were resuspended in 4.5 mL PBS. 200 mg/mL of dithiothreitol (DTT) (ThermoFischer Scientific, R0862) was then added to reduce free proteins

and remove the highly abundant urinary Tamm-Horsfall protein that can complex with SEVs decreasing their overall sample yield and purity (Gonzales et al., 2009; Wachalska et al., 2016; Z. Wang et al., 2012). Resuspended pellets mixed with DTT were incubated at 37℃ for 10 minutes at a shaking frequency of 450 rpm. Lastly, samples were centrifuged at 200,000 g for 1 hour and pellets were resuspended in 120 $\mu L$ PBS for analysis.

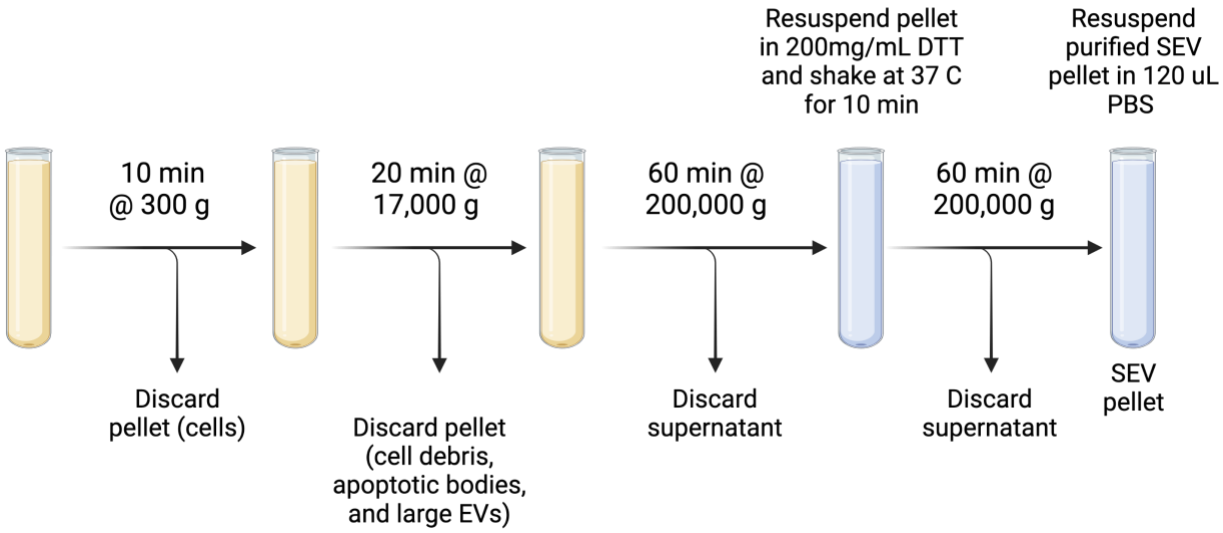


**Figure 4.2.** Differential ultracentrifugation method for the isolation of urine small extracellular vesicles (SEVs). Created with BioRender.com.

## 4.2.7. Urinary SEV Characterization

### *4.2.7.1. Nanoparticle Tracking Analysis*

Four samples, two from the 2017 sampling year and two from the 2018 sampling year were used to determine average SEV size and concentration for each quartile (n=12). 3000 X dilutions of samples in PBS were run through the ZetaView nanoparticle microscope PMS-110 (Particle Matrix) for determination of SEV concentration and size distribution. For analysis the size detection range was set from 10-500 nm and the minimum brightness was set to 15. 102 nm

polystyrene beads (Microtrac, 900383) were used to focus the instrument and sample size distribution was detected at 85 and 40 camera shutter speeds. Welch's t-test was used to determine if there were any significant differences in SEV size or concentration between sampling years.

#### *4.2.7.2. Exo-check Antibody Array*

Exo-check antibody arrays (Systems Bioscience, EXORAY200B-4) were used to confirm the origin of SEV populations by detecting 8 known SEV markers (CD63, CD81, ALIX, FLOT1, EpCam, ICAM1, ANXA5, and TSG101). Additionally, GM130 cis-Golgi marker was analyzed to determine the extent of cellular contamination in SEV samples. Briefly, 90 mL of pooled urine samples were used for SEV isolation. Isolated SEVs were loaded onto gel membranes and antibody staining was conducted in accordance to manufacture instructions (System Biosciences, 2021). Advansta WesternBright Sirius HRP Substrate (Advansta, K12043-C20) was used to develop the blots. Imaging was done on the UVP ChemStudio PLUS Imaging System, Analytik Jena, with CCD camera and automatic exposure.

### 4.2.8 SEV Protein Content

Pierce BCA Protein Assay Kit (Thermo Fischer, 23227) was used to measure the total protein content of urine SEV samples. 8 $\mu L$ of sample (Unknown, Bovine Serum Albumin (BSA) standard or PBS) was added to 2 $\mu L$ of RIPA buffer (ThermoFischer Scientific, 89900) with dissolved Pierce protease inhibitor mini tablet (ThermoFischer Scientific, A32953) and sonicated three times at 3-minute intervals with intermediate incubation on ice for SEV membrane lysis (Lässer et al., 2012). The samples were then incubated at 60 ℃ for 1 hour. 2 $\mu L$ of sample was then added to Nanodrop 2000 Spectrophotometer (ThermoFischer Scientific, ND-2000) and

absorbance was read at a wavelength of 560 nm. PBS was used as the reference buffer and BSA was used to produce the standard curves required for protein content determination. A new standard curve was constructed for each batch of samples analyzed. All samples were analyzed in triplicates and the average protein concentration was reported.

### 4.2.9 Statistical Analysis

Statistical analysis was performed using R studio (Version 1.4.1103 © 2009-2021 "Wax Begonia"). Total urinary inorganic arsenic (uiAs) was calculated by the sum of urinary inorganic arsenic species ($As^{III}$ and $As^{V}$) and their metabolites (MMA and DMA). Descriptive statistics for arsenic species ($As^{III}$, $As^{V}$, MMA, DMA, uiAs, AsB), creatinine, other metals (Pb and Cd), and protein biomarkers (TGFBR1 and RNH1) were calculated. Normality of the urine data was assessed using the Shapiro-Wilk normality test. All urinary measurements (chemicals and biomarkers) were log transformed prior to regression analysis. The use of creatinine adjustment as a means of normalizing urinary SEV biomarkers is widely debated (Tonomura et al., 2015; Blijdorp et al., 2021a; Fernández-Llama et al., 2010; Gheinani et al., 2018). For this analysis, data is presented with and without creatinine adjustment and the use of creatinine adjustment is further explored using SEV concentration and biomarker concentration regression analysis.

Association between effect (TGFBR1 and RNH1) and exposure (arsenic and other metals) biomarkers as well as other potential effect modifiers (age and sex) was assessed using Welch's t-test. For statistical significance, $\alpha < 0.05$ was used. Simple and multivariable linear regressions were used to assess the relationship between exposure and effect biomarkers. For multivariable linear regression age and sex were used. Box plot analysis and Welch's t-test was used to

determine if effect biomarkers were significantly different between the previously defined urinary arsenic quartiles of low (<25$^{th}$ percentile), medium (25$^{th}$-75$^{th}$ percentile), and high (>75$^{th}$ percentile) uiAs concentrations (n=12 per quartile).

## 4.3. Results

### 4.3.1. Population Characteristics

Characteristics of the 36 participants included in this study are described in **Table 4.1** showing arithmetic mean (AM) and standard deviation (SD) for continuous variables (age and years spent living in Yellowknife) and sample size and percentage for categorical variables (gender and past smoking status). Furthermore, the urinary concentration of arsenic species, other metals, creatinine, and effect biomarkers are summarized in **Table 4.2**.

**Table 4.1.** Characteristics of the included study participants (n=36) with arithmetic mean (AM) and standard deviation (SD) provided for continuous variables and number (n) and percentage (%) of participants provided for categorical variables.

| **Variable** | | **AM (SD) / n (%)** |
|---|---|---|
| Age (years) | | 44.7 (5.7) |
| Sex | *Male* | 18 (50%) |
| | *Female* | 18 (50%) |
| Years spent living in YK | | 17(11) |
| Past smoker | *Yes* | 17 (47.2%) |
| | *No* | 19 (52.8%) |

**Table 4.2.** Concentrations of chemical and protein biomarkers in the study population (n=36) provided as the arithmetic mean (AM) and geometric mean (GM) with appropriate standard deviations (SD) as well as the median, minimum, and maximum concentrations.

| Biomarker | | AM (SD) | GM (SD) | Median | Min-Max |
|---|---|---|---|---|---|
| **Metals (μg/L)** | *Cadmium (Cd)* | 0.28 (0.26) | 0.19 (2.48) | 0.18 | 0.02-1.22 |
| | *Lead (Pb)* | 0.70 (0.61) | 0.50 (2.31) | 0.50 | 0.12-2.54 |
| **Arsenic Species (μg/L)** | *Arsenobetaine (AsB)* | 2.02 (2.01) | 1.09 (3.69) | 1.37 | 0.03-8.17 |
| | *Arsenite ($As^{III}$)* | 0.36 (0.44) | 0.17 (4.37) | 0.21 | 0.00-2.04 |
| | *Arsenate ($As^{V}$)* | 0.56 (0.41) | 0.37 (2.96) | 0.54 | 0.04-1.50 |
| | *Dimethylarsenic acid (DMA)* | 5.20 (3.91) | 3.95 (2.18) | 4.44 | 0.80-18.35 |
| | *Methylarsonic acid (MMA)* | 0.73 (0.74) | 0.30 (6.68) | 0.52 | 0.00-2.76 |
| | *Total inorganic arsenic (uiAs)* | 6.86 (4.88) | 5.32 (2.11) | 5.69 | 1.30-22.86 |
| **Creatinine (mg/dL)** | | 120.45(51.01) | 110.27(1.55) | 119.05 | 36.90-256.90 |
| **Effect Biomarkers (pg/mL)** | *TGFBR1* | 62.02 (21.99) | 58.37 (1.43) | 60.23 | 29.30-110.74 |
| | *RNH1* | 0.020 (0.038) | 0 (0) | 0.01 | 0.00-0.14 |

## 4.3.2. Urinary SEV Characterization

### *4.3.2.1. Nanoparticle Tracking Analysis*

Based on the results of the Welch's t-test, sampling year did not have a significant effect on SEV concentration (p-value = 0.2735) or SEV size (p-value = 0.7229). The average size of urinary SEVs was 116 nm based on median estimates with size ranging from 91-140 nm and the average concentration of particles per mL was $1.84 \times 10^{10}$ with concentration ranging from $4.10 \times 10^{9}$ to $5.30 \times 10^{10}$ (n = 12) (**Figure 4.3**). Furthermore, regression analysis relating particle

concentration to urine creatinine concentration did not show a significant correlation (p-value = 0.900) (**Appendix Figure 4.1**).

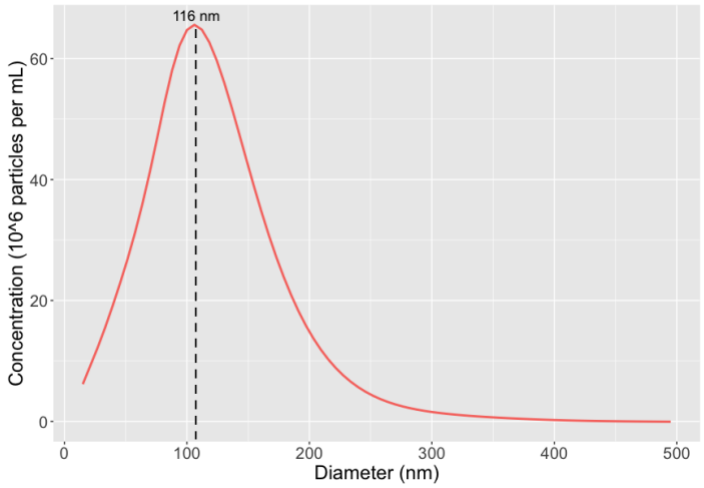


**Figure 4.3.** Nanoparticle tracking analysis results of urine SEV size and concentration characterization averaged across replicates (n=12).

### *4.3.2.2 Exo-check Antibody Array*

The Exo-Check analysis showed no signs of cell contamination as golgi matrix protein 130 (GM130) was absent in urine SEV samples (**Figure 4.4**). Furthermore, there was no expression of epithelial cellular adhesion molecules (EpCAM). As different concentrations of antibodies were used for each protein on the blot the overall abundance can only be determined relative to the previous cell SEV results reported in chapter 2. In comparison to the cell SEV blots there is high expression of cluster of differentiation protein 81 and 63 (CD81 and CD63). Furthermore, compared to cell SEV results the urine SEVs showed lower expression of flotillin-1 (FLOT1), Intercellular adhesion molecules 1 (ICAM), and ALG-2-interacting protein X (ALIX).

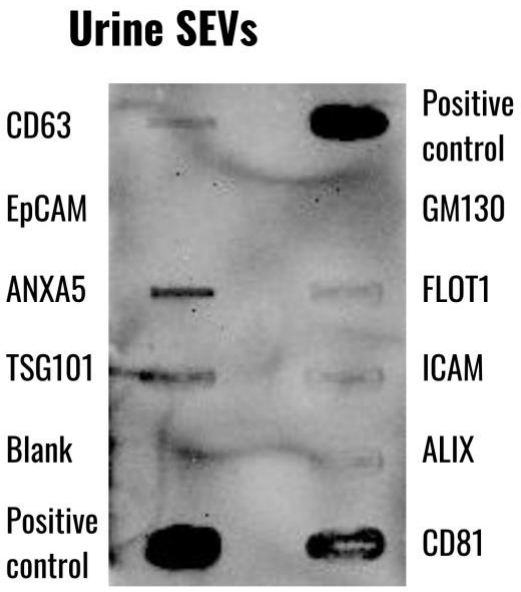


**Figure 4.4.** Exo-check array analysis of urine SEVs for 8 endosomal proteins (CD63, EpCAM, ANXA5, TSG101, FLOT1, ICAM, ALIX, and CD81) and one cell contamination protein (GM130).

#### *4.3.2.3. Protein Content*

The results of the Urine SEV BCA show high protein concentrations compared to the purified cell media SEV samples which may indicate contaminating urinary proteins (**Table 4.3**).

**Table 4.3** BCA analysis of the total protein concentration in urine SEV samples divided by inorganic arsenic exposure quartiles.

| Sample | Average protein in SEVs ($\mu g/mL$) |
|---|---|
| **Quartile 1** | $4.469 \pm 4.300$ |
| **Quartile 2** | $2.867 \pm 10.880$ |
| **Quartile 3** | $1.661 \pm 1.206$ |

### 4.3.4. TGFBR1 ELISA

The standard curve plotted for TGFBR1 best fit a Rational model ($R^2 = 0.9998$) and thus this model was used to determine the concentration of TGFBR1 in each sample based on measured absorbance values (**Appendix Figure 2.3**).

#### *4.3.4.1. Urine SEVs*

**Assessing Normality**

Before determining if data needed to be log transformed, normality of the effect and exposure biomarkers was assessed using a Shapiro Wilk test for quantitative analysis. All the conducted Shapiro Wilk tests except for TGFBR1 (p-value = 0.07) showed significant (p-value < 0.001) deviation from normality (**Appendix Table 4.2**). Therefore, data were not normally distributed and were log-transformed prior to analysis for normalization.

**Urine Creatinine Adjustment**

Based on the current literature there is no consensus on whether creatinine adjustment is an appropriate method for urinary SEV biomarker normalization (Tang et al., 2015). We further explored this method of normalization by relating measured creatinine levels with the concentration of urinary SEVs as determined by nanoparticle tracking analysis (**Figure 4.5**). The results show no correlation between urine creatinine levels and total SEV counts (particles per mL) (p-value = 0.900) (**Table 4.4**). Furthermore, there was a positive correlation between urine creatine and TGFBR1 levels, however, this was not a significant association (p-value = 0.068, $R^2$ = 0.068) (**Appendix Figure 4.2** and **Appendix Table 4.3**).

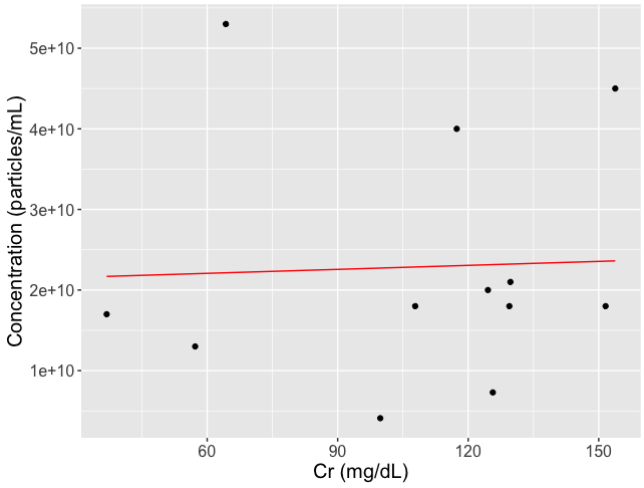


**Figure 4.5.** Univariate regression correlation of particle counts with urine creatinine concentration (n=12).

**Table 4.4.** Regression statistics for the correlation of particle counts with urine creatinine concentration (n=12)

| | **SEV Concentration** | | | |
|---|---|---|---|---|
| | **Model 1** | | **Model 2** | |
| **Variable** | $\beta$ | P value | $\beta$ | P value |
| Intercept | 2.108e+10 | 0.179 | 1.153e+11 | 0.224 |
| Cr | 1.648e+07 | 0.900 | -1.261e+08 | 0.546 |
| Age | | | -1.912e+09 | 0.255 |
| Sex | | | 1.949e+09 | 0.860 |
| Adjusted $R^2$ | -0.098 | | -0.1404 | |
| P value | 0.900 | | 0.6631 | |

**TGFBR1 and Exposure Biomarkers**

Regression analysis was performed using both a univariate model (model 1) and a multivariate model (model 2) that considered age and sex as covariates. TGFBR1 was positively correlated with inorganic arsenic levels with a p-value of 0.066 for univariate analysis (**Figure 4.6 and**

**Table 4.5**). The strength of the correlation decreased following creatinine adjustment but still had a positive regression slope. Other nephrotoxic metals including lead and cadmium that had been previously measured in the urine samples were correlated with TGFBR1 to see if similar relationships were present. TGFBR1 levels had no correlation with the concentration of urinary lead (**Appendix Figure 4.3** and **Appendix Table 4.4**) but did show a significant (P-value = 0.022) positive correlation with urinary cadmium (**Figure 4.7** and **Table 4.6**). Finally urinary inorganic arsenic and cadmium were run together in the same model to determine if this would make for a stronger model than assessing each exposure biomarker separately (**Table 4.7**). From this analysis, it was found that incorporating cadmium into the model provided a stronger correlation with a greater $R^2$ value than when assessing the relationship of inorganic arsenic alone (p-value = 0.059, $R^2$ =0.107).

In addition to the regression analysis, the concentration of TGFBR1 was assessed between the three arsenic exposure quartiles using a boxplot analysis and Welch's t-test for significance (**Figure 4.8**). These results also display that TGFBR1 is elevated in higher exposure quartiles, with a significant (p-value = 0.027) increase in TGFBR1 between the first and second exposure quartile.

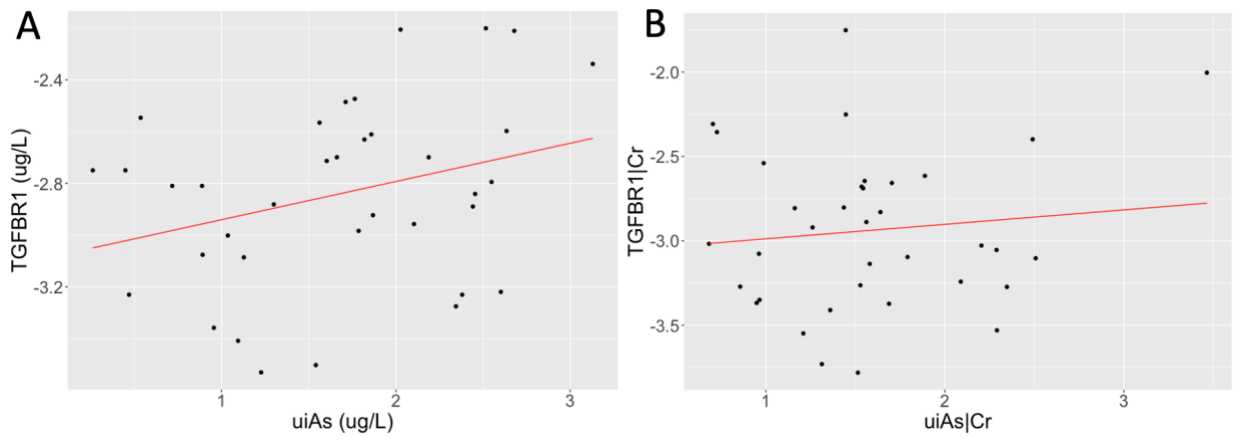


**Figure 4.6.** Univariate regression analysis of (A) log transformed SEV derived TGFBR1 against log transformed urinary inorganic arsenic without creatinine adjustment and (B) log transformed SEV derived TGFBR1 against log transformed urinary inorganic arsenic with creatinine adjustment.

**Table 4.5.** Model regression statistics of the association of SEV derived TGFBR1 with urinary inorganic arsenic using both univariate (Model 1) and multivariate (Model 2) models displayed with and without creatinine adjustment following log transformation.

| | **uiAs** | | | | **Creatinine adjusted uiAs** | | | |
|---|---|---|---|---|---|---|---|---|
| | **Model 1** | | **Model 2** | | **Model 1** | | **Model 2** | |
| **Variable** | *β* | P value | *β* | P value | *β* | P value | *β* | P value |
| Intercept | -3.088 | **<0.001** | -3.410 | **<0.001** | -3.074 | **<0.001** | -3.758 | **<0.001** |
| Log(uiAs) | 0.148 | 0.066 | 0.177 | **0.041** | 0.0858 | 0.526 | 0.122 | 0.429 |
| Age | | | 0.010 | 0.345 | | | 0.012 | 0.455 |
| Sex | | | -0.127 | 0.273 | | | 0.064 | 0.698 |
| Adjusted $R^2$ | 0.069 | | 0.0769 | | -0.017 | | -0.056 | |
| P value | 0.066 | | 0.138 | | 0.526 | | 0.768 | |

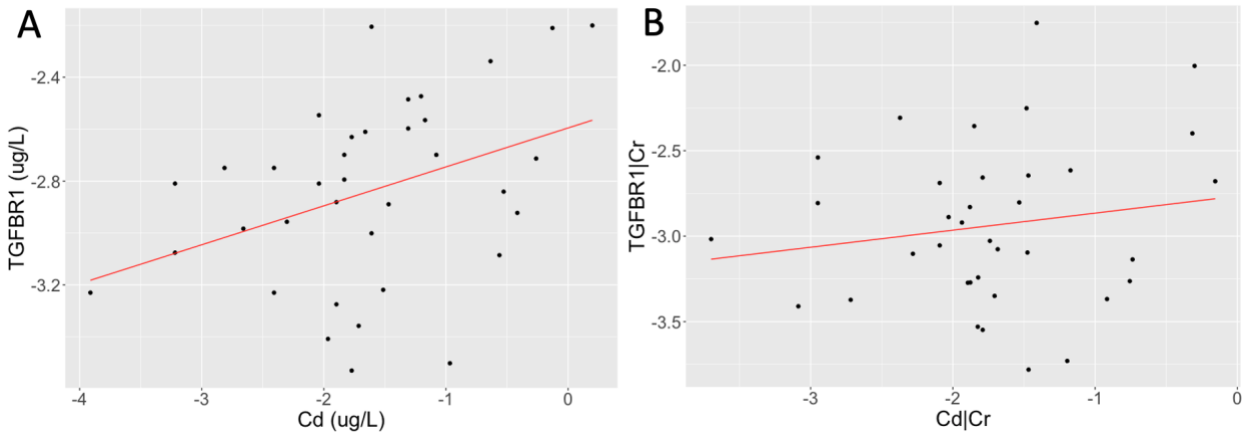


**Figure 4.7.** Univariate regression analysis of (A) log transformed SEV derived TGFBR1 against log transformed urinary cadmium without creatinine adjustment and (B) log transformed SEV derived TGFBR1 against log transformed urinary cadmium with creatinine adjustment.

**Table 4.6.** Model regression statistics of the association of SEV derived TGFBR1 with urinary cadmium using both univariate (Model 1) and multivariate (Model 2) models displayed with and without creatinine adjustment following log transformation.

| | **Cd** | | | | **Creatinine adjusted Cd** | | | |
|---|---|---|---|---|---|---|---|---|
| | **Model 1** | | **Model 2** | | **Model 1** | | **Model 2** | |
| **Variable** | *β* | P value | *β* | P value | *β* | P value | *β* | P value |
| Intercept | -2.595 | **<0.001** | -2.283 | **<0.001** | -2.766 | **<0.001** | -3.758 | **<0.001** |
| Log(Cd) | 0.150 | **0.022** | 0.162 | **0.015** | 0.100 | 0.339 | 0.122 | 0.429 |
| Age | | | -0.001 | 0.923 | | | 0.012 | 0.455 |
| Sex | | | -0.167 | 0.146 | | | 0.064 | 0.698 |
| Adjusted $R^2$ | 0.121 | | 0.126 | | -0.002 | | -0.056 | |
| P value | **0.022** | | 0.063 | | 0.339 | | 0.768 | |

**Table 4.7.** Model regression statistics of the association of TGFBR1 with both urinary inorganic arsenic and cadmium (model 1) as well as with age and sex as covariates (model 2) displayed with and without creatinine adjustment.

| | **uiAs and Cd** | | | | **Creatinine adjusted uiAs and Cd** | | | |
|---|---|---|---|---|---|---|---|---|
| | **Model 1** | | **Model 2** | | **Model 1** | | **Model 2** | |
| **Variable** | $\beta$ | P value | $\beta$ | P value | $\beta$ | P value | $\beta$ | P value |
| Intercept | -2.753 | **<0.001** | -2.643 | **0.002** | -2.854 | **<0.001** | -3.459 | **0.004** |
| Log(iAs) | 0.064 | 0.495 | 0.068 | 0.539 | 0.042 | 0.775 | 0.087 | 0.625 |
| Log(Cd) | 0.120 | 0.129 | 0.126 | 0.152 | 0.087 | 0.446 | 0.054 | 0.677 |
| Age | | | 0.003 | 0.806 | | | 0.009 | 0.601 |
| Sex | | | -0.157 | 0.177 | | | 0.047 | 0.784 |
| Adjusted $R^2$ | 0.107 | | 0.109 | | -0.029 | | -0.084 | |
| P value | 0.059 | | 0.1087 | | 0.611 | | 0.861 | |

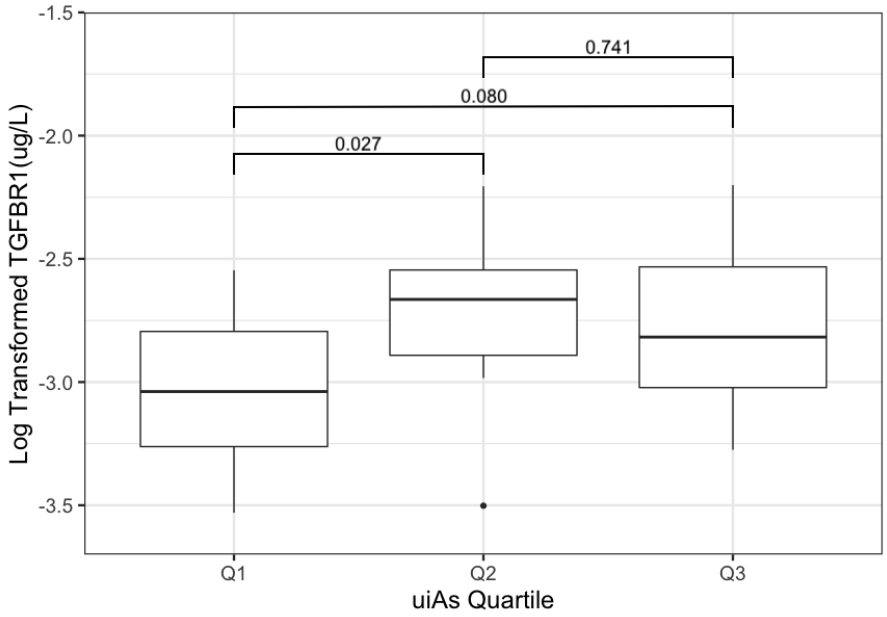


**Figure 4.8.** Box plot analysis of log TGFBR1 concentrations in urine SEV samples in each exposure quartile (Q1: <25$^{th}$ percentile, Q2: 25$^{th}$ – 75$^{th}$ percentile, Q3: >75$^{th}$ percentile) with Welch's t-test results.

### 4.3.5. RNH1 ELISA

The standard curve plotted for RNH1 best fit a Rational model ($R^2 = 0.9999$) and thus, this model was used to determine the concentration of RNH1 in each sample based on measured absorbance values (**Appendix Figure 2.4**).

#### *4.3.5.1. Urine SEVs*

Urinary concentrations of RNH1 were below the lower limit of detection (0.313 $pg/mL$) in all urine SEV samples examined. Therefore, RNH1 was not further examined as a candidate urinary SEV biomarker of arsenic induced urological injury.

## 4.4. Discussion

### 4.4.1. SEV Characterization

Despite the wide use of SEVs as clinical disease biomarkers, this is one of the few studies that has measured SEV biomarkers as a tool in in human health exposure risk assessment. The initial characterization of urine SEVs in this study provided evidence to support that the EVs examined did fall into the SEV characterization. Looking more closely at specific endosomal protein markers, CD81 and CD63 showed higher expression in urinary SEVs than in the previously characterized cell SEV samples. The exact composition of typical SEV biomarkers can vary between the types of media examined (e.g. urine vs cell media) as well as between the types of secreting cells (e.g. urothelial vs stem cell) so it is not surprising that the composition of their endosomal markers would vary (Doyle & Wang, 2019). Furthermore, the effect of long-term storage at -80℃ has been shown to affect the composition of endosomal biomarkers in urine samples. Zhou et al., 2006, found that following storage at -80℃ many endosomal proteins were

conserved almost completely, however, some such as ALIX degraded following storage. This study also noted the importance of extensive vortexing following the thawing of urine samples as was done during sample preparation in the present study (Zhou et al., 2006). A recent genetic analysis of urinary SEVs determined that SEVs had mainly tissue-specific genes for the bladder with high genetic specificity to urothelial (or 'endothelial') cells (Zhu et al., 2021). Nevertheless, our results demonstrate the applicability of urine SEVs as biomarkers.

### 4.4.2 Urinary SEV Normalization

Creatinine is a waste product formed from muscle metabolism that is excreted in high volumes through glomerular filtration at a relatively consistent rate. The normalization process with creatinine involves dividing the urinary biomarker concentration by the total concentration of urinary creatinine to get the amount of biomarker per milligram of creatinine (Wagner et al., 2010). There are, however, several challenges that may hinder the applicability of creatinine normalization. First, urinary creatinine varies by gender, age, and dietary protein consumption which may result in its use biasing the interpretation of the biomarker analysis (Barr et al., 2005; Neubert & Remer, 1998). Secondly, the applicability of creatinine normalization for SEV biomarkers is further debated as there is no consensus on whether the concentration of urine creatinine is proportional to the concentration of urinary SEVs. In the present literature there are studies that use urine creatinine adjustment (Blijdorp et al., 2021b; Mizutani et al., 2019) and studies that do not (Gheinani et al., 2018) or use a different variable for adjustment such as total protein (Fernández-Llama et al., 2010) or particle count (Oosthuyzen et al., 2013). We further calculated total urinary SEV protein concentrations but found higher concentrations than anticipated based on cell SEV samples. These high concentrations were likely due to the highly

abundant urinary Tamm Horsfall protein, which often poses an issue in urinary SEV research (Fernández-Llama et al., 2010). Because of the contaminating Tamm Horsfall protein and high variance in calculated urinary protein concentration the total protein content could not be used for effect biomarker normalization. Blijdorp et al. (2021b) found that urine particle and creatinine concentrations were highly correlated ($R^2$=0.96), showing promise as a method of biomarker normalization. However, in the present study there was no apparent correlation between particle and creatinine concentration ($R^2$ = -0.098, p-value = 0.900). Similarly, Gheinani et al. (2018) found that using urinary creatinine for SEV normalization can lead to bias in the results interpretation, as they did not find any correlation between SEV cargo and creatinine concentration. In the present analysis we also compared urine creatinine to concentrations of the TGFBR1 effect biomarker and did not see a significant correlation, however there was a positive association. Lastly, elevated creatinine is commonly used as an indicator of negative kidney health (Lopez-Giacoman & Madero, 2015). The present study examined the relation of effect biomarkers with several nephrotoxic chemicals (inorganic arsenic, cadmium, and lead) but as creatinine is predicted to increase with elevated metal exposure its use in normalization may bias the interpretation of the effect biomarker data (Orr & Bridges, 2017). Altogether, the results of the present study suggest that urine creatinine may not be a reliable method of urinary SEV biomarker normalization for the present samples and thus the urine results were presented both with and without creatinine adjustment.

### 4.4.3. Population Exposure Assessment

Based on the most recent Canadian Health Measures Survey (CHMS) data (2018-2019) which also measured inorganic arsenic as the sum of urinary metabolites ($iAs^{III}$ + $iAs^{V}$ + MMA + DMA), the geometric mean of exposure was 5.5 $\mu g/L$ in the Canadian general population

(Health Canada, 2021a). In the present study, the geometric mean of arsenic exposure was comparable at 5.32 $\mu g/L$ urine. Using the quartile approach the individuals included in quartile three all had exposure levels greater than the mean of the Canadian general population with exposure ranging from 6.83 to 22.86 $\mu g/L$ urine. In the most recent CHMS (2018-2019), which only measured blood and not urine cadmium, the geometric mean of exposure was 0.25 $\mu g/L$ blood (Health Canada, 2021b). Comparatively, the geometric mean of urinary cadmium in the present study group was 0.19 $\mu g/L$ urine with a maximum concentration of 1.22 $\mu g/L$ urine reported. Lastly, in the most recent CHMS (2018-2019) which only measured blood and not urinary lead, the geometric mean was 0.82 $\mu g/L$ blood (Health Canada, 2021c). Comparatively, the geometric mean of urinary lead in our study group was 0.50 $\mu$g/L urine with a maximum concentration of 2.54 $\mu$g/L urine. Therefore, our examined population had exposure levels comparable to or below the Canadian general population for the examined chemicals with some individuals having elevated arsenic exposure as was selected for in our quartile study design.

### 4.4.4 TGFBR1 Effect Biomarker

Concentrations of TGFBR1 were positively correlated with both urinary inorganic arsenic and cadmium concentrations, with no association with urinary lead. In fact, urinary cadmium had the strongest relationship with TGFBR1 with a significant p-value in the univariate model (p-value = 0.022) and an $R^2$ of 0.121. In a model including both urinary inorganic arsenic and cadmium as covariates in TGFBR1 expression, the model neared significance (p-value = 0.059) with an $R^2$ of 0.107. Furthermore, based on the initial quartile design, a boxplot analysis of TGFBR1 expression in the three inorganic arsenic quartiles revealed elevated expression in both quartile 2 ($25^{th}$-$75^{th}$ percentile) and quartile 3 ($75^{th}$ – $100^{th}$ percentile) in comparison to the lowest exposure

quartile. As discussed, TGFB family proteins have previously been observed to be upregulated during low-dose arsenic exposure but as these proteins are related to fibrosis, they have also been positively associated with cadmium exposure. In a study assessing the effects of low-dose chronic cadmium exposure on mouse liver metabolism, researchers found that TGFBR1 was significantly increased (LFC = 1.2, P-value = 0.04) in the cadmium exposure group (Go et al., 2015). Another study found that TGFB1 enhanced cytotoxicity through increasing intracellular cadmium accumulation in vascular endothelial cells (Ito et al., 2021). Lastly, genes associated with the TGFB pathway were shown to increase in cadmium treated trophoblasts and were similarly associated with rates of preeclampsia, which is a complication during pregnancy that may be caused by kidney damage (Brooks et al., 2016). Overall, the effect of creatinine adjustment weakened the correlation between effect and exposure markers, but a positive slope remained when assessing the association of adjusted TGFBR1 with adjusted urinary arsenic and cadmium. Altogether, these results suggest that TGFBR1 may be a promising biomarker for assessing the impact of arsenic and cadmium exposure on the urinary tract with further research required to decipher the role of TGFBR1 in urothelial injury and fibrosis.

### 4.4.5. RNH1 Effect Biomarker

RNH1 was also assessed as a potential effect biomarker in this study with predicted downregulation during exposure. However, RNH1 had low expression in all urine SEV samples which fell below the limit of detection of the ELISA. Therefore, future studies in the Yellowknife Health Effects Monitoring Program and other arsenic exposure studies should focus efforts on TGFBR1 and the development of further SEV biomarkers.

### 4.4.6. Urinary SEV Biomarkers

ELISA proved to offer a high throughput analysis tool for the measurement of SEV markers, however, more work is required to standardize SEV isolation and protein extraction protocols before it may be implemented as common practice in human health risk assessment. The present study implemented differential ultracentrifugation for SEV isolation as it is the gold standard for SEV isolation and is reported to be used in over 60% of all SEV related publications returning high sample yield and purity (Théry et al., 2018). This approach may be cost effective given access to an ultracentrifuge, but it is highly labour intensive and does not offer the high throughput required for implementation into large scale risk assessment efforts. Other isolation techniques including on bead precipitation and ultrafiltration may reduce the isolation time however further work is needed to standardize these methods (Cheruvanky et al., 2007; P. Li et al., 2017).

## 4.5 Conclusion

The research objective in chapter 4 was to assess SEV derived biomarkers of urothelial health in relation to urinary arsenic concentrations to establish their applicability as novel effect biomarkers. In this study TGFBR1 and RNH1 were examined as potential biomarkers in urine SEV samples collected from participants of the YKHEMP. Overall, the results of this study showed that TGFBR1 has greater promise as an effect biomarker compared to RNH1. RNH1 could not be measured above the limit of detection in urine samples. TGFBR1 showed promising results as a urinary biomarker as it was measurable in all samples and positively associated with both urinary inorganic arsenic and cadmium concentrations. The future considerations of TGFBR1 as an effect biomarker of arsenic exposure should include increasing samples sizes to

capture the heterogeneity of human populations. This investigation serves as one of few studies analyzing SEVs as biomarkers in human health risk assessment despite their widespread clinical applications. Urinary SEVs show promise as effect biomarkers as they can be collected in a minimally invasive manner, have a high stability in stored samples, and can protect sensitive genetic cargo that would otherwise be degraded in whole urine analysis. The present pilot study suggests that TGFBR1 shows promising prospects as a biomarker of urothelial health in relation to inorganic arsenic as well as cadmium exposure.

## 4.6 References


Barr, D. B., Wilder, L. C., Caudill, S. P., Gonzalez, A. J., Needham, L. L., & Pirkle, J. L. (2005). Urinary creatinine concentrations in the U.S. population: implications for urinary biologic monitoring measurements. *Environmental Health Perspectives*, *113*(2), 192–200. https://doi.org/10.1289/EHP.7337

Barreiro, K., Dwivedi, O. P., Valkonen, S., Groop, P. H., Tuomi, T., Holthofer, H., Rannikko, A., Yliperttula, M., Siljander, P., Laitinen, S., Serkkola, E., af Hällström, T., Forsblom, C., Groop, L., & Puhka, M. (2021). Urinary extracellular vesicles: Assessment of pre-analytical variables and development of a quality control with focus on transcriptomic biomarker research. *Journal of Extracellular Vesicles*, *10*(12). https://doi.org/10.1002/JEV2.12158

Batlle, E., & Massagué, J. (2019). Transforming Growth Factor-β Signaling in Immunity and Cancer. *Immunity*, *50*(4), 924–940. https://doi.org/10.1016/J.IMMUNI.2019.03.024

Tonomura, Y., Matsubara, M., & Kazama, I. (2015). Biomarkers in Urine and Use of Creatinine. *General methods in biomarker research as their applications.* 165-186. https://doi.org/10.1007/978-94-007-7696-8_18

Blijdorp, C. J., Tutakhel, O. A. Z., Hartjes, T. A., van den Bosch, T. P. P., van Heugten, M. H., Rigalli, J. P., Willemsen, R., Musterd-Bhaggoe, U. M., Barros, E. R., Carles-Fontana, R., Carvajal, C. A., Arntz, O. J., van de Loo, F. A. J., Jenster, G., Clahsen-Van Groningen, M. C., Cuevas, C. A., Severs, D., Fenton, R. A., van Royen, M. E., … Hoorn, E. J. (2021a). Comparing approaches to normalize, quantify, and characterize urinary extracellular vesicles. *Journal of the American Society of Nephrology*, *32*(5), 1210–1226. https://doi.org/10.1681/ASN.2020081142/-/DCSUPPLEMENTAL

Blijdorp, C. J., Tutakhel, O. A. Z., Hartjes, T. A., van den Bosch, T. P. P., van Heugten, M. H., Rigalli, J. P., Willemsen, R., Musterd-Bhaggoe, U. M., Barros, E. R., Carles-Fontana, R., Carvajal, C. A., Arntz, O. J., van de Loo, F. A. J., Jenster, G., Clahsen-Van Groningen, M. C.,

Cuevas, C. A., Severs, D., Fenton, R. A., van Royen, M. E., … Hoorn, E. J. (2021b). Comparing approaches to normalize, quantify, and characterize urinary extracellular vesicles. *Journal of the American Society of Nephrology*, *32*(5), 1210–1226. https://doi.org/10.1681/ASN.2020081142/-/DCSUPPLEMENTAL

Boukouris, S., & Mathivanan, S. (2015). Exosomes in bodily fluids are a highly stable resource of disease biomarkers. *PROTEOMICS – Clinical Applications*, *9*(3–4), 358–367. https://doi.org/10.1002/PRCA.201400114

Brooks, S. A., Martin, E., Smeester, L., Grace, M. R., Boggess, K., & Fry, R. C. (2016). miRNAs as common regulators of the transforming growth factor (TGF)-β pathway in the preeclamptic placenta and cadmium-treated trophoblasts: Links between the environment, the epigenome and preeclampsia. *Food and Chemical Toxicology: An International Journal Published for the British Industrial Biological Research Association*, *98*, 50–57. https://doi.org/10.1016/J.FCT.2016.06.023

Chan, H. M., Hu, X. F., Cheung, J. S., Parajuli, R. P., Rosol, R., Yumvihoze, E., Williams, L., & Mohapatra, A. (2020). Cohort profile: Cohort profile: health effects monitoring programme in Ndilǫ, Dettah and Yellowknife (YKHEMP). *BMJ Open*, *10*(9). https://doi.org/10.1136/BMJOPEN-2020-038507

Chen, J. X., Gao, Y., Liu, J. W., Tian, Y. X., Zhao, J., & Cui, X. Y. (2005). Antitumor effects of human ribonuclease inhibitor gene transfected on B16 melanoma cells. *The International Journal of Biochemistry & Cell Biology*, *37*(6), 1219–1231. https://doi.org/10.1016/J.BIOCEL.2004.11.020

Cheruvanky, A., Zhou, H., Pisitkun, T., Kopp, J. B., Knepper, M. A., Yuen, P. S. T., & Star, R. A. (2007). Rapid isolation of urinary exosomal biomarkers using a nanomembrane ultrafiltration concentrator. *American Journal of Physiology - Renal Physiology*, *292*(5). https://doi.org/10.1152/ajprenal.00434.2006

Cheung, J. S. J., Hu, X. F., Parajuli, R. P., Rosol, R., Torng, A., Mohapatra, A., Lye, E., & Chan, H. M. (2020). Health risk assessment of arsenic exposure among the residents in Ndilǫ, Dettah, and Yellowknife, Northwest Territories, Canada. *International Journal of Hygiene and Environmental Health*, *230*. https://doi.org/10.1016/J.IJHEH.2020.113623

Dai, J., Xu, M., Zhang, X., Niu, Q., Hu, Y., Li, Y., & Li, S. (2019). Bi-directional regulation of TGF-β/Smad pathway by arsenic: A systemic review and meta-analysis of in vivo and in vitro studies. *Life Sciences*, *220*, 92–105. https://doi.org/10.1016/J.LFS.2019.01.042

de Caestecker, M. P., Piek, E., & Roberts, A. B. (2000). Role of Transforming Growth Factor-β Signaling in Cancer. *JNCI: Journal of the National Cancer Institute*, *92*(17), 1388–1402. https://doi.org/10.1093/JNCI/92.17.1388

Doyle, L. M., & Wang, M. Z. (2019). Overview of Extracellular Vesicles, Their Origin, Composition, Purpose, and Methods for Exosome Isolation and Analysis. *Cells*, *8*(7). https://doi.org/10.3390/CELLS8070727

Fernández-Llama, P., Khositseth, S., Gonzales, P. A., Star, R. A., Pisitkun, T., & Knepper, M. A. (2010). Tamm-Horsfall protein and urinary exosome isolation. *Kidney International*, *77*(8), 736–742. https://doi.org/10.1038/KI.2009.550

Gheinani, A. H., Vögeli, M., Baumgartner, U., Vassella, E., Draeger, A., Burkhard, F. C., & Monastyrskaya, K. (2018). Improved isolation strategies to increase the yield and purity of human urinary exosomes for biomarker discovery. *Scientific Reports 2018 8:1*, *8*(1), 1–17. https://doi.org/10.1038/s41598-018-22142-x

Go, Y. M., Sutliff, R. L., Chandler, J. D., Khalidur, R., Kang, B. Y., Anania, F. A., Orr, M., Hao, L., Fowler, B. A., & Jones, D. P. (2015). Low-Dose Cadmium Causes Metabolic and Genetic Dysregulation Associated With Fatty Liver Disease in Mice. *Toxicological Sciences*, *147*(2), 524–534. https://doi.org/10.1093/TOXSCI/KFV149

Gonzales, P. A., Pisitkun, T., Hoffert, J. D., Tchapyjnikov, D., Star, R. A., Kleta, R., Wang, N. S., & Knepper, M. A. (2009). Large-Scale Proteomics and Phosphoproteomics of Urinary Exosomes. *Journal of the American Society of Nephrology*, *20*(2), 363–379. https://doi.org/10.1681/ASN.2008040406

Health Canada. (2021a). *Arsenic in Canadians*. https://www.canada.ca/en/health-

Health Canada. (2021b). *Cadmium in Canadians*. https://www.canada.ca/en/health-

Health Canada. (2021c). *Lead in Canadians*. https://www.canada.ca/en/health-

Ito, K., Fujie, T., Shimomura, M., Nakano, T., Yamamoto, C., & Kaji, T. (2021). TGF-β 1 Potentiates the Cytotoxicity of Cadmium by Induction of a Metal Transporter, ZIP8, Mediated by the ALK5-Smad2/3 and ALK5-Smad3-p38 MAPK Signal Pathways in Cultured Vascular Endothelial Cells. *International Journal of Molecular Sciences*, *23*(1). https://doi.org/10.3390/IJMS23010448

Lässer, C., Eldh, M., & Lötvall, J. (2012). Isolation and Characterization of RNA-Containing Exosomes. *Journal of Visualized Experiments: JoVE*, *59*, 1–6. https://doi.org/10.3791/3037

Li, P., Kaslan, M., Lee, S. H., Yao, J., & Gao, Z. (2017). Progress in Exosome Isolation Techniques. *Theranostics*, *7*(3). https://doi.org/10.7150/thno.18133

Lin, E., Kuo, P. H., Liu, Y. L., Yang, A. C., & Tsai, S. J. (2017). Transforming growth factor-β signaling pathway-associated genes SMAD2 and TGFBR2 are implicated in metabolic syndrome in a Taiwanese population. *Scientific Reports 2017 7:1*, *7*(1), 1–8. https://doi.org/10.1038/s41598-017-14025-4

Lopez-Giacoman, S., & Madero, M. (2015). Biomarkers in chronic kidney disease, from kidney function to kidney damage. *World Journal of Nephrology*, *4*(1), 57. https://doi.org/10.5527/WJN.V4.I1.57

Lowry, L. K. (1995). Role of biomarkers of exposure in the assessment of health risks. *Toxicology Letters*, *77*(1–3), 31–38. https://doi.org/10.1016/0378-4274(95)03268-1

Mizutani, K., Kawakami, K., Horie, K., Fujita, Y., Kameyama, K., Kato, T., Nakane, K., Tsuchiya, T., Yasuda, M., Masunaga, K., Kasuya, Y., Masuda, Y., Deguchi, T., Koie, T., & Ito, M. (2019). Urinary exosome as a potential biomarker for urinary tract infection. *Cellular Microbiology*, *21*(7), e13020. https://doi.org/10.1111/CMI.13020

Neubert, A., & Remer, T. (1998). The impact of dietary protein intake on urinary creatinine excretion in a healthy pediatric population. *The Journal of Pediatrics*, *133*(5), 655–659. https://doi.org/10.1016/S0022-3476(98)70107-6

Oosthuyzen, W., Sime, N. E. L., Ivy, J. R., Turtle, E. J., Street, J. M., Pound, J., Bath, L. E., Webb, D. J., Gregory, C. D., Bailey, M. A., & Dear, J. W. (2013). Quantification of human urinary exosomes by nanoparticle tracking analysis. *The Journal of Physiology*, *591*, 5833. https://doi.org/10.1113/JPHYSIOL.2013.264069

Sarangdhar, M. A., & Allam, R. (2021). Angiogenin (ANG)—Ribonuclease Inhibitor (RNH1) System in Protein Synthesis and Disease. *International Journal of Molecular Sciences*, *22*(3), 1287. https://doi.org/10.3390/IJMS22031287

System Biosciences. (2021). *Exo-Check Exosome Antibody Arrays*.

Tang, K. W. A., Toh, Q. C., & Teo, B. W. (2015). Normalisation of urinary biomarkers to creatinine for clinical practice and research – when and why. *Singapore Medical Journal*, *56*(1), 7. https://doi.org/10.11622/SMEDJ.2015003

Tang, Y., Liu, P., Tian, Y., Xu, Y., Ren, F., Cui, X., & Fan, J. (2015). Overexpression of ribonuclease inhibitor defines good prognosis and suppresses proliferation and metastasis in human colorectal cancer cells via PI3K/AKT pathway. *Clinical and Translational Oncology*, *17*(4), 306–313. https://doi.org/10.1007/S12094-014-1228-0/FIGURES/4

Théry, C., Witwer, K. W., Aikawa, E., Alcaraz, M. J., Anderson, J. D., Andriantsitohaina, R., Antoniou, A., Arab, T., Archer, F., Atkin-Smith, G. K., Ayre, D. C., Bach, J. M., Bachurski, D., Baharvand, H., Balaj, L., Baldacchino, S., Bauer, N. N., Baxter, A. A., Bebawy, M., … Zuba-Surma, E. K. (2018). Minimal information for studies of extracellular vesicles 2018 (MISEV2018): a position statement of the International Society for Extracellular Vesicles and update of the MISEV2014 guidelines. *Journal of Extracellular Vesicles*, *7*(1). https://doi.org/10.1080/20013078.2018.1535750

Vargas, J., & Varga, J. (2002). Scleroderma and Smads: Dysfunctional Smad family dynamics culminating in fibrosis Scleroderma and Smads Dysfunctional Smad Family Dynamics

Culminating in Fibrosis. *Arthritis & Rheumatism*, *46*(7), 1703–1713. https://doi.org/10.1002/art.10413

Wachalska, M., Koppers-Lalic, D., van Eijndhoven, M., Pegtel, M., Geldof, A. A., Lipinska, A. D., van Moorselaar, R. J., & Bijnsdorp, I. v. (2016). Protein Complexes in Urine Interfere with Extracellular Vesicle Biomarker Studies. *Journal of Circulating Biomarkers*, *5*. https://doi.org/10.5772/62579

Wang, Z., Hill, S., Luther, J. M., Hachey, D. L., & Schey, K. L. (2012). Proteomic Analysis of Urine Exosomes by Multidimensional Protein Identification Technology (MudPIT). *Proteomics*, *12*(2), 329. https://doi.org/10.1002/PMIC.201100477

Yao, X., Li, D., Xiong, D. M., Li, L., Jiang, R., & Chen, J. X. (2013). A novel role of ribonuclease inhibitor in regulation of epithelial-to-mesenchymal transition and ILK signaling pathway in bladder cancer cells. *Cell and Tissue Research*, *353*(3), 409–423. https://doi.org/10.1007/S00441-013-1638-2/FIGURES/10

Zhou, H., Yuen, P. S. T., Pisitkun, T., Gonzales, P. A., Yasuda, H., Dear, J. W., Gross, P., Knepper, M. A., & Star, R. A. (2006). Collection, storage, preservation, and normalization of human urinary exosomes for biomarker discovery. *Kidney International*, *69*(8), 1471. https://doi.org/10.1038/SJ.KI.5000273

Zhu, Q., Cheng, L., Deng, C., Huang, L., Li, J., Wang, Y., Li, M., Yang, Q., Dong, X., Su, J., Lee, L. P., & Liu, F. (2021). The genetic source tracking of human urinary exosomes. *Proceedings of the National Academy of Sciences of the United States of America*, *118*(43). https://doi.org/10.1073/PNAS.2108876118/SUPPL_FILE/PNAS.2108876118.SD07.XLSX

# Chapter 5: General Conclusions

## 5.1 Future Directions

### *5.1.1 Future SEV investigation using a chronic exposure model*

In the present *in vitro* analysis, acute exposure over a 48-hour period was conducted to determine the changes arsenic has on SEV response in urothelial cells. As arsenic induced bladder cancer is the result of chronic low dose exposure, future investigation using a chronic exposure model would be useful to provide insight into the role SEVs have in arsenic induced carcinogenesis. Previous studies have outlined models of arsenite transformed urothelial cells typically involving chronic exposure to arsenite at concentrations below 2 $\mu M$ for up to 40 weeks (Jou et al., 2019; Mengdan et al., 2017; Su et al., 2006; Zhou et al., 2018). This chronic exposure model was outside the scope of the present investigation but has been shown to provide valuable insight into the precise mechanisms and pathways important in arsenite-induced transformation of urothelial cells. Mengdan et al. (2017) found that chronic exposure of SVHUC1 cells to 0.5 $\mu M$ $NaAsO_2$ induced Janus kinase 2/Signal transducer or activator of transcription 3 signalling pathways that through knockdown experiments proved to be pivotal in arsenite-induced cell proliferation. Furthermore, Zhou et al., 2018, found that human epidermal growth factor receptor and proto-oncogenic tyrosine protein kinase play an important role in arsenite-induced transformation of SVHUC1 cells and inhibition of human epidermal growth factor receptor 2 inhibited cell growth and migration highlighting potential therapeutic interventions to prevent malignant changes. The changes in SEVs following chronic exposure of cells of the urinary tract has never been studied but based off the current results detailing the activation of cancer associated pathways in SEVs it is likely that they would play a role in arsenite-induced cell transformation. This hypothesis could be studied through a similar SEV exposure model as was implemented in chapter 2 to

monitor proliferation rates in cells exposed to SEVs from arsenic treated cells. Similar methods have been implemented in other studies to monitor the effects incubation with cancer cell SEVs has on healthy cells (Beckham et al., 2014a; Olsen et al., 2014; Yoshida et al., 2019). Moreover, changes inflicted by SEV exposure may provide insight on the systemic effects of arsenic as SEVs serve important roles in autocrine, paracrine, and endocrine signalling.

### *5.1.2 Representative population sample sizes and advances in SEV research*

In the present study, urine samples from 36 participants of the Yellowknife Health Effects Monitoring Program were selected for SEV biomarker analysis. The results of this study revealed that SEVs are promising avenues for urine biomarker discovery even in samples that have been stored for prolonged periods of time. Despite the promising results much more work is needed to further validate the use of SEV biomarkers in human health risk assessment. To adequately represent the heterogeneity of human's larger sample sizes are required to further validate TGFBR1 as an effect biomarker. In epidemiological studies of biomarkers population composition often poses a threat to statistical power as biomarkers often have non-linear relationships with other population variables such as age, disease, and co-exposures. To account for these variations, increased sample sizes as well as multivariable analyses are necessary to capture the true applicability of proposed biomarkers (Cohen et al., 2018). The methodology laid out in the present thesis to accurately characterize and isolate urinary SEVs may be used as the groundwork for future investigations into SEVs as urinary effect biomarkers. Another important factor to consider in the applicability of human biomarkers is the ease and reproducibility of measurement.

Despite the benefits of having stable enveloped membranes and being released by all cell types SEVs are not the easiest to isolate and require characterization to accurately assess their origin and size. The method of differential ultracentrifugation used in the present study is one of the more labor-intensive methods of SEV isolation but still serves as the gold standard in the field with approximately 60% of all publications reporting its use (Théry et al., 2018). Alternative isolation procedures such as on-bead precipitation and membrane filtration techniques are available and can reduce sample processing time; however further work is required to standardize these methods (Butz et al., 2016; Cheruvanky et al., 2007). Moreover, as several SEV isolation techniques exist it is possible that different subpopulations of extracellular vesicles may be isolated when implementing different methods which can lead to poor reproducibility between studies. Takov et al. (2019) found that the functional activity of SEVs can change depending on the method of isolation used which highlights the importance of setting standard protocols for isolation and characterization before SEVs can be implemented as biomarkers in human health risk assessment.

## 5.2 Concluding Remarks

This thesis examined the application of SEVs as novel effect biomarkers and characterized their potential roles in mediating arsenic induced urothelial toxicity. The results of this thesis revealed that SEVs derived from SVHUC1 human urothelial cells are predicted to activate important cancer cell signaling and cell viability pathways during arsenic exposure. The pathways and functions predicted to be activated in SEVs following arsenic exposure shared similarities with SEVs derived from T24 urothelial carcinoma cells. Further examination of paired cell samples displayed that cell lysate analysis provides a more encompassing view of the pathways and functions altered during exposure. However, many of the important functions indicating

hallmarks of early carcinogenesis including activation of cell survival, viability, and migration signaling were conserved between SEV and cell samples. The proteomics investigation in chapters 2 and 3 supported my first hypothesis that the biology and protein packaging profile of SEVs is altered following arsenic exposure and confirmed the induction of cell stress and cancer signaling pathways. The initial proteomics analysis of SEV samples was used to identify potential candidate biomarkers and from that analysis TGFBR1 and RNH1 were further investigated in cell media and urine samples. Cell media SEV ELISA analysis of both biomarkers presented some conflicting findings in comparison to the previous proteomics investigation highlighting the need for further analysis and investigation with new methods such as western blot or flow cytometry. The chapter 3 investigation into urinary SEV biomarkers supported the second hypothesis leading this thesis work that urinary SEV proteins can be used as biomarkers of arsenic exposure. The ELISA analysis proved to be a useful tool in the assessment of urinary TGFBR1 and TGFBR1 was significantly associated with both urinary arsenic and cadmium concentrations. This thesis work adds to the growing body of evidence supporting the important roles SEVs play in chemical exposure. The present investigation will hopefully lead the way for further studies into the use of SEVs as biomarkers of exposure and bring forth the consideration of the diverse functions SEVs serve in toxic responses.

## 5.3 References

Beckham, C. J., Olsen, J., Yin, P. N., Wu, C. H., Ting, H. J., Hagen, F. K., Scosyrev, E., Messing, E. M., & Lee, Y. F. (2014). Bladder cancer exosomes contain EDIL-3/Del1 and facilitate cancer progression. *Journal of Urology*, *192*(2), 583–592. https://doi.org/10.1016/j.juro.2014.02.035

Butz, H., Nofech-Mozes, R., Ding, Q., Khella, H. W. Z., Szabó, P. M., Jewett, M., Finelli, A., Lee, J., Ordon, M., Stewart, R., Krylov, S., & Yousef, G. M. (2016). Exosomal MicroRNAs Are Diagnostic Biomarkers and Can Mediate Cell-Cell Communication in Renal Cell Carcinoma. *European Urology Focus*, *2*(2), 210–218. https://doi.org/10.1016/j.euf.2015.11.006

Cheruvanky, A., Zhou, H., Pisitkun, T., Kopp, J. B., Knepper, M. A., Yuen, P. S. T., & Star, R. A. (2007). Rapid isolation of urinary exosomal biomarkers using a nanomembrane ultrafiltration concentrator. *American Journal of Physiology - Renal Physiology*, *292*(5). https://doi.org/10.1152/ajprenal.00434.2006

Cohen, A. A., Legault, V., Fuellen, G., Fülöp, T., Fried, L. P., & Ferrucci, L. (2018). The risks of biomarker-based epidemiology: Associations of circulating calcium levels with age, mortality, and frailty vary substantially across populations. *Experimental Gerontology*, *107*, 11. https://doi.org/10.1016/J.EXGER.2017.07.011

Jou, Y. C., Wang, S. C., Dai, Y. C., Chen, S. Y., Shen, C. H., Lee, Y. R., Chen, L. C., & Liu, Y. W. (2019). Gene expression and DNA methylation regulation of arsenic in mouse bladder tissues and in human urothelial cells. *Oncology Reports*, *42*(3), 1005–1016. https://doi.org/10.3892/OR.2019.7235

Mengdan, L., Chen, W., Jieyu, L., Peiyu, J., Fei, W., & Shengnan, L. (2017). *Low concentration arsenite activated JAK2 / STAT3 signal and increased proliferative factor expressions in SV-HUC-1cells after short and long time treatment*. 2154–2162. https://doi.org/10.1002/tox.22428

Olsen, J., Flax, J., Messing, E., & Beckham, C. (2014). Bladder cancer exosomes contain tumor-associated mrna and long non-coding rna and facilitate tumor progression. *Journal of Urology*, *191*. https://doi.org/http://dx.doi.org/10.1016/j.juro.2014.02.1326

Su, P., Hu, Y., Ho, I., Cheng, Y., & Lee, T. (2006). Distinct Gene Expression Profiles in Immortalized Human Urothelial Cells Exposed to Inorganic Arsenite and Its Methylated Trivalent Metabolites. *Enviornmental Health Perspectives*, *3*, 394–403. https://doi.org/10.1289/ehp.8174

Takov, K., Yellon, D. M., & Davidson, S. M. (2019). Comparison of small extracellular vesicles isolated from plasma by ultracentrifugation or size-exclusion chromatography: yield, purity, and functional potential. *Journal of Extracellular Vesicles*, *8*(1). https://doi.org/10.1080/20013078.2018.1560809

Théry, C., Witwer, K. W., Aikawa, E., Alcaraz, M. J., Anderson, J. D., Andriantsitohaina, R., Antoniou, A., Arab, T., Archer, F., Atkin-Smith, G. K., Ayre, D. C., Bach, J. M., Bachurski, D., Baharvand, H., Balaj, L., Baldacchino, S., Bauer, N. N., Baxter, A. A., Bebawy, M., … Zuba-Surma, E. K. (2018). Minimal information for studies of extracellular vesicles 2018 (MISEV2018): a position statement of the International Society for Extracellular Vesicles and update of the MISEV2014 guidelines. *Journal of Extracellular Vesicles*, *7*(1). https://doi.org/10.1080/20013078.2018.1535750

Yoshida, K., Tsuda, M., Matsumoto, R., Semba, S., Wang, L., Sugino, H., Tanino, M., Kondo, T., Tanabe, K., & Tanaka, S. (2019). Exosomes containing ErbB2/CRK induce vascular growth in premetastatic niches and promote metastasis of bladder cancer. *Cancer Science*, *110*(7), 2119–2132. https://doi.org/10.1111/cas.14080

Zhou, Q., Jin, P., Liu, J., Wang, F., & Xi, S. (2018). HER2 and Src co-regulate proliferation, migration, and transformation by downstream signaling pathways in arsenite-treated human uroepithelial cells. *Metallomics, 10*. https://doi.org/10.1039/c8mt00131f

# Appendix

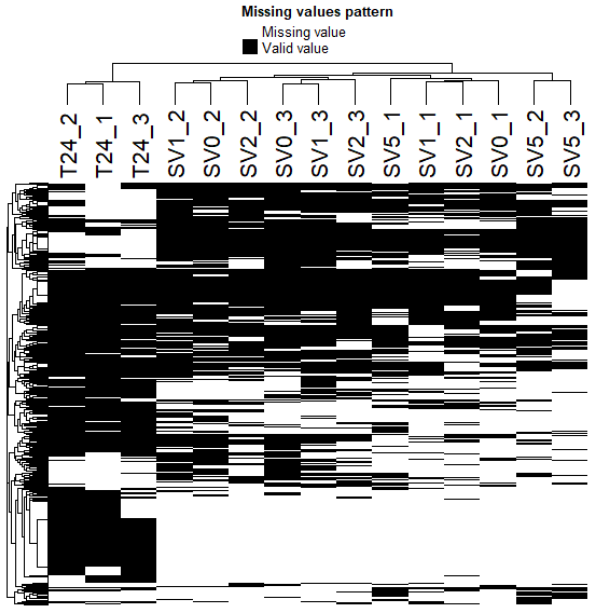


**Appendix Figure 2.1.** Heatmap with hierarchal clustering of all SEV proteins with missing values in at least one sample.

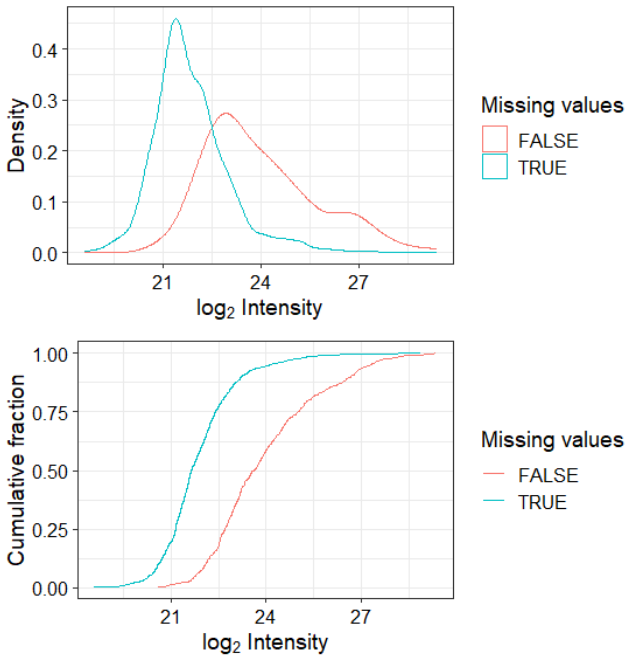

**Appendix Figure 2.2.** Intensity plots for proteins with missing and valid values based on density (top) and cumulative fraction (bottom).

**Appendix Table 2.1.** List of differentially expressed proteins shown to be upregulated in conditions versus control samples ranked based on log fold change.

| Condition | No. | Gene name | Adjusted p-value | Log Fold Change |
|---|---|---|---|---|
| SVHUC1 – 1$\mu$m | 1 | CHMP2A | 5.86E-03 | 3.71 |
| | 2 | TGFBR1 | 1.39E-11 | 3.03 |
| | 3 | NAP1L1 | 3.30E-06 | 2.86 |
| | 4 | IL10RB | 4.55E-06 | 2.68 |
| SVHUC1 – 2$\mu$m | 1 | TGFBR1 | 7.65E-09 | 3.2 |
| | 2 | NAP1L1 | 4.96E-04 | 2.86 |
| | 3 | IL10RB | 7.96E-04 | 2.65 |
| | 4 | ZDHHC5 | 2.48E-02 | 0.882 |
| SVHUC1 -5$\mu$m | 1 | LRP1 | 2.51E-03 | 6.57 |
| | 2 | C4A | 2.63E-02 | 4.78 |
| | 3 | PSMB3 | 3.33E-02 | 4.38 |
| | 4 | THBS1 | 8.58E-05 | 4.36 |
| | 5 | PXDN | 6.23E-08 | 4.07 |
| | 6 | COL6A1 | 4.89E-02 | 3.68 |
| | 7 | LAMA3 | 1.00E-07 | 3.6 |
| | 8 | MAN2B1 | 1.74E-02 | 3.05 |
| | 9 | TPP2 | 2.14E-02 | 3.01 |
| | 10 | TGFBR1 | 2.79E-05 | 2.97 |
| | 11 | PSMA1 | 2.05E-02 | 2.93 |
| | 12 | BMP1 | 5.07E-03 | 2.84 |
| | 13 | COL5A1 | 3.10E-02 | 2.65 |
| | 14 | THBS4 | 2.99E-04 | 2.48 |
| | 15 | LAMC2 | 1.94E-02 | 2.41 |
| | 16 | FN1 | 3.12E-04 | 2.37 |
| | 17 | PSMB5 | 1.55E-05 | 2.37 |
| | 18 | PSMB1 | 4.09E-03 | 2.34 |
| | 19 | PSMB2 | 2.63E-07 | 2.21 |
| | 20 | PSMA3 | 5.32E-08 | 2.16 |
| | 21 | PSMA4 | 2.26E-02 | 2.13 |
| | 22 | PSMA2 | 5.66E-05 | 2.11 |
| | 23 | CTSC | 3.99E-04 | 2.03 |
| | 24 | PSMA5 | 2.68E-05 | 1.95 |
| | 25 | PLAT | 3.38E-02 | 1.76 |
| | 26 | PSMA7 | 9.07E-06 | 1.72 |
| T24 | 1 | TAGLN | 4.28E-02 | 5.96 |
| | 2 | BASP1 | 5.13E-08 | 5.57 |
| | 3 | EPB41L2 | 2.59E-04 | 5.4 |

| | | | |
|---|---|---|---|
| 4 | CLDN11 | 2.88E-03 | 5.34 |
| 5 | DDAH1 | 3.10E-04 | 5.02 |
| 6 | PTX3 | 3.05E-04 | 4.76 |
| 7 | CD70 | 2.19E-03 | 4.68 |
| 8 | CDH2 | 1.95E-03 | 4.65 |
| 9 | GDI1 | 3.09E-02 | 4.5 |
| 10 | NQO1 | 9.41E-04 | 4.47 |
| 11 | NF2 | 8.22E-03 | 4.26 |
| 12 | SH3GL1 | 9.88E-03 | 4.14 |
| 13 | FERMT2 | 1.23E-03 | 3.84 |
| 14 | PTPRJ | 4.90E-02 | 3.72 |
| 15 | PRSS23 | 4.79E-02 | 3.46 |
| 16 | EVA1A | 1.17E-03 | 3.27 |
| 17 | ZDHHC5 | 1.60E-07 | 3.21 |
| 18 | AXL | 1.73E-02 | 3.18 |
| 19 | UAP1 | 8.07E-04 | 2.93 |
| 20 | ENG | 3.37E-02 | 2.92 |
| 21 | CSNK1G1 | 2.53E-02 | 2.9 |
| 22 | ANXA6 | 3.17E-02 | 2.8 |
| 23 | KRAS | 2.91E-02 | 2.6 |
| 24 | ITGB5 | 4.25E-02 | 2.3 |
| 25 | CD59 | 2.60E-02 | 2.07 |
| 26 | TGM2 | 1.99E-02 | 1.98 |
| 27 | ITGA6 | 2.28E-02 | 1.84 |
| 28 | MYO1C | 2.79E-02 | 1.75 |
| 29 | EPHA2 | 1.82E-02 | 1.74 |
| 30 | RRAS2 | 3.83E-02 | 1.63 |

**Appendix Table 2.2.** List of differentially expressed proteins shown to be downregulated in conditions versus control samples ranked based on log fold change.

| Condition | No. | Gene name | Adjusted p-value | Log Fold Change |
|---|---|---|---|---|
| SVHUC1 – 2$\mu$m | 1 | RNH1 | 1.46E-03 | -1.58 |
| SVHUC1 -5$\mu$m | 1 | ANXA5 | 3.38E-02 | -1.14 |
| | 2 | GNAI1 | 3.83E-03 | -1.73 |
| | 3 | GNA11 | 3.92E-03 | -2.1 |
| | 4 | SMPDL3B | 7.28E-05 | -2.91 |
| | 5 | RNH1 | 8.75E-10 | -2.99 |
| | 6 | CAPZA2 | 3.56E-02 | -3 |
| | 7 | PTPRC | 1.53E-13 | -3.54 |
| | 8 | ITGA2B | 1.53E-13 | -6.12 |
| T24 | 1 | ALDH1A3 | 3.20E-02 | -1.66 |
| | 2 | AKR1B1 | 8.66E-03 | -1.81 |
| | 3 | PDLIM1 | 9.31E-03 | -1.88 |

| | | | |
|---|---|---|---|
| 4 | ITGB4 | 6.31E-03 | -2.21 |
| 5 | TUBA4A | 3.85E-02 | -2.49 |
| 6 | F11R | 1.30E-03 | -2.52 |
| 7 | HSPB1 | 2.18E-03 | -2.69 |
| 8 | CLTC | 2.62E-02 | -2.82 |
| 9 | SLC20A1 | 3.56E-02 | -2.99 |
| 10 | SSBP1 | 9.45E-03 | -3.03 |
| 11 | ICAM1 | 1.84E-05 | -3.04 |
| 12 | HGS | 4.67E-02 | -3.17 |
| 13 | SLC26A2 | 1.25E-03 | -3.18 |
| 14 | ADAMTSL4 | 3.87E-02 | -3.21 |
| 15 | HNRNPC | 2.13E-03 | -3.21 |
| 16 | ST14 | 1.68E-03 | -3.36 |
| 17 | SMPDL3B | 3.90E-02 | -3.4 |
| 18 | NONO | 2.52E-02 | -3.42 |
| 19 | DHX9 | 2.14E-03 | -3.57 |
| 20 | HNRNPL | 3.56E-02 | -3.58 |
| 21 | OCLN | 3.94E-02 | -3.68 |
| 22 | TINAGL1 | 4.66E-02 | -3.75 |
| 23 | HNRNPU | 3.41E-03 | -3.86 |
| 24 | PROM2 | 1.37E-02 | -3.93 |
| 25 | S100A14 | 3.15E-02 | -4.01 |
| 26 | CDH1 | 1.10E-03 | -4.03 |
| 27 | STEAP4 | 3.92E-03 | -4.05 |
| 28 | DNM2 | 2.84E-03 | -4.18 |
| 29 | NID2 | 1.21E-03 | -4.26 |
| 30 | ASS1 | 3.53E-06 | -4.51 |
| 31 | FAM3C | 3.39E-03 | -4.55 |
| 32 | H2AFY | 2.26E-02 | -4.66 |
| 33 | HTRA1 | 6.77E-04 | -4.7 |
| 34 | HIST1H4A | 3.60E-02 | -4.9 |
| 35 | H2AFX | 7.19E-03 | -5.24 |
| 36 | HIST2H2AC | 3.90E-03 | -5.33 |
| 37 | CLDN7 | 5.52E-03 | -5.37 |
| 38 | CLDN4 | 1.22E-11 | -5.39 |
| 39 | H3F3A | 6.73E-03 | -5.81 |
| 40 | EEF1A2 | 9.61E-14 | -6.08 |
| 41 | H2AFV | 1.84E-03 | -6.53 |
| 42 | EPCAM | 9.61E-14 | -7.18 |
| 43 | HIST1H1B | 1.11E-03 | -7.26 |
| 44 | ITGB6 | 9.61E-14 | -8.04 |

**Appendix Table 2.3.** Biological importance and protein identification details of the eight proposed SEV biomarkers. Bolded values are those groups that show significant up or down regulation based upon a fold change >1.5 and a p-value <0.05.

| Name and UniProt accession # | Cellular location | # Unique peptides and sequence coverage | Differential expression | Predicted function (UniProt database) | Previous reports in urological disease/function | Previous reports in arsenic exposure |
|---|---|---|---|---|---|---|
| Transforming growth factor beta receptor 1 (TGFBR1) (P36897) | Plasma membrane | Unique peptides (10)<br><br>Sequence Coverage (27.8%) | **SV1: 3.03, p<0.001**<br>**SV2: 3.2, p<0.001**<br>**SV5: 2.97, p<0.001**<br>T24: 0.27, 0.904 | Molecular function: kinase, receptor, serine/threonine-protein kinase, transferase<br>Biological process: apoptosis, differentiation, growth regulation<br>Ligand: ATP-binding, magnesium, manganese, metal-binding, nucleotide-binding | Up-regulation of other components of the TGF-beta system is seen in renal fibrosis and RCC studies (Dai et al., 2019).<br><br>Prognostic marker in fibrosis and tumor microenvironment (Chung et al., 2021). | Meta-analysis showed that low does (<5uM/L) arsenic exposure up-regulated TGF-B1, whereas high doses had the tendency to downregulate. Subgroup analysis showed that low or short-term arsenic exposure induced expression of TGF-B1 and fibrosis markers (Dai et al., 2019). |
| Prolow-density lipoprotein receptor-related protein 1 (LRP1) (Q07954) | Plasma membrane, nucleus, cytoplasm, and cytosol | Unique peptides (77)<br><br>Sequence Coverage (25.3%) | SV1: 0.53, 0.984<br>SV2: 1.13, 0.977<br>**SV5: 6.57, 0.002**<br>T24: -0.40, 0.914 | Molecular function: Developmental protein, receptor<br>Biological process: Endocytosis<br>Ligand: Calcium, metal-binding | In meta-analysis of 4,629 cancer patients, LRP1 mRNA expression was correlated with decreased urothelial carcinoma patient survival (Gonias et al., 2017). | Not available |
| Peroxidasin homolog (PXDN) (Q92626) | Extracellular matrix and endoplasmic reticulum | Unique peptides (37)<br><br>Sequence Coverage (39.1%) | SV1: 0.126, 0.987<br>SV2: 1.00, 0.857<br>**SV5: 4.07, p <0.001**<br>T24: -1.13, 0.804 | Molecular function: Oxidoreductase, peroxidase<br>Biological process: Hydrogen peroxide<br>Ligand: Calcium, Heme, Iron, Metal-binding | High expression of PXDN was significantly upregulated in BC patients and was related to poor prognosis of BC (Di et al., 2019).<br><br>High expression of PXDN in ovarian cancer patients was associated with poor overall survival (Zheng & Liang, 2018). | Not available |
| Proteasome subunit beta- type 3 (PSMB3) | Nucleus and cytoplasm | Unique peptides (10) | SV1: 1.02, 0.961<br>SV2: 2.06, 0.849<br>**SV5: 4.38, 0.033** | Molecular function: Endopeptidase activity<br>Biological process: | Meta-analysis of PSMs showed that proteasome induction was involved in cancer cell resistance to environmental | Increased PSMB3 expression in immortalized human keratinocytes |

| | | | | | | |
|---|---|---|---|---|---|---|
| (P49720) | | Sequence Coverage (56.1%) | T24: 2.02, 0.829 | Proteasomal ubiquitin-independent protein catabolism<br>Proteasomal ubiquitin-dependent protein catabolism | stress and was involved with the induction of antioxidant enzymes (Voutsadakis, 2017). | exposed to 100 nM NaAsO2 for 7 weeks (Al-Eryani et al., 2017).<br><br>Transcriptomic analysis of zebrafish exposed to iAs revealed enrichment of the protein ubiquitination pathway and upregulation of PSMB3 along with other genes (Bambino et al., 2018).<br><br>Upregulation of PSMB3 in an arsenic induced cutaneous squamous cell carcinoma. Exposure to 100 nM iAs for 28-weeks (Banerjee et al., 2021). |
| Ribonuclease inhibitor (RNH1) (P13489) | Cytoplasm and cytosol | Unique peptides (22)<br><br>Sequence Coverage (79.1%) | SV1: - 0.76, 0.507<br>**SV2: -1.58, 0.0014**<br>**SV5: -2.99, p <0.001**<br>T24: 1.54, 0.386 | Molecular function: ribonuclease inhibitor activity<br>Biological process: mRNA catabolic process and regulation of angiogenesis | Down regulation of RNH1 enhances metastasis in BC cells through regulating the epithelial-mesenchymal transition (Xiong et al., 2014). | Not available |
| Guanine nucleotide binding protein G(i) subunit alpha-1 (GNAI1) (P63096) | Centrosome (mitosis), cell membrane, cytosol, cytoplasm, nucleus, and others | Unique peptides (6)<br><br>Sequence Coverage (51.7%) | SV1: 0.15, 0.986<br>SV2: 0.01, 0.991<br>**SV5: -1.72, 0.004**<br>T24: 0.048, 0.918 | Molecular function: Transducer<br>Biological process: Cell cycle, cell division, mitosis, transport<br>Ligand: GTP-binding, metal-binding, nucleotide binding | Not available | Increased expression of GNAI1 mRNA in mouse urinary bladder following 12-week arsemsnate exposure in drinking water (Clewell et al., 2011). |
| Guanine nucleotide binding protein subunit alpha-11 (GNA11) (P29992) | Cell membrane and cytoplasm | Unique peptides (11)<br><br>Sequence Coverage (63.8%) | SV1: 0.07, 0.988<br>SV2: - 0.14, 0.988<br>**SV5: - 2.1, 0.004**<br>T24: 2.77, 0.071 | Molecular function: GTP-binding, metal ion binding, GTPase activity, G protein-coupled receptor binding<br>Biological process: Action potential, adenylate cyclase-modulating G- | Not available | Decreased expression in lung epithelial cells exposed to arsenic (Stueckle et al., 2012). |

| | | | | | | |
|---|---|---|---|---|---|---|
| | | | | protein couple receptor signaling pathway, cellular response to pH, Signal transduction<br><u>Ligand:</u><br>GTP-binding, metal-binding, nucleotide binding | | |
| Acid sphingomyelinase-like phosphodiesterase 3b (SMPDL3B) (Q92485) | Cell membrane and extracellular region | Unique peptides (5)<br><br>Sequence Coverage (16.5%) | SV1: -0.04, 0.989<br>SV2: - 0.12, 0.989<br>**SV5: -2.91, p<0.001**<br>**T24: -3.40, 0.039** | <u>Molecular function:</u><br>Glycosidase, hydrolase<br><u>Biological process:</u><br>Immunity, inflammatory response, innate immunity, lipid degradation, lipid metabolism<br><u>Ligand:</u><br>Metal binding, zinc | Involved in podocyte injury, downregulation following radiation led to elevated podocyte damage (Ahmad et al., 2017). | Not available |

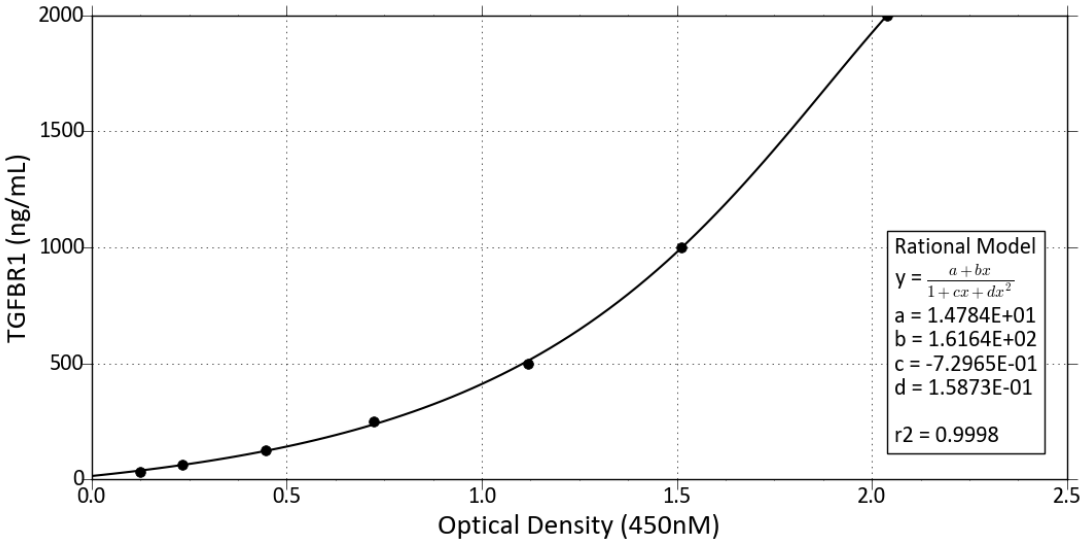


**Appendix Figure 2.3.** TGFBR1 standard curve fitted to a Rational model.

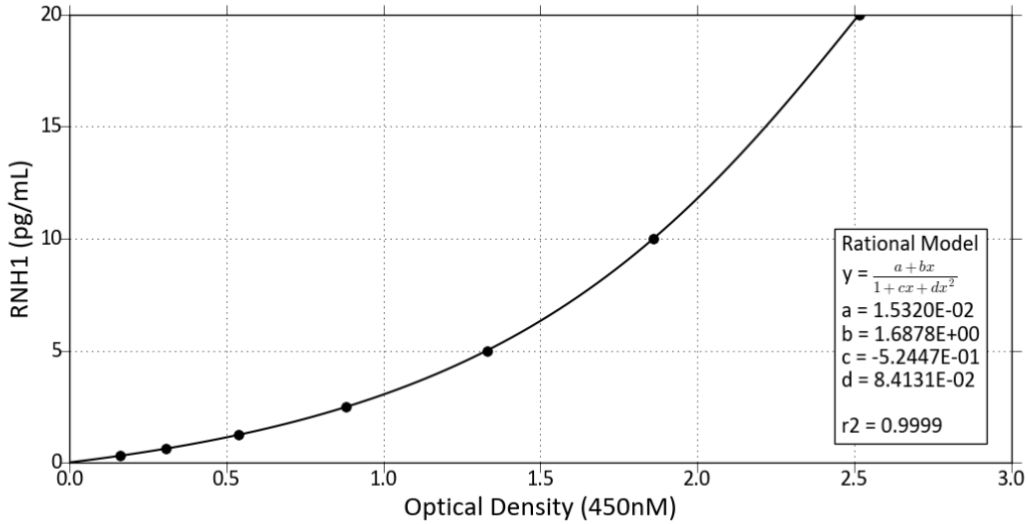


**Appendix Figure 2.4.** RNH1 standard curve fitted to a Rational model.

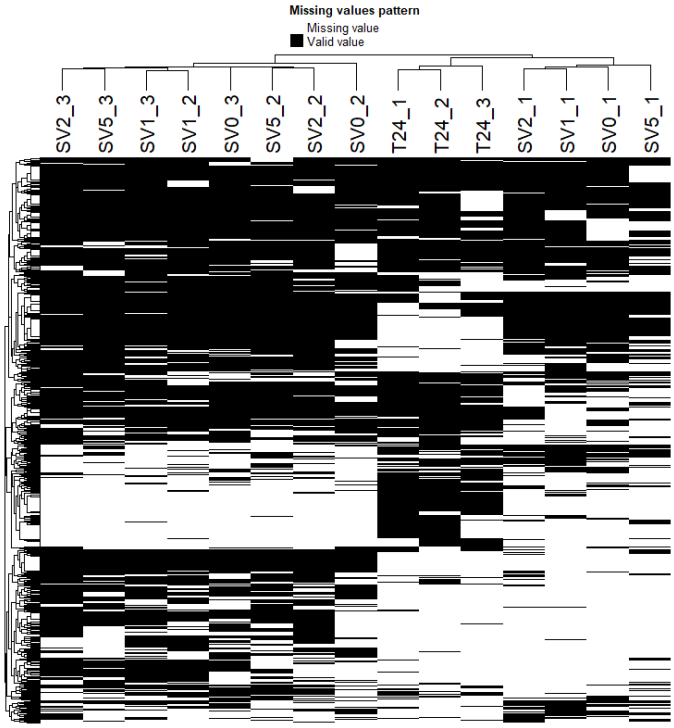


**Appendix Figure 3.1.** Heatmap with hierarchal clustering of all cell lysate proteins with missing values in at least one sample. Passage 6 samples are shown here as replicate 1.

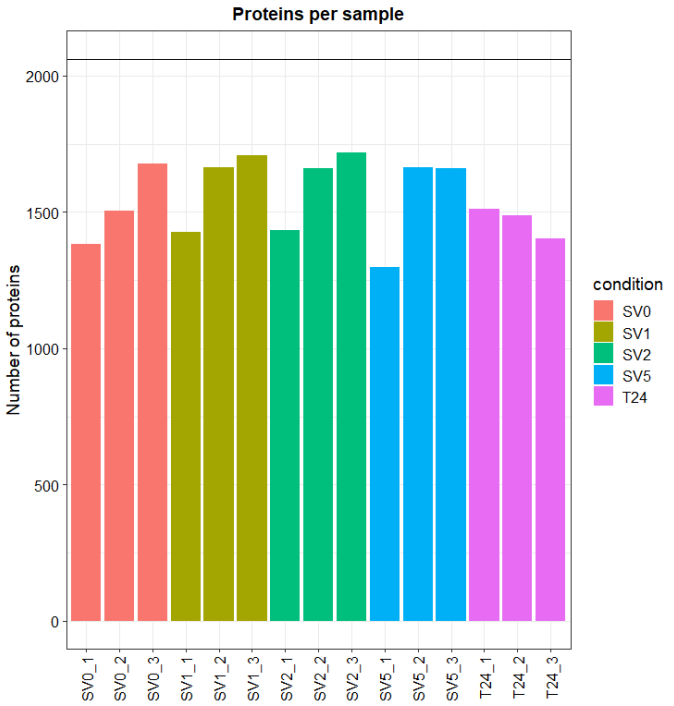


**Appendix Figure 3.2.** Bar chart of the total number of proteins in each cell lysate sample. Passage 6 samples are shown here as replicate 1.

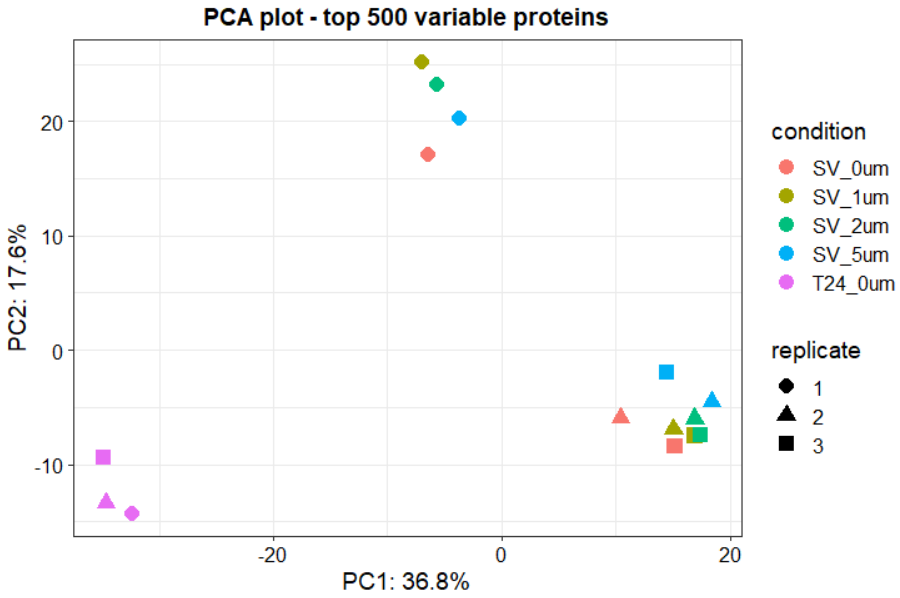


**Appendix Figure 3.3.** Unsupervised principal component analysis of the top 500 variable cell lysate proteins. Passage 6 samples are shown here as replicate 1.

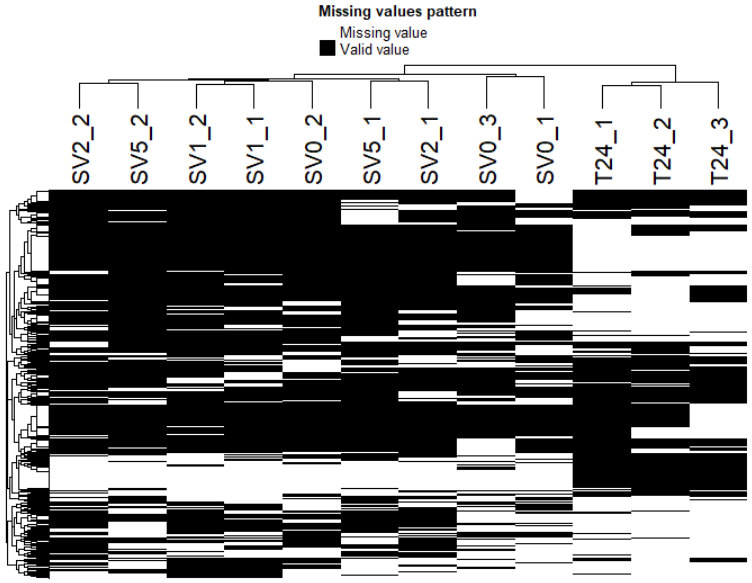


**Appendix Figure 3.4.** Revised heatmap with hierarchal clustering excluding passage 6 sample of all cell lysate proteins with missing values in at least one sample.

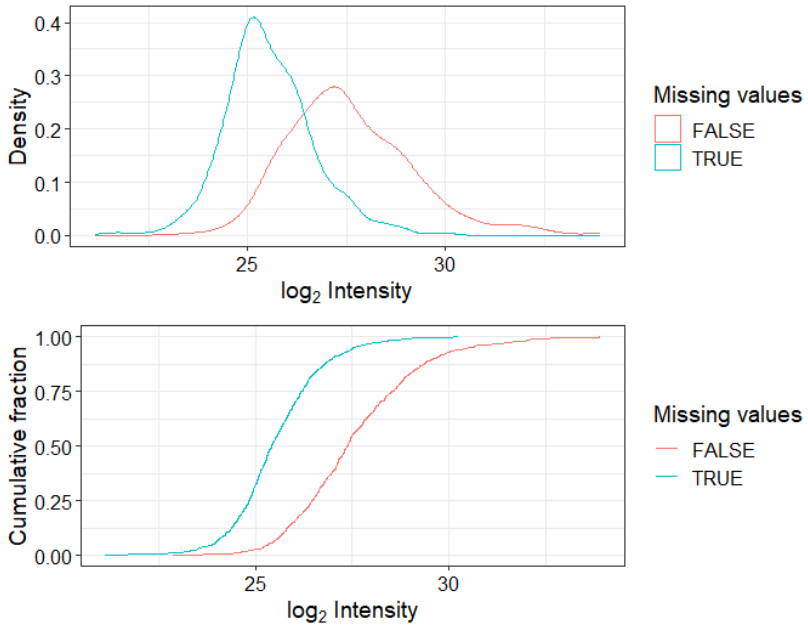


**Appendix Figure 3.5.** Intensity plots for cell lysate proteins with missing and valid values based on density (top) and cumulative fraction (bottom).

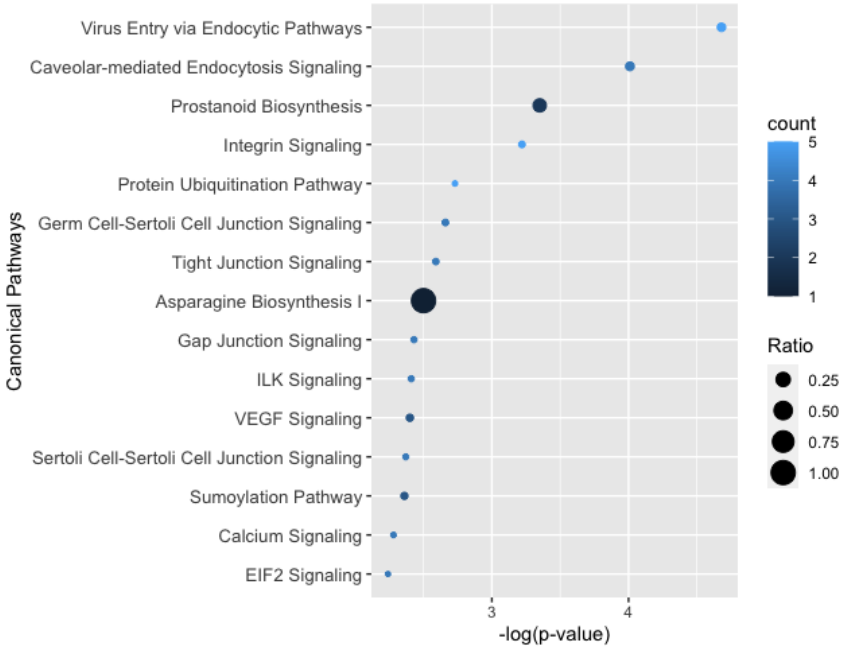


**Appendix Figure 3.6**. Canonical pathway analysis of the top 15 pathways significantly (p-value <0.05) associated with 1-um arsenic exposure cell lysate proteins.

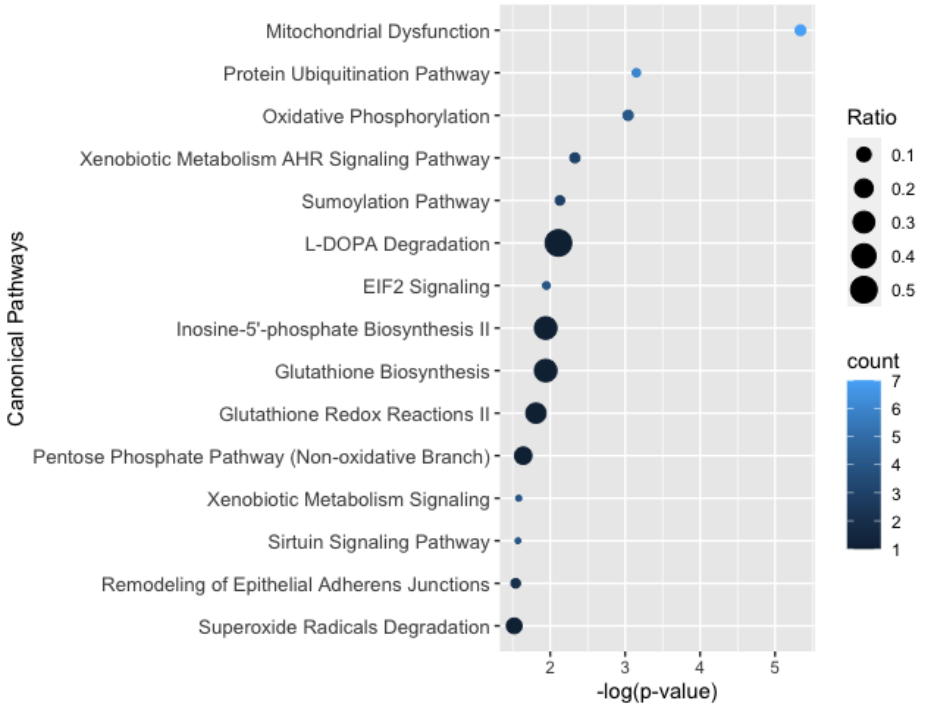


**Appendix Figure 3.7.** Canonical pathway analysis of the top 15 pathways significantly (p-value <0.05) associated with 2-um arsenic exposure cell lysate proteins.

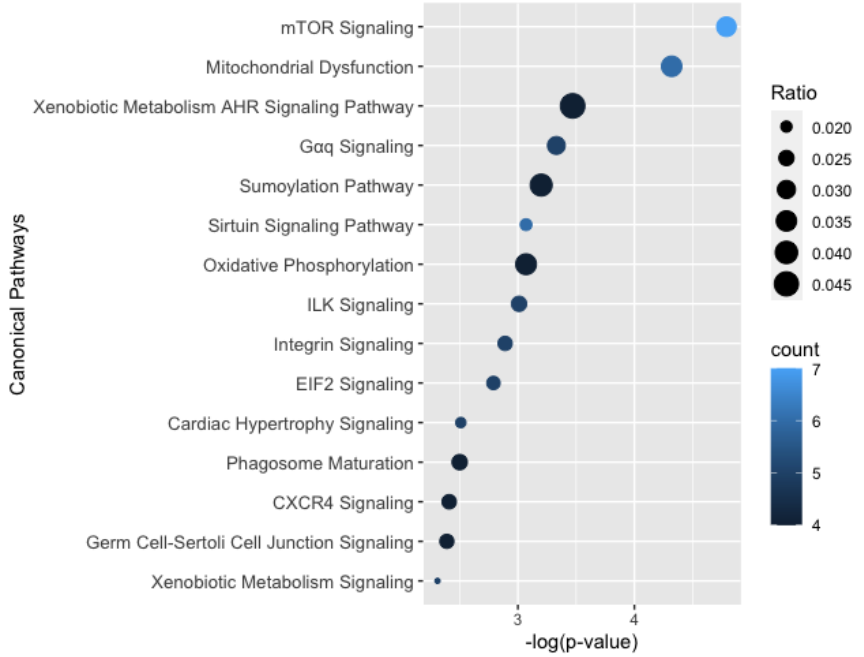


**Appendix Figure 3.8.** Canonical pathway analysis of the top 15 pathways significantly (p-value <0.05) associated with 5-um arsenic exposure cell lysate proteins.

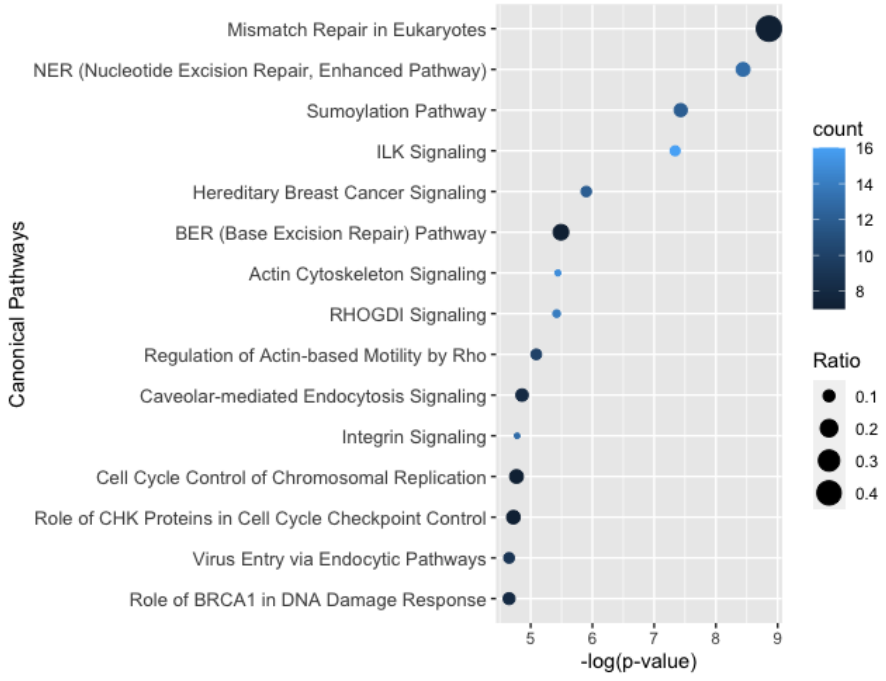


**Appendix Figure 3.9.** Canonical pathway analysis of the top 15 pathways significantly (p-value <0.05) associated with T24 cell lysate proteins.

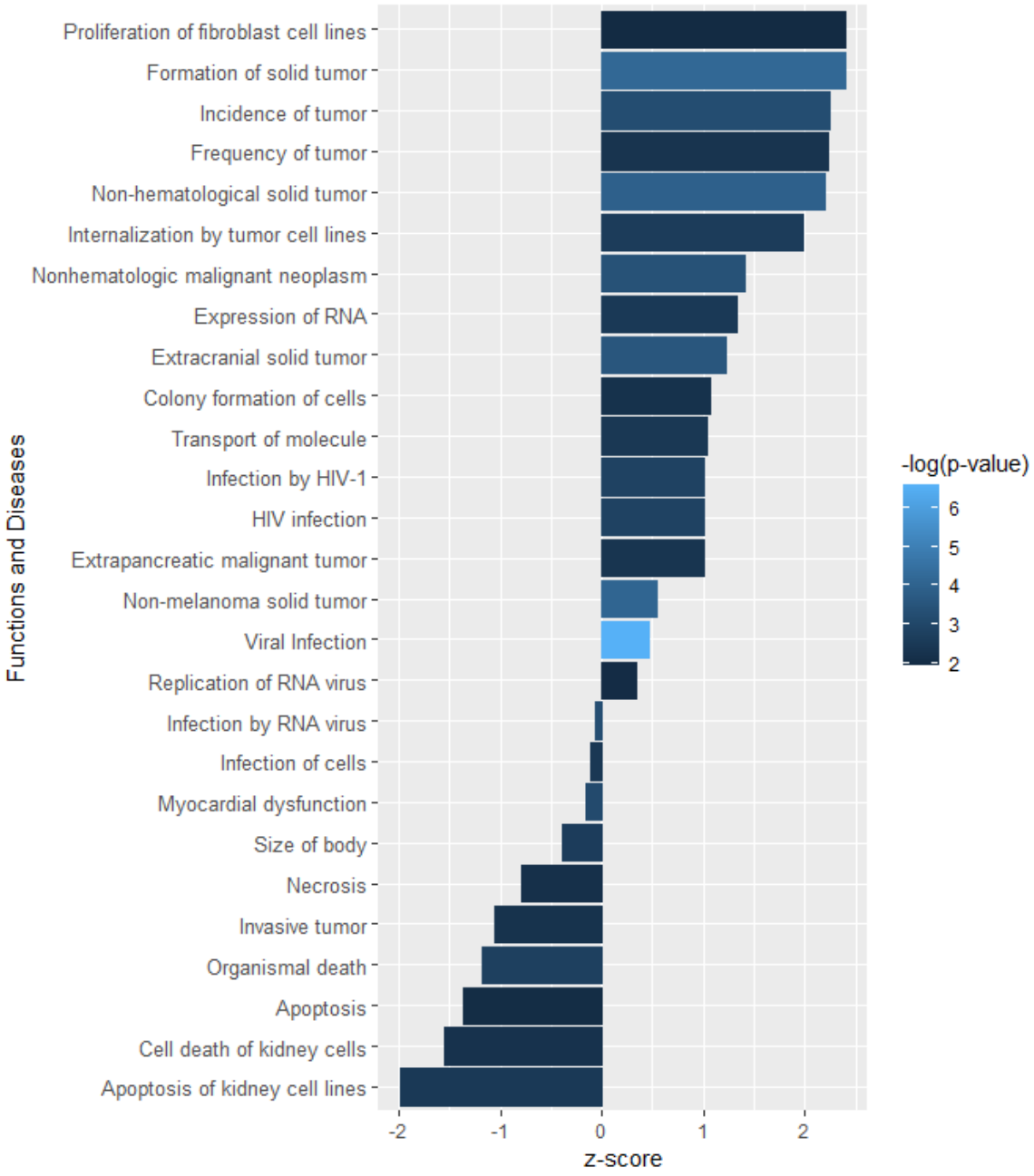


**Appendix Figure 3.10.** Analysis of the significant functions and diseases (p-value <0.05) predicted to be activated (z-score > 2) or inactivated (z-score < -2) in the 1-um arsenic exposure cell lysate group.

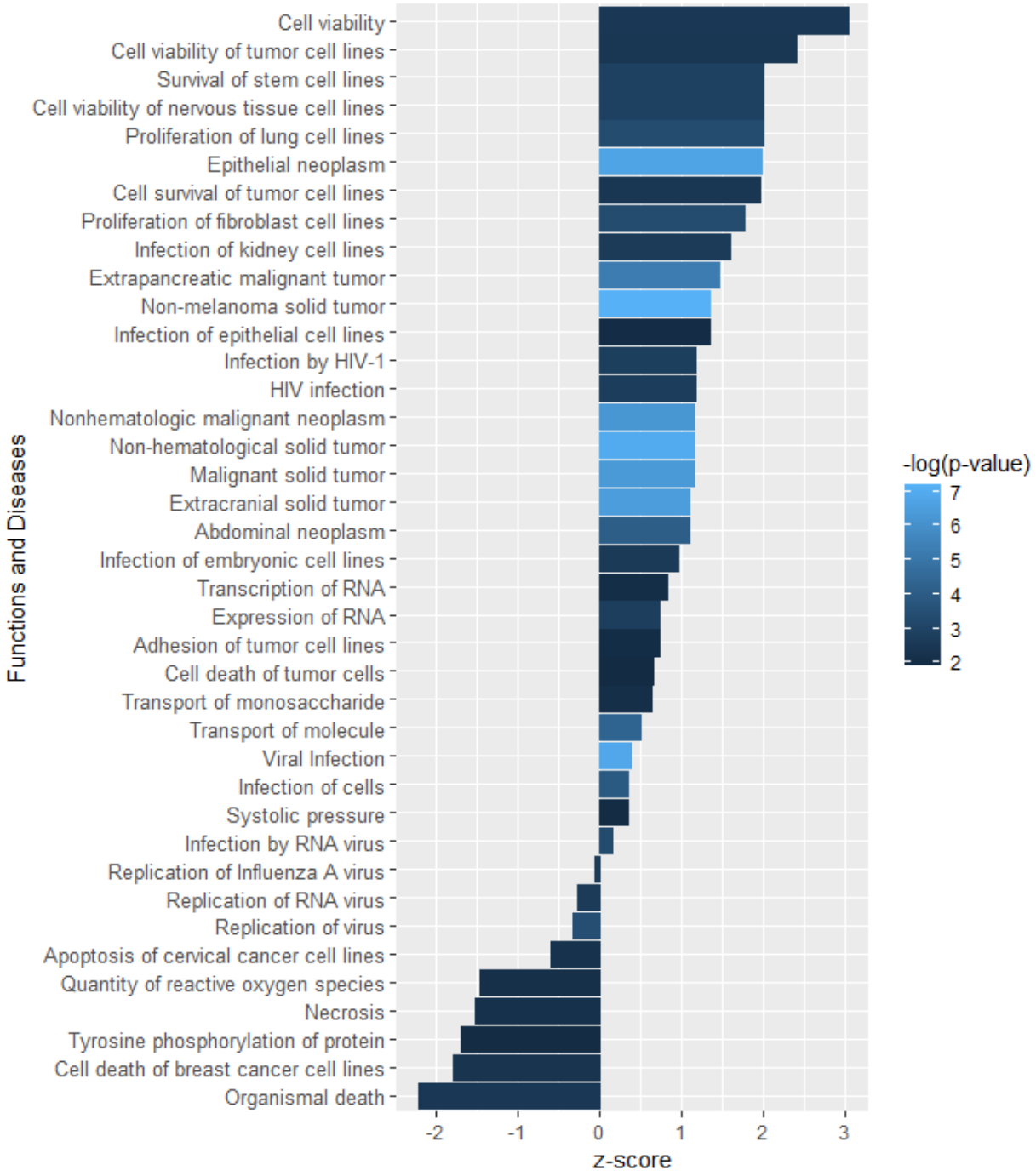


**Appendix Figure 3.11.** Analysis of the significant functions and diseases (p-value <0.05) predicted to be activated (z-score > 2) or inactivated (z-score < -2) in the 2-um arsenic exposure cell lysate group.

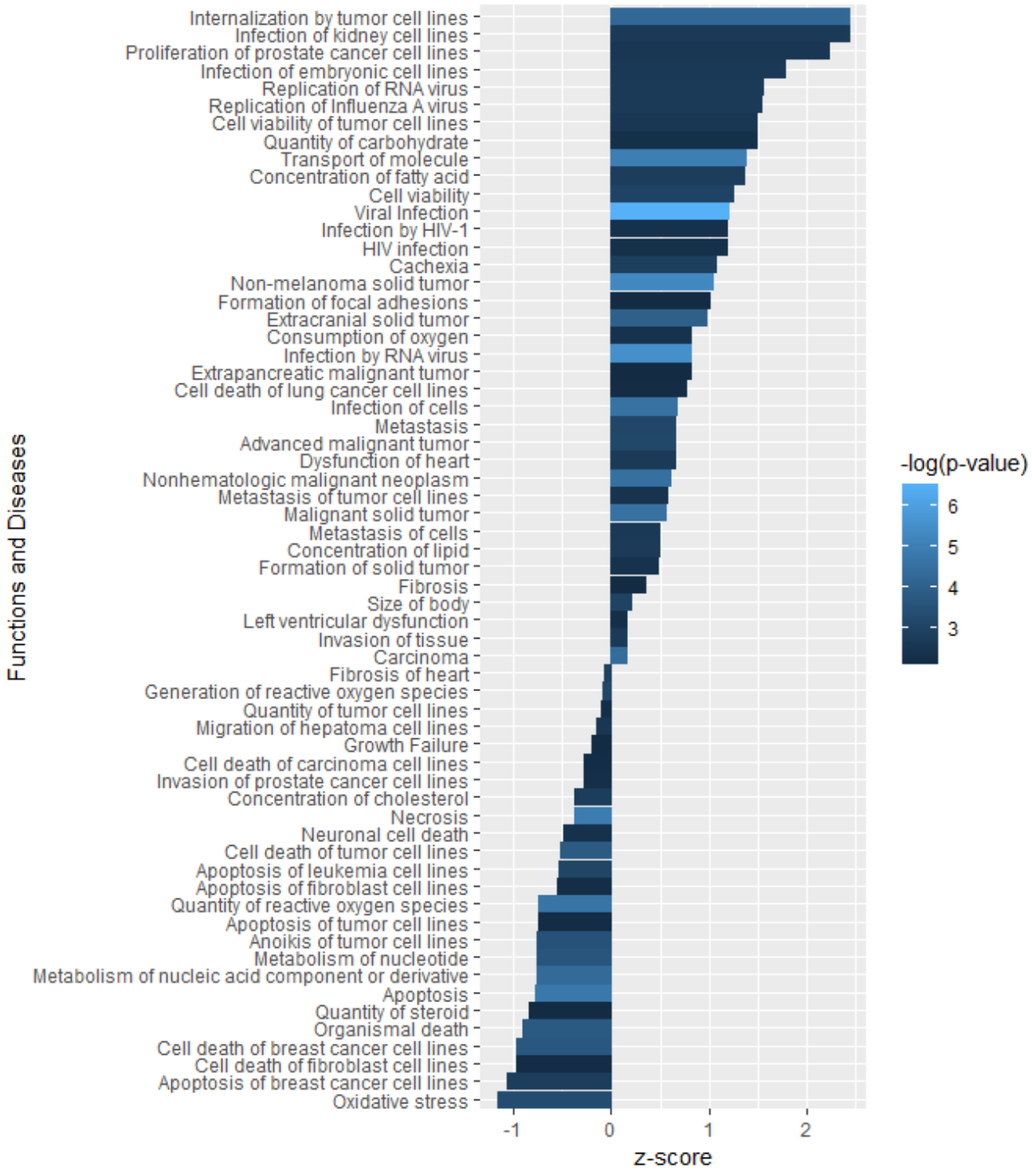


**Appendix Figure 3.12.** Analysis of the significant functions and diseases (p-value <0.05) predicted to be activated (z-score > 2) or inactivated (z-score < -2) in the 5-um arsenic exposure cell lysate group.

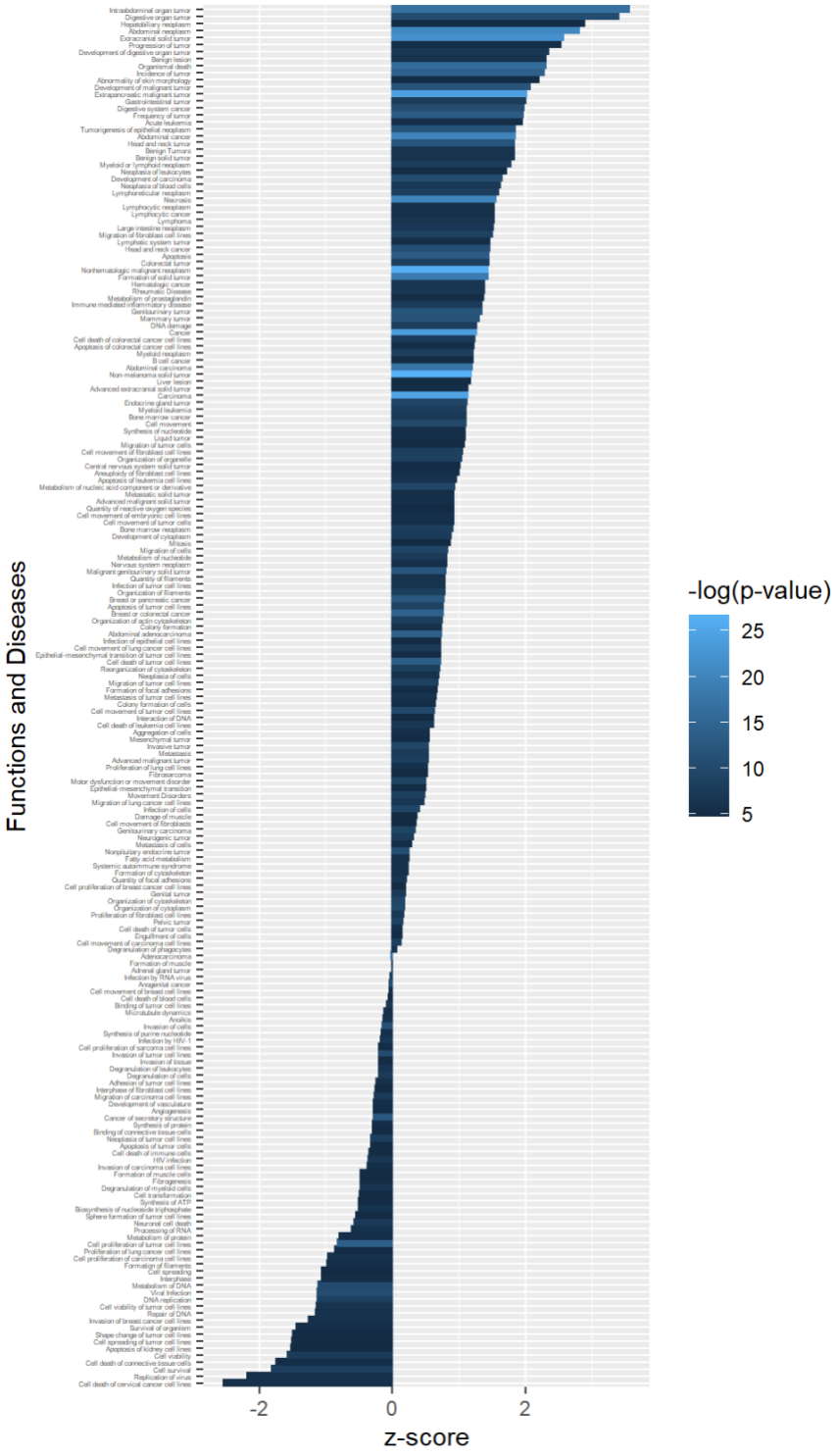


**Appendix Figure 3.13.** Analysis of the significant functions and diseases (p-value <0.05) predicted to be activated (z-score > 2) or inactivated (z-score < -2) in the T24 cell lysate group.

**Appendix Table 3.1.** Top 10 cell compartments of the 535 proteins observed in only SEV samples and not cell lysate groups. Percent of proteins details the percent of proteins in that compartment over the total proteins examined (535).

| Cell Compartment | Protein Count | Percent of Proteins (%) |
|---|---|---|
| Plasma membrane | 331 | 63.8 |
| Extracellular exosome | 235 | 45.3 |
| Integral component of membrane | 203 | 39.1 |
| Cytosol | 185 | 35.6 |
| Cytoplasm | 177 | 34.1 |
| Membrane | 169 | 32.6 |
| Integral component of plasma membrane | 116 | 22.4 |
| Extracellular region | 91 | 17.5 |
| Extracellular space | 87 | 16.8 |
| Cell surface | 78 | 15.0 |

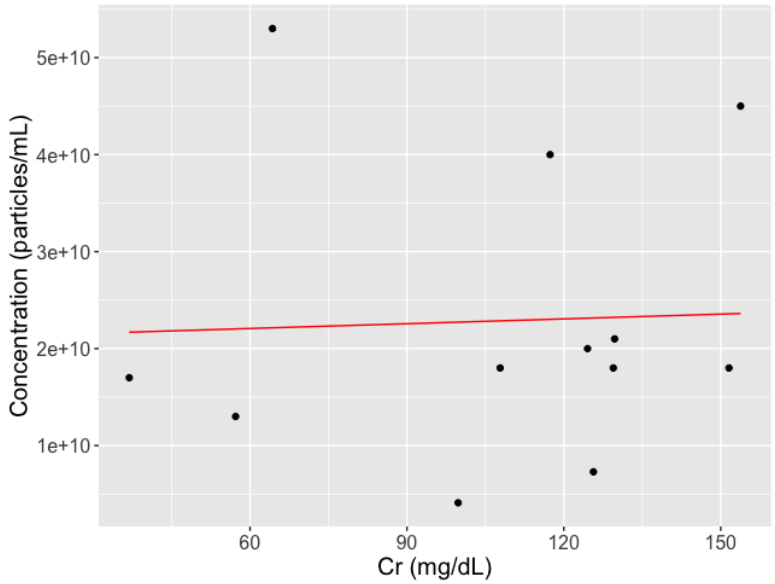


**Appendix Figure 4.1.** Univariate regression analysis of particle counts against urinary creatinine concentration.

**Appendix Table 4.1.** Model regression statistics of the association of particle count with urinary creatinine.

| | SEV Concentration _ Cr | | | |
|---|---|---|---|---|
| | Model 1 | | Model 2 | |
| **Variable** | $\beta$ | P value | $\beta$ | P value |
| Intercept | 2.108e+10 | 0.179 | 1.153e+11 | 0.224 |
| Cr | 1.648e+07 | 0.900 | -1.261e+08 | 0.546 |
| Age | | | -1.912e+09 | 0.255 |
| Sex | | | 1.949e+09 | 0.860 |
| Adjusted $R^2$ | -0.098 | | -0.1404 | |
| P value | 0.900 | | 0.6631 | |

**Appendix Table 4.2.** Results of Shapiro Wilk tests for normality in urinary biomarker data.

| Variable | W test statistic | p-value |
|---|---|---|
| **TGFBR1** | 0.944 | 0.070 |
| **uiAs** | 0.887 | **0.001** |
| **Cd** | 0.788 | **<0.001** |
| **Pb** | 0.822 | **<0.001** |

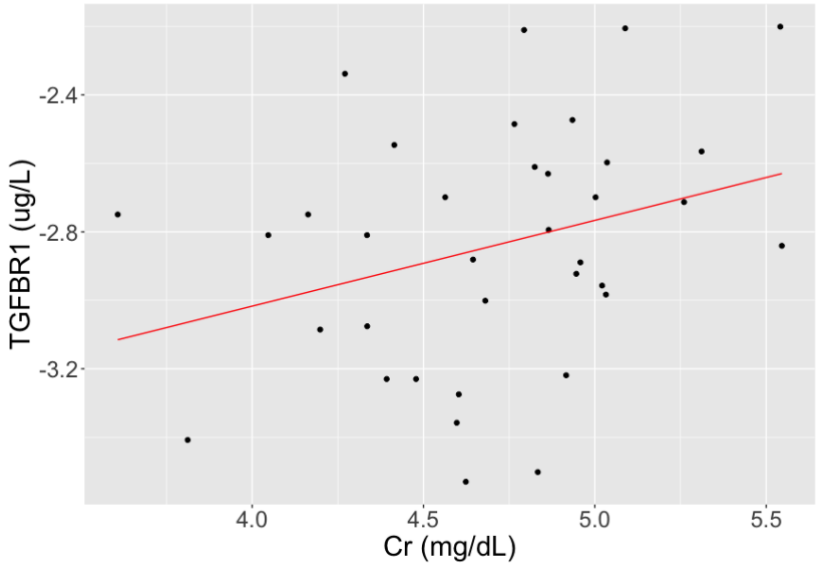


**Appendix Figure 4.2.** Univariate regression analysis of log transformed SEV derived TGFBR1 against log transformed urinary creatinine.

**Appendix Table 4.3.** Model regression statistics of the association of TGFBR1 with urinary creatinine (model 1) as well as with age and sex as covariates (model 2).

| | Creatinine (Cr) | | | |
|---|---|---|---|---|
| | Model 1 | | Model 2 | |
| **Variable** | $\beta$ | P value | $\beta$ | P value |
| Intercept | -4.020 | **<0.001** | -3.939 | **<0.001** |
| Cr | 0.251 | 0.068 | 0.229 | 0.114 |
| Age | | | 0.003 | 0.764 |
| Sex | | | -0.080 | 0.513 |
| Adjusted $R^2$ | 0.068 | | 0.026 | |
| P value | 0.068 | | 0.286 | |

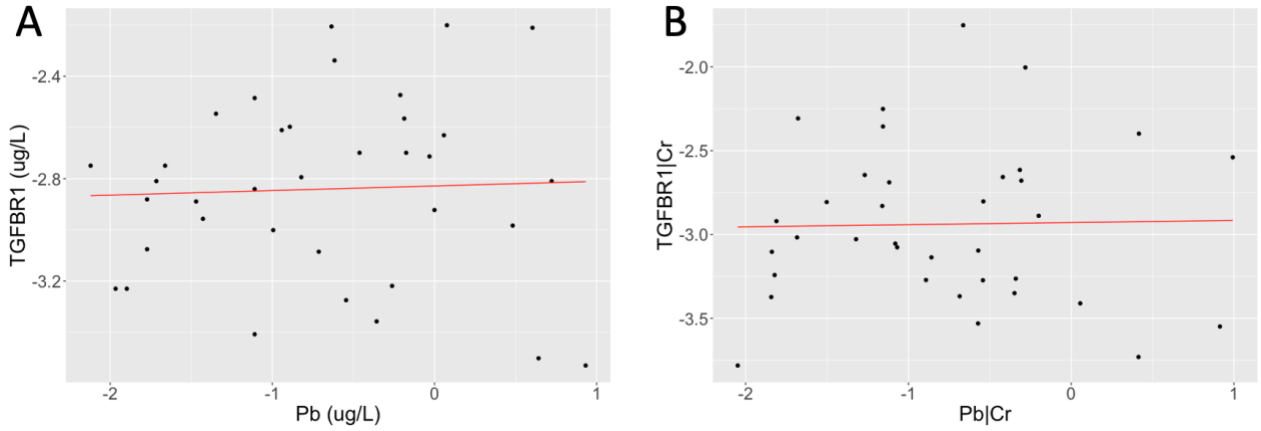


**Appendix Figure 4.3.** Univariate regression analysis of (A) log transformed SEV derived TGFBR1 against log transformed urinary lead without creatinine adjustment and (B) log transformed SEV derived TGFBR1 against log transformed urinary lead with creatinine adjustment.

**Appendix Table 4.4.** Model regression statistics of the association of SEV derived TGFBR1 with urinary lead using both univariate (model 1) and multivariate (model 2) models displayed with and without creatinine adjustment following log transformation.

| | **Pb** | | | | **Creatinine adjusted Pb** | | | |
|---|---|---|---|---|---|---|---|---|
| | **Model 1** | | **Model 2** | | **Model 1** | | **Model 2** | |
| **Variable** | *β* | P value | *β* | P value | *β* | P value | *β* | P value |
| Intercept | -2.828 | **<0.001** | -2.707 | **<0.001** | -2.929 | **<0.001** | -3.389 | <0.001 |
| Log(Pb) | 0.078 | 0.808 | 0.018 | 0.806 | 0.013 | 0.904 | -0.007 | 0.950 |
| Age | | | 0.002 | 0.877 | | | 0.007 | 0.644 |
| Sex | | | -0.132 | -0.288 | | | 0.091 | 0.588 |
| Adjusted $R^2$ | -0.028 | | -0.052 | | -0.029 | | -0.077 | |
| P value | 0.808 | | 0.737 | | 0.904 | | 0.920 | |

# References


Ahmad, A., Mitrofanova, A., Bielawski, J., Yang, Y., Marples, B., Fornoni, A., & Zeidan, Y. H. (2017). Sphingomyelinase-like phosphodiesterase 3b mediates radiation-induced damage of renal podocytes. *FASEB Journal*, *31*(2), 771–780. https://doi.org/10.1096/FJ.201600618R

Al-Eryani, L., Waigel, S., Jala, V., Jenkins, S. F., & States, J. C. (2017). Cell cycle pathway dysregulation in human keratinocytes during chronic exposure to low arsenite. *Toxicology and Applied Pharmacology*, *331*, 130–134. https://doi.org/10.1016/J.TAAP.2017.06.002

Bambino, K., Zhang, C., Austin, C., Amarasiriwardena, C., Arora, M., Chu, J., & Sadler, K. C. (2018). Inorganic arsenic causes fatty liver and interacts with ethanol to cause alcoholic liver disease in zebrafish. *Disease Models & Mechanisms*, *11*(2). https://doi.org/10.1242/DMM.031575

Banerjee, M., Ferragut Cardoso, A., Al-Eryani, L., Pan, J., Kalbfleisch, T. S., Srivastava, S., Rai, S. N., & States, J. C. (2021). Dynamic alteration in miRNA and mRNA expression profiles at different stages of chronic arsenic exposure-induced carcinogenesis in a human cell culture model of skin cancer. *Archives of Toxicology*, *95*(7), 2351. https://doi.org/10.1007/S00204-021-03084-2

Chung, J. Y. F., Chan, M. K. K., Li, J. S. F., Chan, A. S. W., Tang, P. C. T., Leung, K. T., To, K. F., Lan, H. Y., & Tang, P. M. K. (2021). TGF-β Signaling: From Tissue Fibrosis to Tumor Microenvironment. *International Journal of Molecular Sciences*, *22*(14). https://doi.org/10.3390/IJMS22147575

Clewell, H. J., Thomas, R. S., Kenyon, E. M., Hughes, M. F., Adair, B. M., Gentry, P. R., & Yager, J. W. (2011). Concentration- and time-dependent genomic changes in the mouse urinary bladder following exposure to arsenate in drinking water for up to 12 weeks. *Toxicological Sciences : An Official Journal of the Society of Toxicology*, *123*(2), 421–432. https://doi.org/10.1093/TOXSCI/KFR199

Dai, J., Xu, M., Zhang, X., Niu, Q., Hu, Y., Li, Y., & Li, S. (2019). Bi-directional regulation of TGF-β/Smad pathway by arsenic: A systemic review and meta-analysis of in vivo and in vitro studies. *Life Sciences*, *220*, 92–105. https://doi.org/10.1016/J.LFS.2019.01.042

Di, Y., Chen, D., Yu, W., & Yan, L. (2019). Bladder cancer stage-associated hub genes revealed by WGCNA co-expression network analysis. *Hereditas*, *156*, 7. https://doi.org/10.1186/S41065-019-0083-Y

Gonias, S. L., Karimi-Mostowfi, N., Murray, S. S., Mantuano, E., & Gilder, A. S. (2017). Expression of LDL receptor-related proteins (LRPs) in common solid malignancies correlates with patient survival. *PLoS ONE*, *12*(10). https://doi.org/10.1371/JOURNAL.PONE.0186649

Stueckle, T. A., Lu, Y., Davis, M. E., Wang, L., Jiang, B. H., Holaskova, I., Schafer, R., Barnett, J. B., & Rojanasakul, Y. (2012). Chronic occupational exposure to arsenic induces carcinogenic gene signaling networks and neoplastic transformation in human lung epithelial cells. *Toxicology and Applied Pharmacology*, *261*(2), 204. https://doi.org/10.1016/J.TAAP.2012.04.003

Voutsadakis, I. (2017). Proteasome expression and activity in cancer and cancer stem cells. *Tumor Biology*, 1–12. https://journals.sagepub.com/doi/pdf/10.1177/1010428317692248

Xiong, D., Liou, Y., Shu, J., Li, D., Zhang, L., & Chen, J. (2014). Down-regulating ribonuclease inhibitor enhances metastasis of bladder cancer cells through regulating epithelial-mesenchymal transition and ILK signaling pathway. *Experimental and Molecular Pathology*, *96*(3), 411–421. https://doi.org/10.1016/J.YEXMP.2014.04.012

Zheng, Y. Z., & Liang, L. (2018). High expression of PXDN is associated with poor prognosis and promotes proliferation, invasion as well as migration in ovarian cancer. *Annals of Diagnostic Pathology*, *34*, 161–165. https://doi.org/10.1016/J.ANNDIAGPATH.2018.03.002